ELECTRONIC MATERIALS RESEARCH LABORATORY

THE UNIVERSITY OF TEXAS

COLLEGE OF ENGINEERING

AUSTIN

RESEARCH ON DIGITAL

TRANSDUCER PRINCIPLES

VOLUME IV

CHARGE TRANSPORT MECHANISMS IN

THIN SILICON NITRIDE FILMS

for the

NATIONAL AERONAUTICS AND SPACE ADMINISTRATION

GRANT NGR 44-012-043

Covering the Period

July 1, ~~1967~~ *1966* – June 30, 1967

by

Jerry R. Yeargan

H. Lyndon Taylor

William H. Hartwig

The University of Texas

Austin, Texas 78712

PAGES II THRU VII MISSING FROM ORIGINAL DOCUMENT.

TABLE OF CONTENTS

LIST OF ILLUSTRATIONS

CHAPTER I

Introduction

Since its introduction in thin film form in 1965, silicon
nitride has been the object of an intense research effort, mainly by
industrial laboratories, to explore its possible use in the technology
and manufacture of integrated circuits and microelectronic devices.
In announcing a technology employing silicon nitride as the diffusion
mask and dielectric in a new material, Tombs[76] et.al. described it as
more uniform with fewer pinhole defects, having a relatively large
dielectric constant and larger breakdown voltage, and permitting greater
control of the surface state density than silicon dioxide. Silicon
dioxide is currently the most important dielectric material in the micro-
electronics industry. It serves as both the diffusion mask and the
dielectric material in silicon field effect transistors. Its major
advantage is the ease with which it grows by thermal oxidation on sili-
con substrates. However, silicon dioxide has two major disadvantages
in device applications, it grows thermally on only silicon substrates
and it has an affinity for sodium. The sodium ions move through the
silicon oxide causing a space charge which changes the electrical char-
acteristics of the metal-oxide-semiconductor (MOS) devices, thus causing
the devices to fail. Only elaborate techniques can prevent contami-
nation of the oxide with sodium. The possible advantages of silicon
nitride for device stability encourages industrial interest in the
material.

Vapor plating the nitride permits its use on a large variety

1

of substrates. The deposited material does not require a specific element in the substrate for film growth. Its successful application to gallium-arsenide has recently been announced.[33] The fact that the films are uniform, with fewer pinholes than silicon dioxide suggests its use in thin film tunneling devices. Mead[61] described in 1962 a new class of devices employing tunneling from a metal through an insulator into another insulator. To date, no commercial devices using this technique are available, mainly because of the technological problems involved in obtaining films of the required thickness (< 100 Å) with existing insulators. These desirable properties suggested a detailed study of silicon nitride to obtain basic information about the material itself.

A) Other Work on Silicon Nitride Films:

The first published successful preparation and deposition of thin films of silicon nitride is the work of Sterling and Swann[74] in 1965. Tombs[77] et.al. followed with a letter in the Proceedings of the IEEE reporting the use of silicon nitride in place of silicon oxide as the diffusion mask, the passivating layer, and the gate insulator in planar silicon insulated-gate field effect transistors. They report improvements in the device stability, the dielectric strength of the gate, and the control of the surface state densities. Hu[51] and Doo[37] followed Tombs, et.al. in July of 1966. In October of 1966, the Electrochemical Society sponsored a symposium of silicon nitride at which almost every device manufacturer was represented. References (1) - (18) give the topics discussed at that meeting. In general the work to date is very qualitative and little quantitative information exists. The only information on the electrical properties of the material in the literature

are the works of Hu[51, 52]. There are at least two papers on the
electrical properties scheduled for publication[30,*]. This work both
supports and complements their conclusions.

B) Significance of This Work:

The major result of this work is a knowledge of the conduction
behavior of silicon nitride films on silicon and quartz substrates
with different contacts. Measurements on substrates of these materials
with film thicknesses ranging from < 80 $\overset{\circ}{\text{A}}$ to 2500 $\overset{\circ}{\text{A}}$ established the ma-
jor current injection mechanism as thermal emission from the bulk of
the film. We find two different thermal emission mechanisms. The so-
called Poole-Frenkel emission mechanism is characteristic of the material.
It is identified with a barrier height of approximately 1.5 eV and a
distribution of traps such that a carrier density of from 10^6 to 10^8
carriers/cm^3 exists in the conduction band at zero field. The other
type of emission arises from non-stoichiometric conditions of some of
the films and this mechanism exhibits transient effects in about one-
fourth the devices. It differs from the Poole-Frenkel emission in
that the current readings are less stable, the resistivity is lower
at a given field, and the slope of the Schottky plots (lnI vs. $V^{1/2}$)
are approximately 1/2 those of the Poole-Frenkel type. Trap levels
for this mechanism vary from 0.85 eV to 1.05 eV below the conduction
band compared to 1.5 eV for the Poole-Frenkel emission.

At film thicknesses less than 200 $\overset{\circ}{\text{A}}$ the current appears
essentially ohmic on the quartz substrates but remains non-ohmic on the
silicon substrates. This is the first known work on silicon nitride below

---

* G. Brown, private communication

300 $\overset{\text{o}}{\text{A}}$. Pinhole-free films form with areas greater than 2.0 mm^2 at thicknesses of 50 $\overset{\text{o}}{\text{A}}$.

The theory review presents a more complete description of the Poole-Frenkel theory than exists in the literature. This involves writing down the equations for thermal carrier concentrations in an insulator and the effect of the applied field on the barrier height, considering that a coulomb attraction exists between the emitted carrier and its ionized state. A description of an ideal insulator includes the presence of traps and how they affect the barrier at the metal-insulator interface and determine whether the current injection is electrode or bulk controlled. Thermal barrier heights and approximate trap densities result from data analysis. No difference in the current characteristic appears in the thickness range from ~ 50 $\overset{\text{o}}{\text{A}}$ to 2300 $\overset{\text{o}}{\text{A}}$. The nitride supports a steady current of the order of 1 microamp before breakdown. The breakdown strength of the nitride approaches the theoretical limit of 10^7 V/cm at thickness over 200 $\overset{\text{o}}{\text{A}}$ at room temperature but decreases to about 5 x 10^6 V/cm below 200 $\overset{\text{o}}{\text{A}}$. The room temperature resistivity of the nitride is about 10^{16} ohm-cm at low fields but decreases to about 10^{10} ohm-cm before breakdown.

C) Experimental Techniques

The little material in any thin film structure makes the study of physical properties difficult. Thin film insulators are usually amorphous making it very difficult to obtain information about their composition and structure. Since thin films have been of such great interest only in the last decade, techniques for their study require further development along with the theory of the thin film state. Since the material holds such interest for engineers, an engineering study

seemed a worthwhile endeavor.

The main experimental technique applicable to thin film dielectrics is a study of their electrical properties. The information obtained applies directly to devices by interpreting it through physical models.

Two basic techniques apply to the study of the electrical properties: capacitance versus frequency and temperature and dc current transport. Capacitance data give information about the interface states and ionic conductivity in the material. The dc current transport data give information about the interface barriers, trap levels, and densities, and the band structure of the device.

The differential capacitance versus bias voltage technique helps study the interface between a semiconductor and an insulator. Since silicon nitride will primarily be used on semiconductors, a significant fraction of the specimens measured should have a semiconductor substrate. The dc current transport method offers less chance of commercial application so less industrial work will pursue this technique.

This investigation emphasized the dc current transport properties to obtain information about (a) the breakdown strength of the material, (b) the uniformity of the films, (c) the reproducibility of the films, (d) the current mechanisms present in the films, and (e) the effect of stress from different substrates on the electrical properties.

A knowledge of the current-voltage characteristics is of practical importance to engineers. As well as supplying basic information about the material, the current-voltage characteristics are useful in design of field effect transistors. The leakage current of the dielectric affects the characteristics and must be considered in design.

The leakage current also provides warning that the dielectric approaches breakdown. This type of information pertains to device reliability. Since 1960, a whole new class of devices employing the tunnel emission mechanism has been known and Hartwig[87] recently described the operation of a new tunneling digital transducer. The information gained from a study of the current-voltage behavior has practical as well as theoretical importance.

D) Transport Mechanisms in Thin Insulating Films:

The possibility of current flow in insulators has been recognized for many years (see e.g. Mott and Gurney[24]). Rose[69,27] developed the theory of space charge limited flow. Mead[61] conducted the first work on current transport in thin films of insulating materials in which he described a new class of electronic devices employing the mechanism of tunnel emission. The work by Mead created a lot of interest in these new devices and his work on Ta_2O_3 and Al_2O_3 preceded work on SiO[49,53] SiO_2[54], Al_2O_3[48,27,66], BO[63], polymerized silicon oil[42,78,38] (PSO) and others.

In general, the current densities required for space-charge-limited conditions do not occur. The mechanism by which the carriers appear in the conduction band of the insulator limits the current. Mechanism models proposed for the injection of carriers into the conduction band rely on the energy band representation of the metal-insulator-metal structure as in fig. 1. The mechanisms consist of two general classes, thermionic emission and tunnel emission and subdivide into bulk- and electrode-controlled phenomena.

Thermionic emission occurs when the carrier receives enough
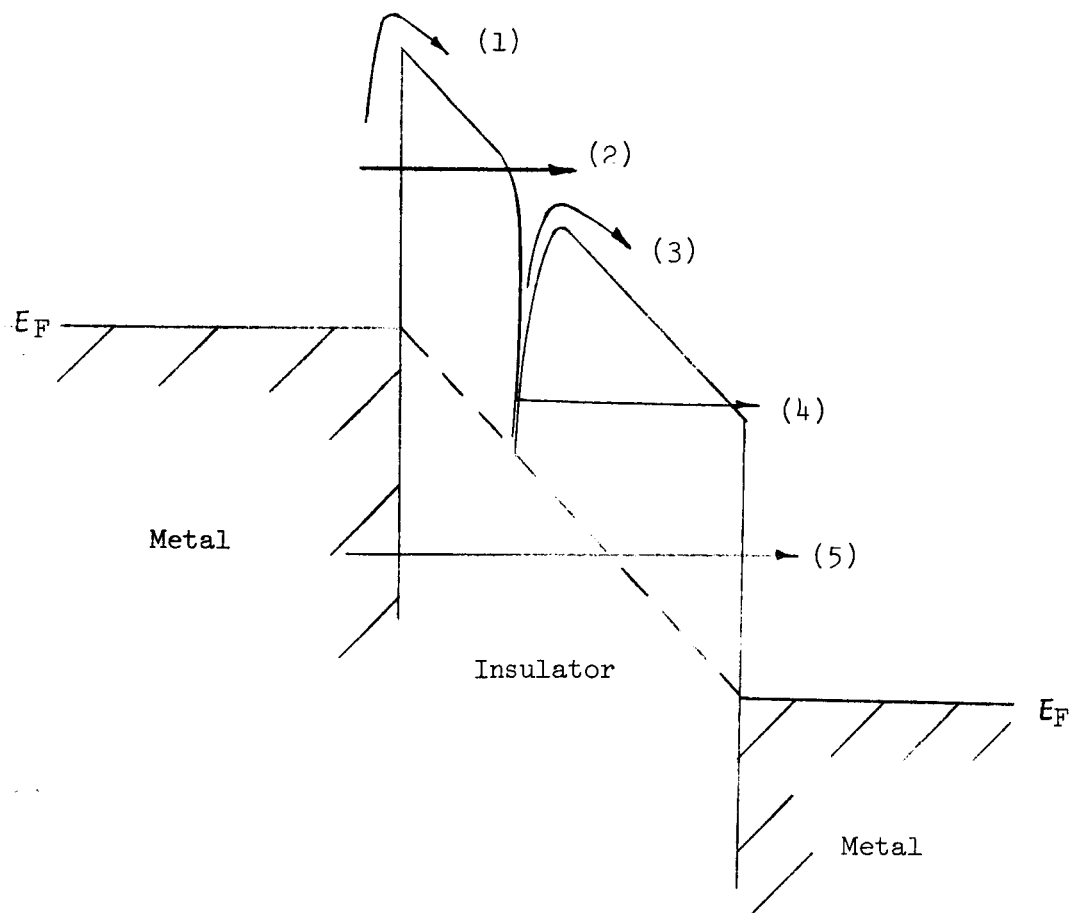
Fig. 1 Current Mechanisms in Thin Film Insulators

(1) Schottky Emission
(2) Fowler-Nordheim Tunneling
(3) Poole-Frenkel Emission
(4) Field Ionization
(5) Metal-Metal Tunneling

thermal energy from the lattice to surmount the restraining potential barrier and the lowest available state in the conduction band of the insulator. Tunneling occurs when the barrier thickness is thin enough to allow a finite probability for the electron to penetrate the barrier and emerge to the other side.

Experimentally, a great deal of similarity exists between the observed current characteristics for the materials mentioned above. In general, the current is proportional to exp $(C\ V^{1/2})$ where C is a constant and V is the applied voltage. For thicknesses greater than 100 $\overset{\circ}{A}$, the current usually depends strongly on temperature at room temperature. Current depends little on temperature at low temperatures. That the theoretical picture is not clear is evidenced by the present number of divergent papers in the literature on the subject which indicates the unsatisfactory theoretical picture. Two recent papers examine the effects of traps on Schottky emission[44] and the effects of electron-phonon interaction on tunneling[39].

CHAPTER II

Current Mechanisms in Insulators

Electronically solid state materials group as conductors, semiconductors, and insulators. The conductivity range of solid materials varies over 10^{25} mhos/meter. Fused quartz, a good insulator, has a conductivity of 2 x 10^{-17} mhos/meter, and silver, a good conductor has a conductivity of 6 x 10^{7} mhos/meter. They illustrate extremes of one of the most variable quantities found in nature. Their energy band structure, shown in fig. 2, best explains the distinguishing features of conductors, insulators, and semiconductors.

The conduction properties of the three classes of materials arise from the size of the energy gap separating the valence band and the conduction band. The gaps in allowed energy are the result of degeneracy conditions in the material. The electrons obey the Pauli exclusion principle and when a large number of atoms with identical electronic structure are brought together, the allowed states separate into closely spaced levels called bands. No conduction occurs in a full band, only in partially filled bands. At normal temperatures, some electrons in narrow gap materials possess enough thermal energy to excite them over the energy barrier between the valence band and the conduction band resulting in partially filled bands thus permitting conduction. This class of materials are semiconductors. In metals the bottom of the conduction band is actually lower in energy than the top of the valance band so that the bands are partially filled at all

9

temperatures. In insulators, however, the amount of carriers in the conduction band due to thermal excitation from the valence band is negligible even to temperatures approaching the melting temperature of the material.

Any real material contains imperfections which allow states to exist within the forbidden band. These states localize around the impurity or defect and differ from the Bloch states found everywhere in the material. These localized states (traps) affect the conduction process by capturing and emitting carriers to the conduction and valence bands.

Insulators are materials with relatively large bandgaps (5-12 eV) and in which any traps contributing free carriers to the conduction process are compensated by traps collecting carriers, i.e. donor traps compensated by acceptor traps. In high purity crystalline materials, the concentration of traps may be as low as 10^{12} cm^{-3}; however, in amorphous or polycrystalline materials the number of traps increases to magnitudes comparable to the atomic density of the material. That the material remains insulating with such high trap concentrations is the result of (a) a high degree of compensation or (b) that the energy difference between traps and the nearer band is large compared to the thermal energy.

At high temperatures and high electric fields, the quantity of free carriers becomes such that significant amounts of current may flow in the insulator. The actual carrier injection mechanism determines to a large extent the electric properties of the material and is therefore of great importance to device designers. Thermal emission occurs when the carrier receives enough energy from the lattice to overcome the potential barrier separating its energy state from

(a) Metal

(b) Insulator

(c) Semiconductor: T = 0

(d) Semiconductor: T > 0
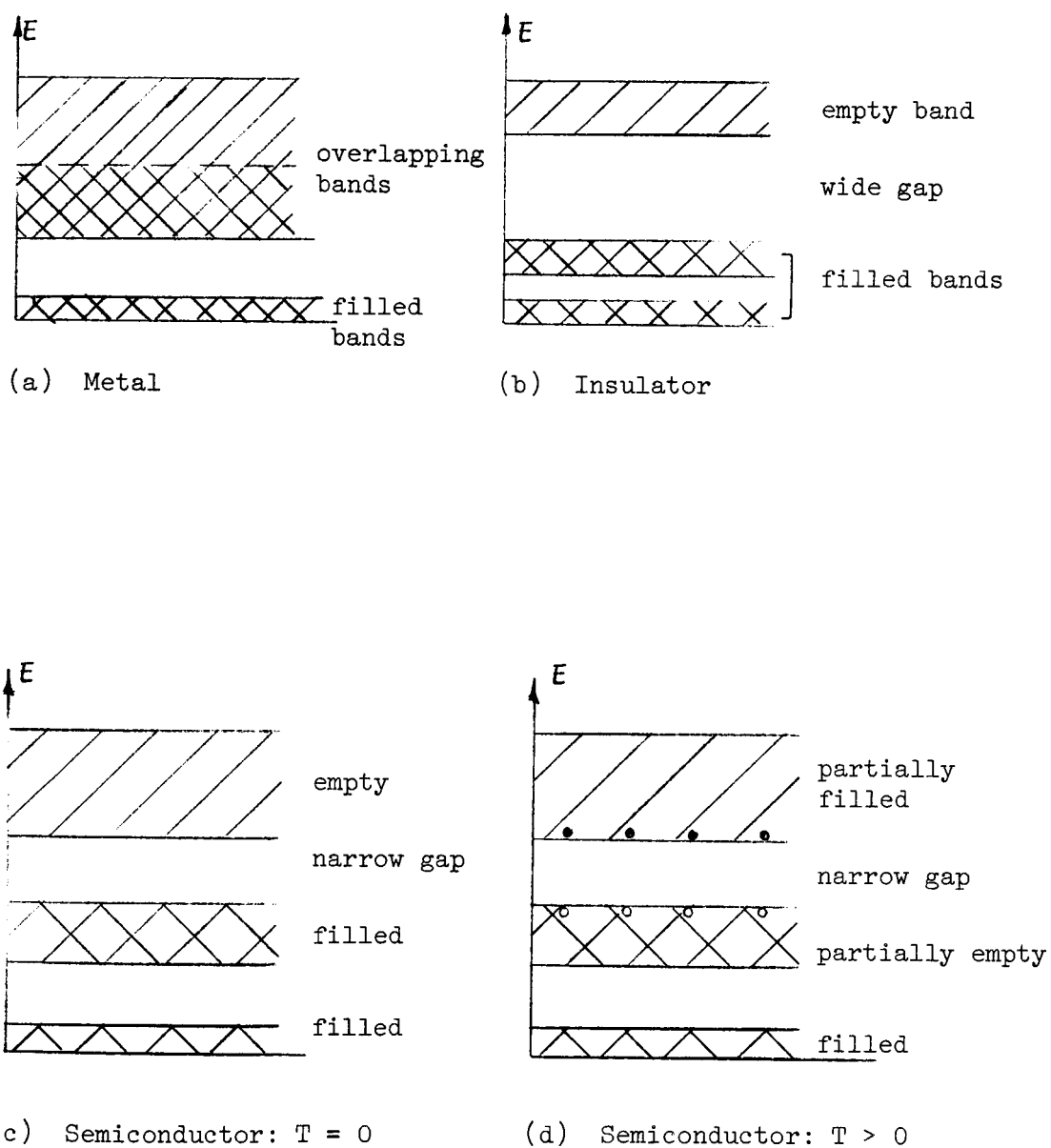
Fig. 2 Band Pictures of the three electrical types of solid materials

the lowest available state in the band. Tunneling occurs when the barrier becomes thin enough for appreciable quantities of electrons to penetrate it while conserving both energy and momentum. Other mechanisms, such as photoexcitation, may inject carriers into the bands, but they are not important to this work.

A study of charge transport through an insulator requires an electrical contact to the material. The contact affects the material behavior, the experimental results and hence, the analysis. Device design also requires knowledge of the contact behavior.

This section presents the model of an insulator used to evaluate its electrical properties, the manner in which the contacts affect the properties, and how information about the material results from an experimental study of the current mechanisms present.

A) The Ideal Insulator:

The number of free electrons in the conduction band of a large bandgap insulator in thermal equilibrium is negligible in most practical cases. Conduction takes place only after the introduction of carriers into the conduction (or valence band) by some mechanism. Once in the conduction band, the carriers move in the conventional manner, describable by a mobility parameter.

Figure 3 (a) gives the simplest case for the energy band structure of an insulator containing no traps and shows the two most common types of contacts, metals and semiconductors. While the band picture is well established only for crystalline materials with periodic potentials, good evidence indicates that some close order exists in all materials and in fact that the band picture may hold for completely random materials[55]. Note that a field exists in the insulator, even
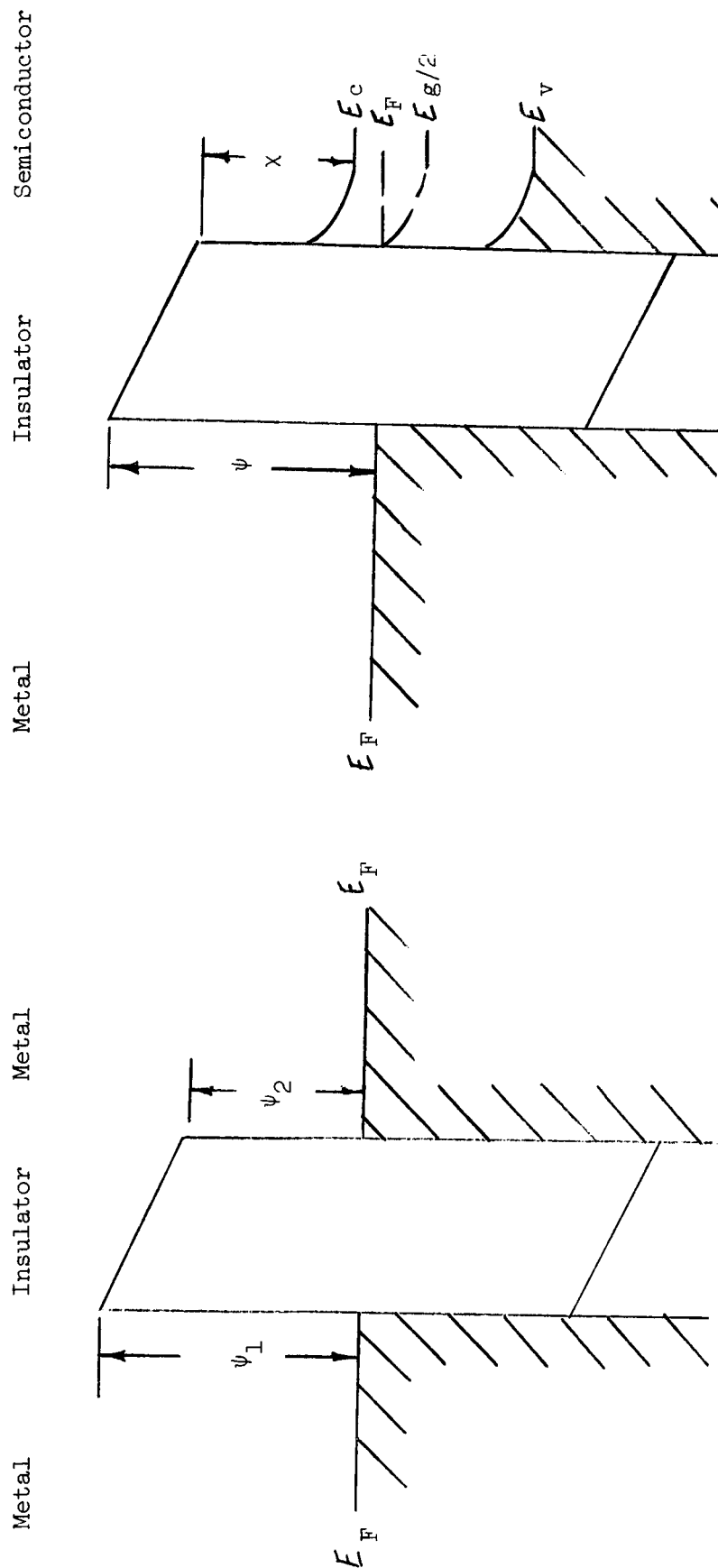
Fig. 3 Band Picture for Metal-Insulator-Metal and Metal-Insulator-Semiconductor Structures

with no applied voltage, due to the difference in the surface work functions. Application of an external bias results in a total field

$$E = E_{ex} + E_{int} \tag{1}$$

where

$$E_{int} = \frac{\phi_1 - \phi_2}{d} \tag{2}$$

$$E_{ex} = \frac{V_{ap}}{d} \tag{3}$$

In the ideal insulator, Schottky emission and tunneling are the mechanisms by which carrier injection into the conduction band occurs.

1) Injection over a Barrier (Schottky Emission)[30]

Consider the metal-insulator interface of fig. 3. For small ϕ's or very high temperatures some electrons possess sufficient energy to pass over the barrier. In equilibrium, an equal number flows in the opposite direction. By applying a small field, the contribution of one group diminishes. Integrating over all electrons in the metal with sufficient energy in the z direction to overcome the barrier gives the current density (J_z). This resembles closely the case of thermionic emission into a vacuum and follows the Richardson-Dushman[28] equation

$$J_z = \frac{1}{(2\pi)^2} \frac{2qm(kT)^2}{h^3} \exp(-q\phi/kT) \tag{4}$$

The mass of the electron which enters the equation is the effective mass "m*" which may differ considerably from the free electron mass "m". In a parabolic band, the effective mass is a single,

well-defined number, and if the effective mass is the same in the in-
sulator and the metal, the Richardson-Dushman equation needs only modi-
fication by replacing "m" by "m*". If the effective masses differ,
the correct mass is the one in the material into which the carriers
are injected, i.e. the insulator.

The thermionic current is negligible at normal temperatures.
However, high fields lower the barrier height and increase the current
to appreciable values in a manner analogous to the Schottky effect in
thermionic emission from metals into a vacuum. Consideration of the
image force on the injected carrier gives the amount of barrier lower-
ing $\Delta\phi$. An emitted electron sees an equal and opposite charge in the
metal which tends to return it to the metal by coulomb attraction.
For emission into a vacuum the force of attraction is

$$F = \frac{q^2}{4\pi\varepsilon_0(2z)^2} \, . \tag{5}$$
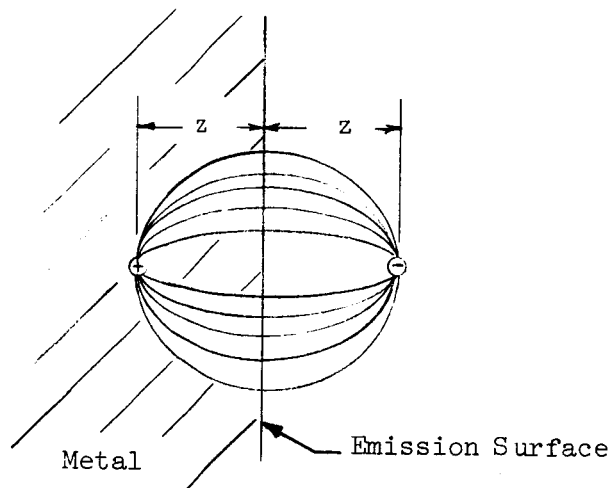
Fig. 4   Force on Electron Emitted From Metal Surface.

Ions in the insulator partially shield the field and reduce the force of attraction in the case of emission into a dielectric. The relative dielectric constant "κ" corrects for the shielding effects.
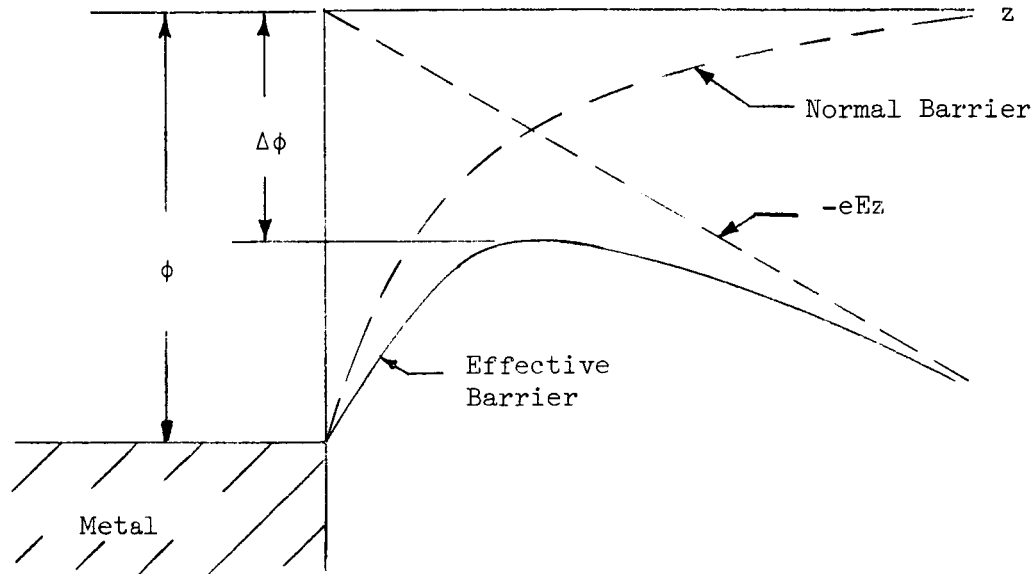
Fig. 5 Reduction of the Surface Barrier at a Metal-Insulator Interface Due to the Application of an External Field.

Equation 6 then gives the correct barrier lowering

$$\Delta\phi = (\frac{qE}{4\pi\kappa\varepsilon_o})^{1/2} \qquad (6)$$

resulting in an effective barrier

$$\phi_{eff} = \phi - \Delta\phi \qquad (7)$$

Substituting the expression for the effective barrier into the equation for thermionic emission gives the Schottky equation

$$J = \frac{2qm^*(kT)^2}{(2\pi)^2 h^3} \exp[-\frac{q\phi - q(qE/4\pi\kappa\varepsilon_o)^{1/2}}{kT}] \qquad (8)$$

$$J = 120\frac{m^*}{m} T^2 e^{-q\phi/kT} \exp[+0.44E^{1/2}/\sqrt{\kappa}T] \qquad (9)$$

for ϕ in electron volts; E in volts/meter.

2) Tunneling or Field Emission:

From above, when the energy of the electron exceeds the barrier
height ϕ, the electron may travel relatively freely over the barrier.
However for $E < \phi$ there is still a finite probability that the electron
will escape the metal due to quantum-mechanical tunneling. Figure 6
shows the one-dimensional case.
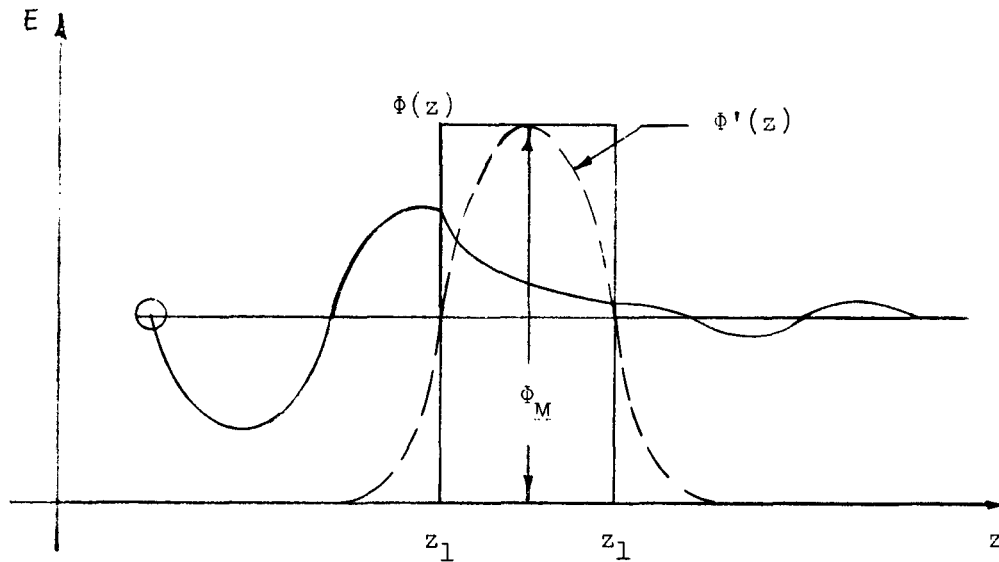
Fig. 6 Tunneling Through a Potential Barrier, $\Phi'(z)$ is the Smoothed
Out Barrier due to Image Force.

Z_1 and Z_2 represent the classical turning points. Solution
of one-dimensional Schrodinger equation

$$- \frac{h2}{2m} \frac{\partial^2 \psi}{\partial z^2} + \Phi(z)\psi = E\psi \tag{10}$$

for the square potential $\Phi(z)$ results in an exponentially decaying
wave function in the forbidden region. We define $P(E)$, the proba-
bility of an electron tunneling through the barrier, as

$$P(E) = \frac{|\psi(z_2)|^2}{|\psi(z_1)|^2} . \tag{11}$$

Stratton[76] uses an expansion which applies rigorously at low voltages
providing the image force can be taken into account exactly. Simmons[71,72]
makes approximations which allow solution of the equation over the
entire range but result in errors as much as a factor of 10^4 for materials
with small dielectric constants. Meyerhofer and Ochs[63] calculate the
tunneling probability numerically with an accuracy of $\pm$ 25%.
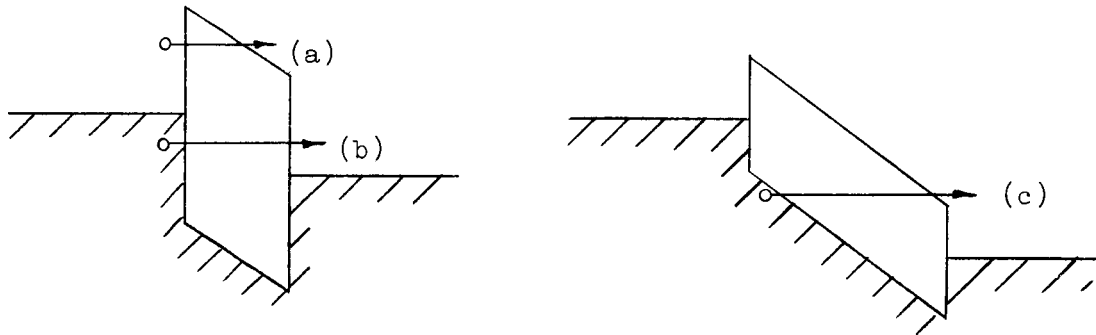
Fig. 7 Various Ways Tunneling Can Occur.

Figure 7 shows three ways tunneling occurs:

(a) direct tunneling from the conduction band of one metal
into the conduction band of the other.

(b) tunneling from the conduction band of the metal into
the conduction band of the insulator.

(c) tunneling from the valence band of the insulator directly
into the conduction band of the insulator.

$|\psi(z)|^2$ is the expected value of finding an electron at z. Real bar-
riers are never infinitely sharp and require approximations for solutions

of the transmission coefficient $P(E)$. The common approach uses the WKB approximation[23].

The result is

$$P(E) = \exp \left(-\int_{z_1}^{z_2} [2m\Phi'(z) - E]^{1/2} \, dz \right), \quad (12)$$

where $\Phi'(z)$ is the shape of the real barrier and E is the energy of the electron measured from the bottom of the conduction band of the metal. Integrating over all electrons then gives the tunnel current

$$J_z = qN(E)f(E)P(E_z)v_z dk_z \quad , \quad (13)$$

where $N(E)$ is the density of states function

$\quad$ $f(E)$ is the Fermi function

$\quad$ v_z $\quad$ is the z component of velocity

$\quad$ k_z $\quad$ is the wave number of the electron and is expressed in terms

$\quad\quad$ of energy.

Of the many attempts to evaluate J_z, most authors calculate approximate forms of the integrals which apply only within certain limits. Two of the most recent and complete calculations are by Stratton[76] and Simmons[72].

Because of the large bandgaps in insulators, mechanism (c) is very unlikely. For very thin films, (a) dominates at low voltages. However for films > 50 Å, the transmission coefficient for (a) is negligible but (b) occurs for any thickness due to narrowing of the barrier by the electric field. For films of this study, mechanism (b) predominates. Simmons[71] gives the expression for (b) as

$$J = \frac{2.2e^2E^2}{8\pi h\phi} \exp[-\frac{8\pi(2m)^{1/2}(q\phi)^{3/2}}{2.96hqE}]. \quad (14)$$

This expression has the same form as high field emission from a metal into a vacuum first considered by Fowler and Nordheim [43].

$$J = AE^2 e^{-B/E} \tag{15}$$

Others[76] obtain the form of this equation although the constants vary with the approximations.

B) Space-Charge-Limited Current:

Carriers injected into the conduction band of the insulator continue to flow toward the anode due to the applied field. For no compensating charge present, the presence of the carriers constitutes a space charge. The space charge in turn changes the field distribution in the insulator. For an unlimited reservior of carriers, the expression for one-carrier, trap-free, space-charge-limited current is

$$J = \frac{8}{9} \varepsilon_0 \kappa \mu \frac{v^2}{d^2} \ , \tag{16}$$

where μ is mobility.

This expression shows that large currents in insulators occur if the carriers are available. Smith and Rose[68] measured currents up to 20 amps/cm^2 through insulating CdS crystals and demonstrated that they obey eq. 16.

In general, the assumption of an unlimited supply of carriers does not hold and traps cause important effects on the current. Space-charge limited currents affect the field distribution which in turn affects the injection process. The field at the cathode decreases compared to the uniform field. Geppert[46] and O'Dwyer[64] consider the effects of space charge on Fowler-Nordheim injection and recently Frank and Simmons[44] considered the effects of space charge on Schottky

emission.

C) The Insulator with Traps

Figure 8 shows the band picture of an insulator or semicon-
ductor with traps. By extending the model used to explain the conduc-
tivity of semiconductors, a model suitable for explaining the conduc-
tivity of insulators with traps results. The model includes the effect
of the metal contacts on the shape of the insulator barrier and shows
how this effect influences the analysis of the experimental data.
Neglecting this effect sometimes results in false conclusions about the
metal-insulator barrier height. The model also considers surface states
and shows how, if they are present, the effect of the metal may be
completely masked. Mott and Gurney[24] give the basic model; however,
the model below includes the effect of both the metal contact and
surface states in a thin film insulator with traps and is the first
time that the complete model appears in print.

$\oplus$ ionized donor state

$\ominus$ ionized acceptor state

$\ominus\!\!\!\!e$ free electron
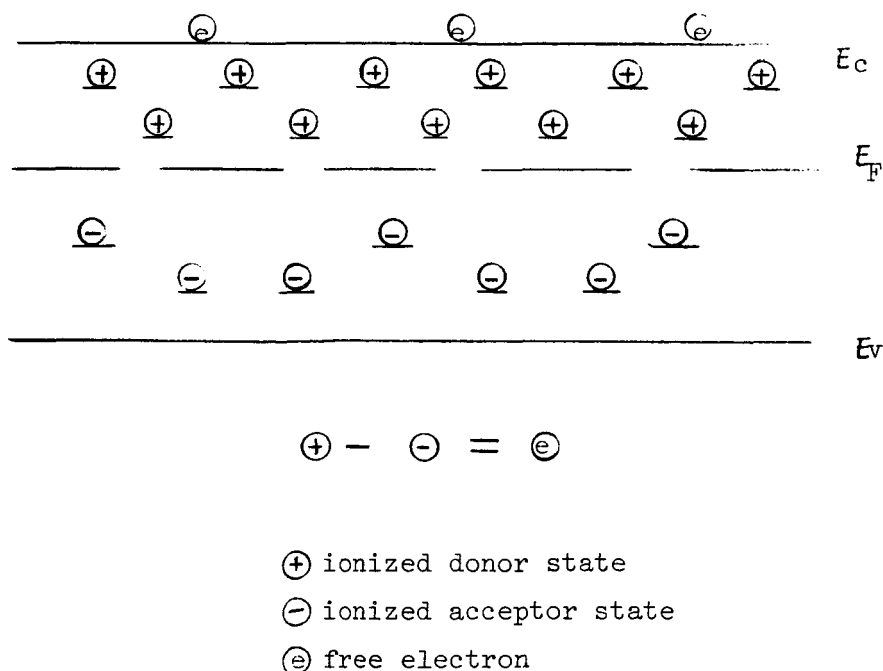
Fig. 8 Band Picture for an n-type Insulator or Semiconductor

1. Effect of the Metal Contact on the Potential Barrier

Figures 9 - 11 show the effect of the metal contact on the shape of the potential barrier at the metal-insulator interface. This condition requires the presence of traps, which exist in any real material. Before contact, the Fermi levels in the insulator and in the metal may differ considerably; however, after contact the levels must be equal for elements in thermodynamic equilibrium. For the case of an insulator whose work function is less than that of the metal, electrons flow from donor impurity levels in the insulator into the metal bringing the Fermi levels into coincidence. (Surface state effects are considered below). The positively ionized impurity levels form an electrical double layer by attracting electrons in the metal toward the interface. Poisson's equation relates the space charge density to the potential at any point.

$$\frac{\partial^2 \phi}{\partial x^2} = - \quad \rho/\kappa\varepsilon_0 \tag{17}$$

Assuming a uniform concentration of ionized donor levels per unit volume, the solution for Poisson's equation is

$$\rho = eN \tag{18}$$

$$\phi = - \frac{2\pi Ne}{\kappa\varepsilon_0} x^2 \tag{19}$$

The thickness "d" of the dipole layer for a potential drop of ϕ_0 is

$$d = (\kappa\varepsilon_0\phi_0/2\pi eN)^{1/2} \tag{20}$$

where ϕ_0 is the difference in the Fermi levels before contact. Taking $N = 10^{18}$ cm^{-3}, $\kappa = 5.5$, $\phi_0 = 0.5$ volt gives a thickness "d" of ≈ 16 Å This distance compares to the total thickness of the insulator in some devices and must then be considered.

(a) before contact   (b) after contact
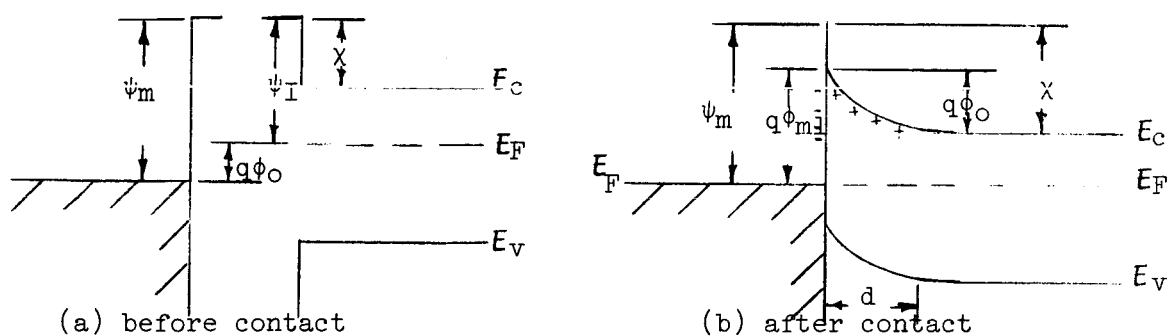
Fig. 9   Band picture for metal-insulator contact barrier when the work function of the insulator (ψ_I) is less than the work function of the metal (ψ_m). (X is the electron affinity of the insulator and $q\phi_o$ is the difference in the work functions before contact.)

(a) before contact   (b) after contact
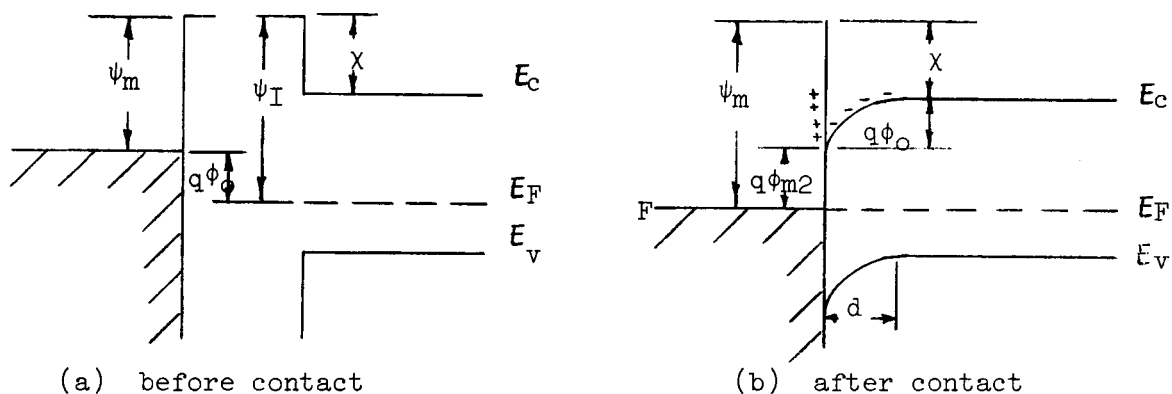
Fig. 10   Band picture for metal-insulator contact barrier when the work function of the insulator is greater than the work function of the metal.
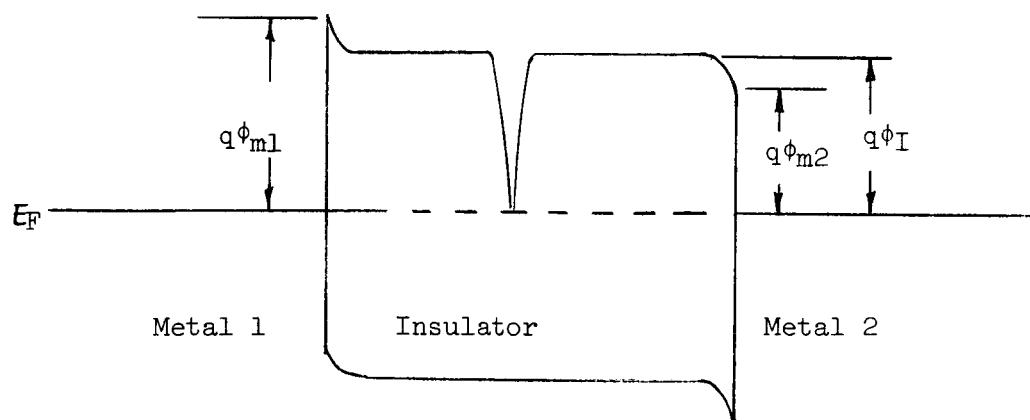
Fig. 11   Band picture for metal-insulator-metal structure with

$$q\phi_{m1} > q\phi_I > q\phi_{m2}$$

For an insulator work function greater than that of the metal, electrons flow from the metal into acceptor states or ionized donor states in the insulator to bring the Fermi levels into coincidence. This charge motion establishes a space charge layer across the metal-insulator interface.

A rectifying junction results when the metal's work function exceeds that of the insulator. For the insulator's work function being larger, the metallic contact is ohmic. Figure 12 shows the band structure for one ohmic and one rectifying contact. This structure helps illustrate the possible effects of the contacts on the current mechanisms. Consider first the case when the rectifying contact is reverse biased, and only thermal emission occurs (tunneling will be considered separately). Figure 12 gives the barrier picture under these conditions.
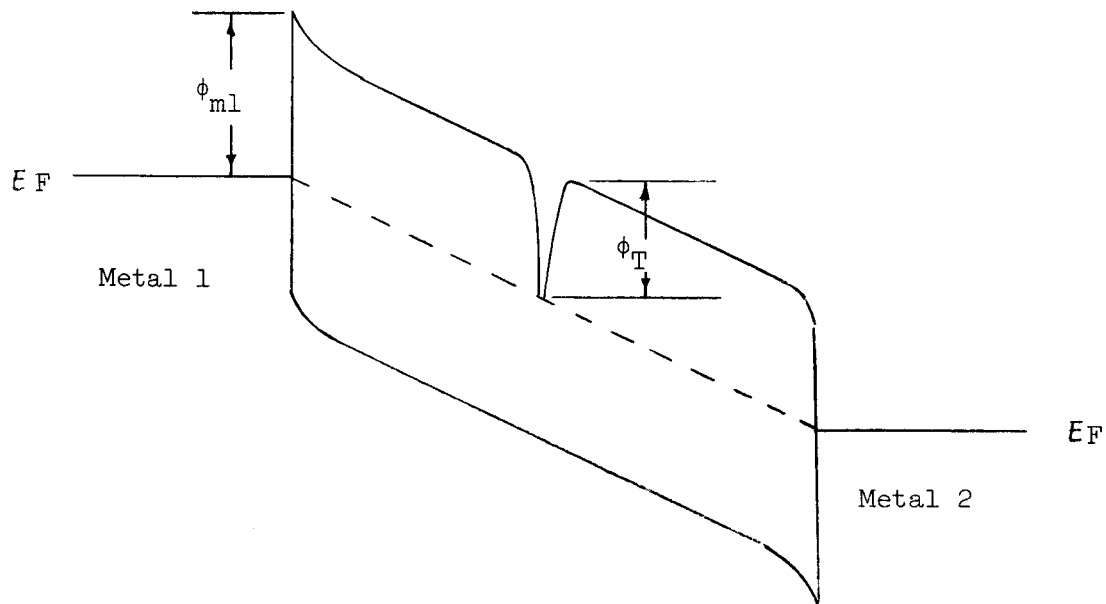
Fig. 12   Band Picture for M-I-M Structure with Rectifying Junction
          Reverse Biased. (metal 1 biased negative).

ϕ_{ml} is the barrier that an electron sees when leaving metal number 1 and entering the insulator. From fig. 9

$$q\phi_{ml} = \psi_{ml} - (\chi - q\phi_o) = \psi_{ml} + q\phi_o - \chi \qquad (21)$$

ϕ_T is the potential difference between the Fermi level of the insulator and the bottom of the conduction band, and from fig. 11 is

$$q\phi_T = \psi_{ml} - \chi \qquad (22)$$

For this situation $\phi_T < \phi_{ml}$ and the emission is from the traps at the Fermi level in the insulator. This is the so-called Poole-Frenkel[45] emission.

$$\phi_{ml} - \phi_T = \phi_o \qquad (23)$$

Consider next the case of forward-biased ohmic contact. In this situation, space charge may limit current flow for a small region of applied bias[44]. At zero bias the maximum barrier is $q\phi_{ml}$, as in fig. 11; however, when a bias greater than the difference in work functions between metal 1 and the insulator $(\psi_{ml} - \psi_I)$ is applied, the maximum barrier becomes $q\phi_{max}$ as in fig. 13. Increased bias reduces the maximum barrier rapidly until the space charge in the insulator is eliminated as shown by fig. 14. The situation when the maximum barrier is that of fig. 14 (a) or (b) is the condition for space charge limited flow because the reservior of the electrons in the conduction band at the metal-insulator interface is larger than needed for the applied field. Further increase in bias reduces the barrier to $q\phi_{ml}$ and the current is then limited by emission of electrons into the conduction band. The condition

for space charge limited current is then

$$\left| \psi_{m1} - \psi_I \right| < qV_{ap} < \left| \psi_{m2} - \psi_I \right| .$$

For ϕ_{m2} over a few kT this effect is small because the flux of electrons which have energies greater than ϕ_{m2} is very small; however, this effect occurs in some insulators.

$$\left| \phi_{m1} - \phi_I \right| < V_{ap} < \left| \phi_{m2} - \phi_I \right|$$
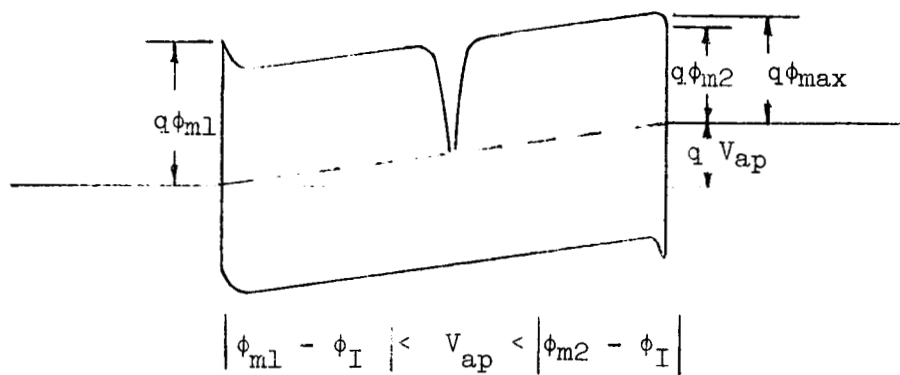
Fig. 13 Conditions of Space-Charge-Limited Current from Ohmic Contact
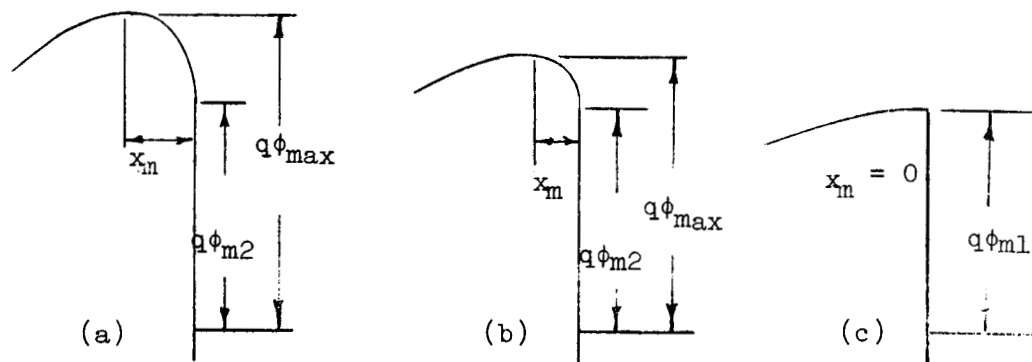
Fig. 14 Effect of increasing the bias on the barrier height and the position of the barrier maximum. (a) no bias, (b) small bias, and (c) large bias.

In summary, the following mechanisms exist for the MIM device described above. For the case of negative bias on the metal at the rectifying junction the barrier at the interface is larger than the barrier from the Fermi level in the bulk of the insulator to the bottom of the conduction band, and any thermal emission present is of the Poole-Frenkel type. When the metal at the ohmic interface is biased negative, space charge limited flow may occur for a small bias range, but at higher voltages the current is limited to Schottky emission from the metal into the insulator.

2. Effect of Surface States:

With no surface states present and a uniform density of traps throughout the insulator, the bands are flat up to the surface as in fig. 15. Making contact to the metal bends the bands according to the discussion on pages 22-27. However, surface states may bend the bands prior to contact with the metal as in fig. 16. The presence of a large density of states at E_s in the forbidden band of the insulator effectively pins the Fermi level at this energy. Making contact to the metal brings the Fermi levels of the metals into coincidence. Figure 17b shows the resulting band picture. If this situation holds, little relation exists between the barrier height and the difference in work functions of the metal and dielectric. The density and location of surface states in the forbidden band then controls the barrier.

Wilmsen[79] and Esaki and Stiles[40,41] have recently noted the effects of surface states in tunneling from a metal into an insulator. Surface states also play a large role in determining the characteristics of MIS field effect transistors and their effect on the capacitance vs.
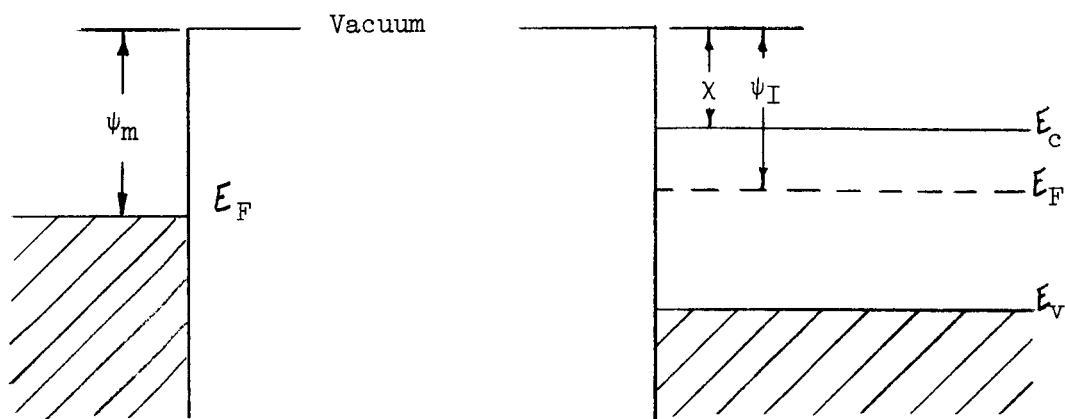
Fig. 15 Metal-Insulator Before Contact (no surface states)
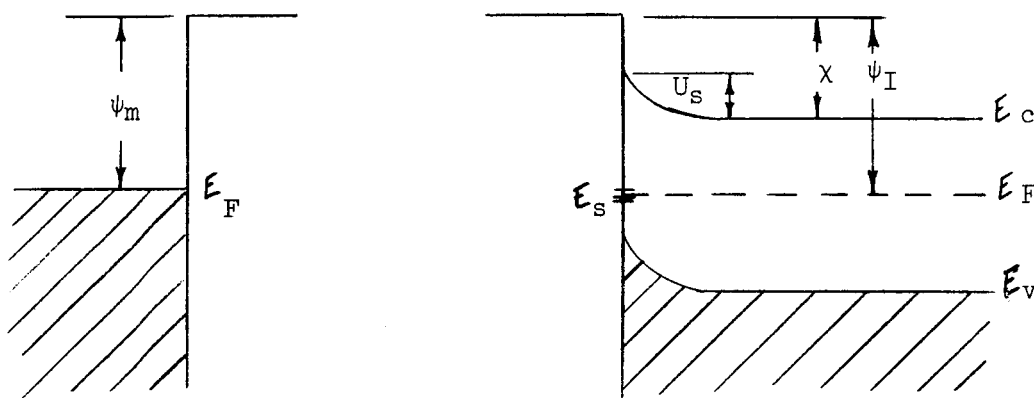
Fig. 16 Metal-Insulator with Surface States Band Picture Before Contact
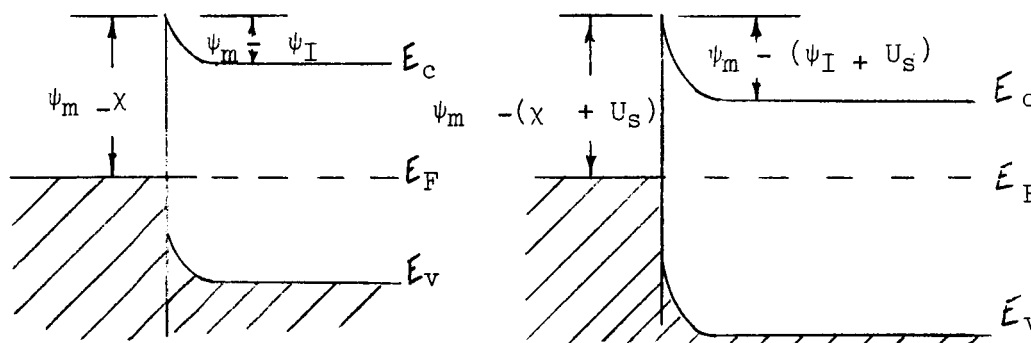
Fig. 17a Metal Insulator after
Contact (no surface
states).

Fig. 17b Metal-Insulator Contact
with Surface States

voltage characteristics is well known.

The most complete information on surface states is for the silicon-silicon oxide interface. The presence of surface states in metal-SiO_2-silicon structures results in a fixed charge at the interface which translates the capacitance-voltage curve along the voltage axis as in fig. 18.
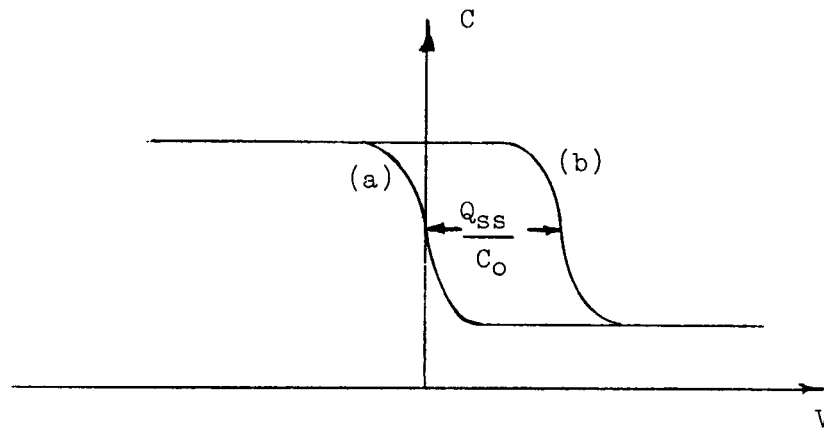
Fig. 18   Effect of Surface States on Capacitance-Voltage Curve of MOS
         Structure (a) Theoretical Curve, (b) Experimental Curve

The density per unit area of the surface state charge is designated as Q_{ss}, and its characteristics have been studied extensively[85] and it has the following properties:

1) It is fixed: it does not charge or discharge with a wide variation of bending of the silicon energy bands.

2) It is unchanged under conditions that would lead to the motion of sodium ions in the oxide, or to the annealing of radiation-induced space charges.

3) It resides within 200 $\overset{o}{A}$ of the oxide-silicon interface.

4) Its density Q_{ss} remains unchanged by the oxide thickness, or by the type or concentration of impurities in the silicon.

5) Q_{ss} depends strongly on the oxidation and annealing conditions and the orientation of the silicon crystal.

In the case of the silicon-silicon oxide system, it appears that the surface-state charge arises from excess ionic silicon present in the oxide during oxidation waiting to react with the oxidizing species that has diffused across the oxide during the oxidation process.

Christian and Taylor[86] investigated a similar charge in Al-Al$_2$O$_3$-Al structures and determined that diffusion of aluminum ions into the dielectric causes a space-charge. They find the density the order of 10^{13} cm^2, and the average thickness of the space charge about one lattice constant.

As an example of how the presence of surface charge dominates the barrier height, consider a metal-insulator-metal structure with no traps in the insulator and a difference of 1 eV in work functions between the metals. Let the insulator thickness be 100 Å and the surface state charge density be 10^{13}cm^{-3}. Assume a relative dielectric constant of 6.0 and an area of one cm^2. The charge transferred to bring the Fermi levels in coincidence is

$$Q = CV \tag{25}$$

where C is the capacitance of the structure

$$C = \frac{\kappa \varepsilon_0 A}{d} = \frac{(6.0)(8.85 \times 10^{-14})}{1 \times 10^{-6}} = 53.1 \times 10^{-8} \tag{26}$$

and V is the difference in work functions of the metals (1 volts). The charge transferred is

$$n = 3.32 \times 10^{12} \text{ carriers} \tag{27}$$

which is only one third of the surface state charge even in this very thin device.

The above discussion leads to the conclusion that the barrier height need not be simply related to the difference in work functions of the various materials in the structure if the current injection mechanism is electrode controlled. Further, if a large density of surface charge exists at each interface, the barriers may essentially mask the electrode effects entirely.

3. Poole-Frenkel Emission

Equation 28 is the expression for the conductivity of a material,

$$\sigma = nq\mu \quad \text{ohm-cm} \tag{28}$$

where σ is the conductivity

  n is the concentration of free carriers

  μ is the mobility of the carriers

  q is the charge on the carriers.

The concentration of free carriers is due to the thermal energy of the material. At high fields, lowering of the barrier drastically increases the concentration. The carriers are, in general, both holes and electrons but, for simplicity, we consider only the case for electrons. The concentration of free electrons is of the form[24]

$$n = n_o \exp[-q\phi/kT] \quad \text{cm}^{-3} \tag{29}$$

where n_o involves the density of states in the conduction band and the concentration of traps. The potential difference, ϕ, exists between the trap level and the lowest state in the conduction band. The contribution to the total concentration of carriers from traps of a single

level ϕ volts below the conduction band is n. The total concentration is

$$n_T = \int_{\phi_V}^{\phi_C} n_0(\phi)e^{-q\phi/kT} \, d\phi \qquad cm^{-3}, \qquad (30)$$

where $n_0(\phi)$ includes the density of traps at each level in the forbidden band.

$$\alpha = 2 \qquad (31)$$

if there are only donor traps and

$$\alpha = 1 \qquad (32)$$

if acceptor traps compensate the donor traps.

Figure 19 shows an insulator with an applied field across it. The solid lines represent the barrier that the electron sees with no applied field and the dashed lines the barrier in the presence of the field. The applied field lowers the potential required to excite thermally an electron into the conduction band by $\Delta\phi$. Frenkel[45] calculates the lowering as

$$\Delta\phi = (\frac{qE}{\pi\epsilon_0 \kappa})^{1/2} \quad volts \qquad (33)$$

where E is the applied field and κ is the dielectric constant. The proper dielectric constant is the electronic component only (square of the index of refraction) since the electron is immediately collected by the field and does not polarize the ions in the vicinity. Note that twice the amount of lowering, $\Delta\phi$, of Schottky emission occurs because the positive charge is rigid and does not move as in the case of the image potential (See figs. 21-24).
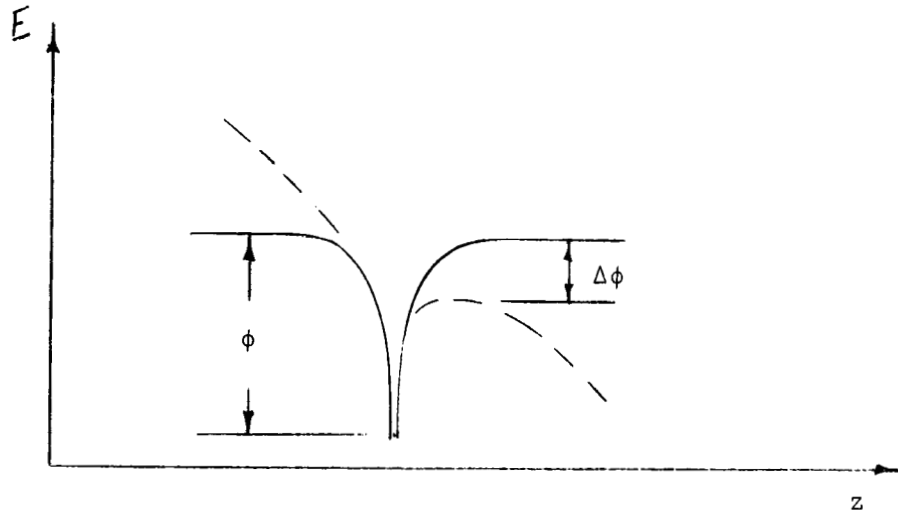
Fig. 19   Lowering of the potential barrier around a trap site in the
insulator by an applied field.

The concentration of carriers due to <u>thermal</u> excitation from
traps is now

$$n_T = \int_{\phi_v}^{\phi_c} n_o(\phi)e^{-q(\phi-\Delta\phi)/\alpha kT} \quad d\phi \quad cm^{-3} \quad (34)$$

$$= \int_{\phi_v}^{\phi_c} n_o(\phi)e^{-q\phi/\alpha kT} \quad e^{q\Delta\phi/\alpha kT} \quad d\phi \quad (35)$$

$$= \int_{\phi_v}^{\phi_c} n_o(\phi)e^{-q\phi/\alpha kT} d\phi \quad e^{\frac{q(qE/\pi\kappa\varepsilon_o)^{1/2}}{kT}}, \quad (36)$$

the conductivity is

$$\sigma = n\mu e \qquad (37)$$

$$\sigma = \sigma_o e^{(q/\alpha kT)[qE/\pi\kappa\epsilon_o]^{1/2}} \quad \text{ohm-cm}, \qquad (38)$$

where

$$q_o = e\mu \int_{\phi_v}^{\phi_c} n_o(\phi)e^{-q\phi/\alpha kT} \, d\phi, \qquad (39)$$

the current is

$$J = \sigma E \qquad (40)$$

$$= \sigma_o E e^{(q/\alpha kT)[qE/\pi\kappa\epsilon_o]^{1/2}} \quad \text{amps/cm}^2. \qquad (41)$$

Equation 38 is the Poole-Frenkel equation. It resembles the expression for Schottky emission from a metal surface. The Schottky equation expresses variation of current with field while the Poole-Frenkel expresses variation of conductivity with field; however, at the fields involved in experimental work, the variation of J is almost identical with the variation of σ.

4) Field Emission

Figure 20 shows the various types of tunneling possible in thin film MIM devices with traps. Although all mechanisms are possible, some are much more likely than others. For thicknesses over 100 Å,

direct tunneling between metals is very unlikely. This is also true
if the applied voltage is more than a few volts because the bottom of
the insulator conduction band is lower than the Fermi level in metal 1
and the shortest barrier thickness is from the metal to the conduction
band of the insulator. Tunneling depends exponentially on the thickness
of the barrier, i.e. the transmission coefficient drops off exponen-
ially as the barrier thickness increases; therefore, this type of tunneling
dominates at applied voltages of over a few volts. The voltage at which
the Fowler-Nordheim mechanism dominates is approximately 1/2 of the band-
gap ($\simeq$ 3-6 volts for the silicon nitride). Note that the dipole layer
at the interface of metal 1 and the insulator causes a larger barrier
thickness at the interface for tunneling from the Fermi level of the
insulator into the conduction band of the insulator. Fowler-Nordheim
emission considers electrons tunneling from the metal's Fermi level into
the insulator's conduction band. The image force increases the small
thickness difference further as the lowering of the barrier is twice
as much for field ionization as for the Fowler-Nordheim emission. The
factor of two arises because the image charge for field ionization re-
mains stationary while the image charge for Fowler-Nordheim moves away
from the electron. Figures 21 through 24 show this schematically.
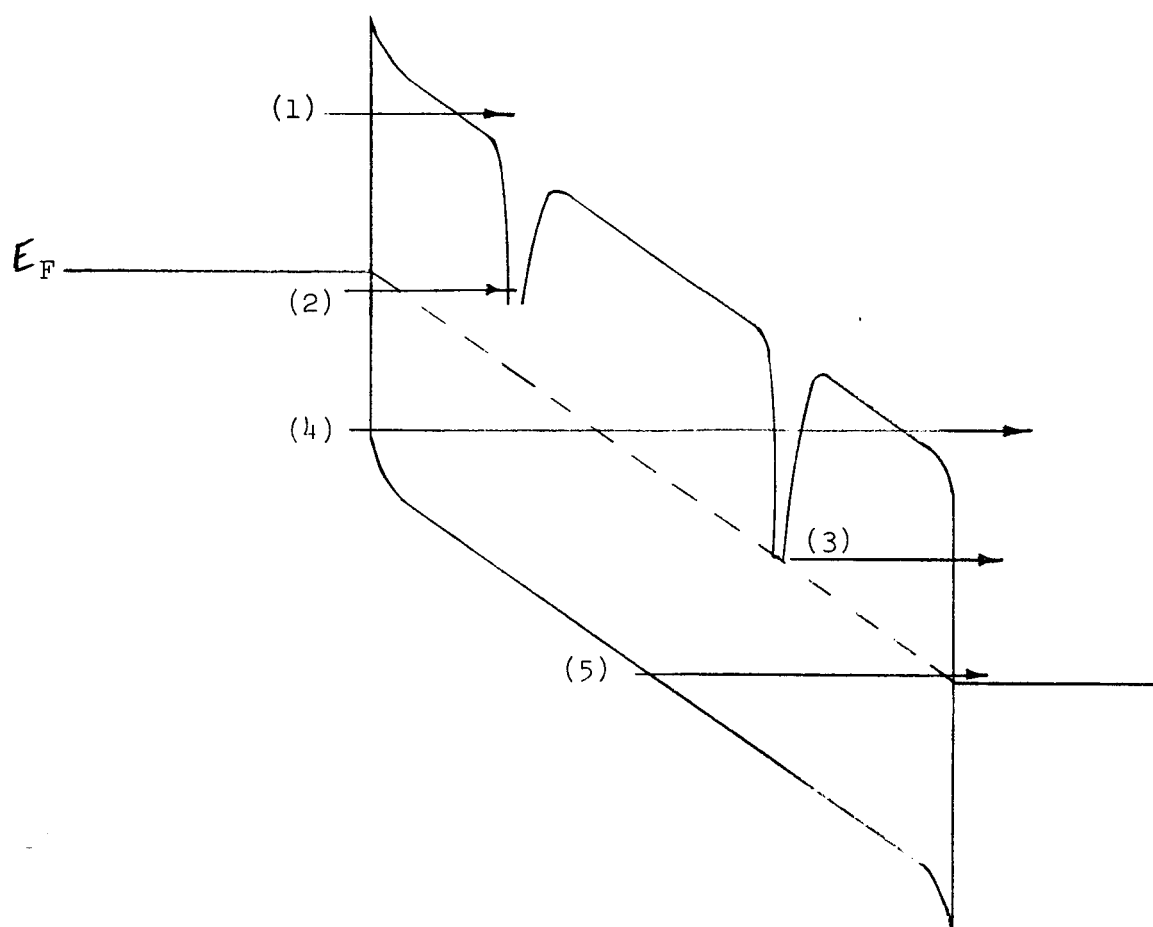
Fig. 20   Diagram illustrating the various tunneling mechanisms possible
in the MIM structure of fig. 3.

1.   Tunneling from the electrode into the conduction band of the insu-
lator (Fowler-Nordheim tunneling).
2.   Tunneling from the metal electrode into empty trap states followed
by thermal emission from the trap.
3.   Tunneling from filled traps at the Fermi level into either the
conduction band of the insulator or into the metal (field ioni-
zation).
4.   Tunneling from one metal directly into the conduction band of the
other metal.
5.   Tunneling from the valence band of the insulator into the metal.
(Fowler-Nordheim emission for holes) 2 and 3 have similar mecha-
nisms for holes.
6.   (not pictured) Tunneling from the valence band of the insulator
into the conduction band of the insulator (Zener Effect).

Actual Barrier

Normal Barrier

Barrier due to
Image Potential

A   B
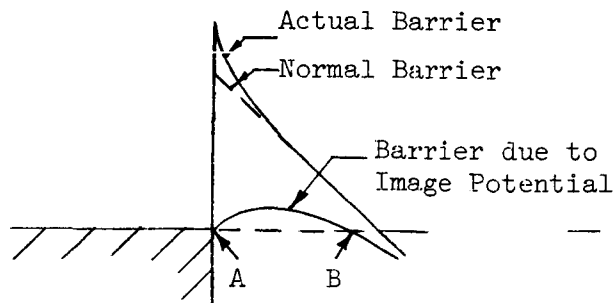
Fig. 21   Barrier for Fowler-Nordheim
Tunneling

Normal Barrier

Barrier due to
Coulomb Potential

A'   B'
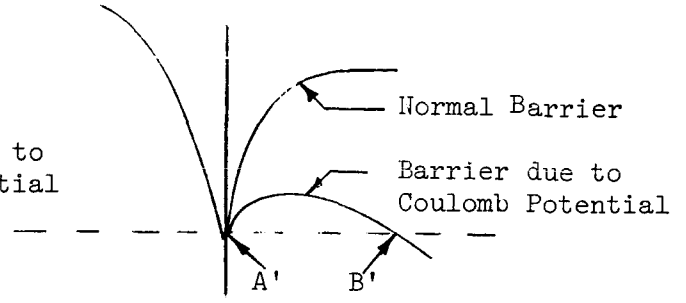
Fig. 22   Barrier for Field
Ionization
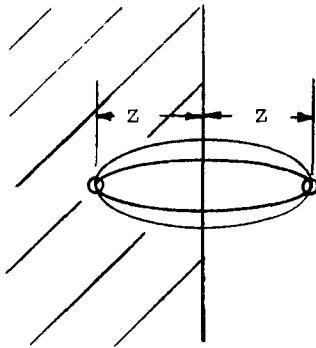
Fig. 23   Image Force on Electron
Leaving Metal Surface
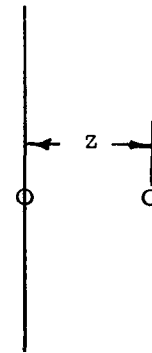
Fig. 24   Coulomb Force on
Electron Leaving
Field Trap

The force seen by the electron leaving the metal surface is

$$F = \frac{q^2}{4\pi\kappa\varepsilon_0(2z)^2}$$
(42)

while the force seen by the electron leaving the ionized trap is

$$F = \frac{q^2}{4\pi\kappa\varepsilon_0(z)^2}$$
(43)

The force seen by the electron leaving the ionized trap is 4 times as

large as the image force seen by the electron leaving the metal. Since

the amount of barrier lowering depends on the magnitude of the image

force, the barrier decreases more in the case of the ionized trap

and the tunneling distance A'B' is less than the distance AB for Fowler-Nordheim.

D) Summary:

The following conclusions result from the above discussion of the thin film current mechanisms involving the effects of contacts, traps, and surface states.

(1) The carrier injection may be from either the electrode or the bulk depending on whether the metal-insulator interface is "ohmic" or "rectifying". Emission tends to occur from the electrode for ohmic contacts since the barrier is lowered by the band bending while the bulk effects tend to dominate for rectifying contacts since the barrier is raised by band bending.

(2) The relative values of the material work functions and the location and type of surface states determine whether the contacts are ohmic or rectifying. With no surface states the contact appears ohmic if the work function of the metal is less than the work function of the insulator. A rectifying contact results if the work function of the metal is greater than that of the insulator. Surface states bend the bands of the insulator up or down depending on whether they are acceptor or donor states. The density of the surface states and their location in the forbidden band control the actual barrier of the metal-insulator interface. The barrier may bear little relation to the difference in work function of the metal and the electron affinity of the insulator for large surface state densities.

(3) Thermal emission and tunneling both occur. The dominant mechanism depends on the trap densities and applied field. The contact again determines whether the mechanism is bulk or electrode controlled.

If the conditions are for bulk emission, both thermal emission and tunneling occur from the bulk. The conditions never favor bulk emission for one mechanism and electrode emission for the other.

(4) Before any conclusions, the mechanisms must be identified as (a) bulk or electrode controlled, and (b) thermal emission or tunneling. The following discussion summarizes the method used to distinguish them.

1) Thermal Emission or Tunneling:

A large dependence of current on temperature is the major identifying characteristic of thermal emission. Temperature influences field emission relatively little because the tunneling current depends mainly on the barrier thickness as opposed to a dependence in barrier height for thermal emission. Figures 25 - 27 show this schematically.
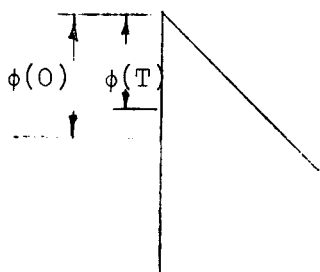
Fig. 25 Variation of Barrier Height With Temperature
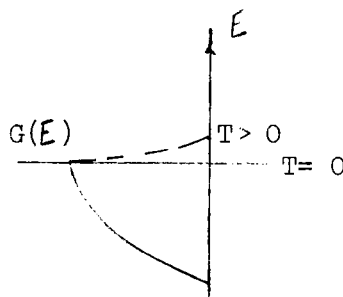
Fig. 26 Variation of State Occupacity with Temperature
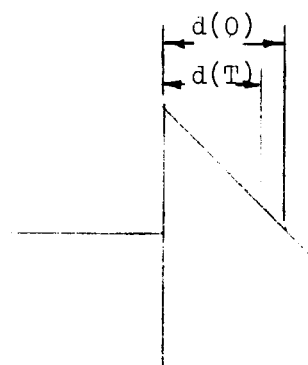
Fig. 27 Variation of Tunneling Distance with Temperature

Simmon's[71] and Stratton's[76] equations predict a T^2 variation of tunneling current with temperature. Hartman and Chivian[48] confirm this and report that the tunneling current drops 30 to 50 percent of its room temperature value at liquid nitrogen temperatures. The characteristic equation for thermal emission shows that the thermal components of current are exponentially dependent on temperature.

$$I \propto \exp (B/T) \qquad\qquad (44)$$

Observing the current variation with temperature then determines whether the injection is thermal or field. Figures 28 and 29 show the expected variation of current with temperature.
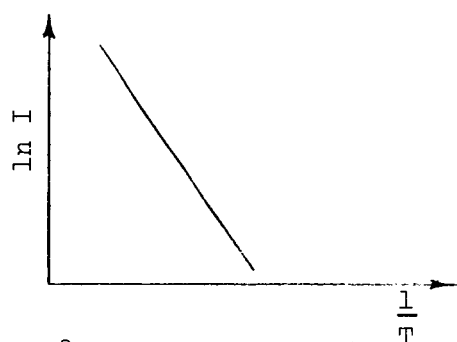
Fig. 28 Expected Current
Variation with Temperature
for Thermal Emission
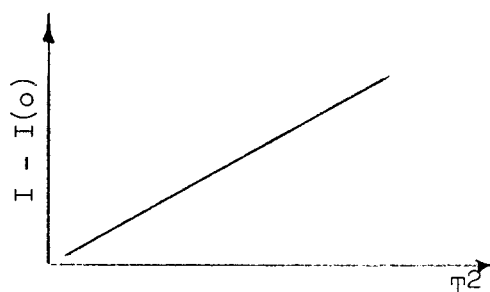
Fig. 29 Expected Current
Variation with Temperature
for Tunneling

The slope of the lnI vs 1/T curve is the activation energy and is proportional to the barrier height. At high fields, both thermal and tunneling components may be present in the observed current. In this situation the current is first strongly temperature dependent and then becomes essentially temperature independent as the thermal component decays as shown in fig. 30.
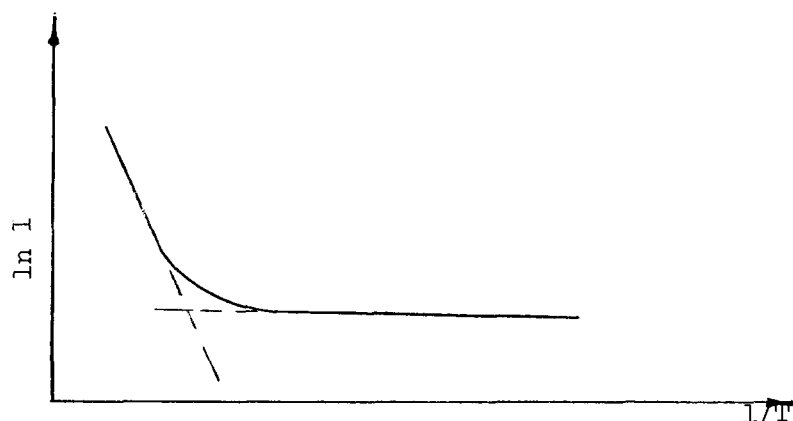
Fig. 30   Current Variation with Temperature with Both Tunneling and
           Thermal Emission Present

2) Bulk or Electrode Controlled:

The magnitude of the current, whether thermal emission or

tunneling, depends on the barrier height. If the current is bulk con-

trolled, the barrier is the same regardless of the polarity of the ap-

plied potential. The current characteristics are then expected to be

the same for the same fields and independent of polarity.

However, the barriers at the two interfaces differ consider-

ably due to differences in the metal work functions and in the surface

states, and when the current is electrode controlled, the current char-

acteristics are very sensitive to polarity. The expected variations

for thermal and tunneling mechanism are shown below. Note that both
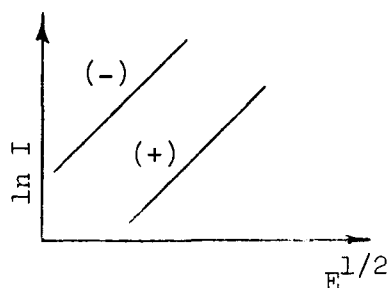
Fig. 31   Polarity dependence for
          electrode controlled
          thermal emission
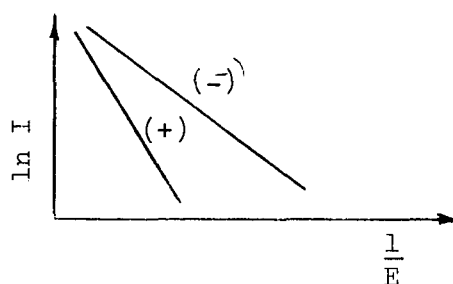
Fig. 32   Polarity dependence for
          electrode controlled
          tunneling

the slope and magnitude vary for tunnel emission while only the magnitude varies with thermal emission. Thermal emission depends sensitively on barrier variations, however. A difference of 0.06 eV in barrier height results in a decade difference in current at the same field at room temperatures.

If Schottky emission (electrode controlled thermal emission) dominates, the following experimental facts appear. First, the current varies exponentially with (1/T). Second, a large difference in current magnitude at equal but opposite fields results when metals with different work functions form the electrodes. Third, the slope of the Schottky plots (ln I vs $E^{1/2}$) agrees with the theoretical value $(q(q/4\pi\kappa\varepsilon_o)^{1/2}/kT)$ and finally the same value of barrier height (ϕ) results whether determined by the zero intercept of the Schottky plot or by the slope of the ln I vs. 1/T curve. Recall that for Schottky emission:

$$J = AT^2 e^{-q\phi/kT} \exp[-q(qE/4\pi\kappa\varepsilon_o)^{1/2}/kT] \qquad (45)$$

Since A and T are known, ϕ can be determined by the ln I vs. $E^{1/2}$ intercept. Variations in A are common, but a factor of 10 variation in A results in only 0.06 eV error in ϕ. The second method of determining ϕ is to bias the MIM device so that a suitable current flows and then observe the change of current with temperature. The slope of ln I vs. 1/T is proportional to the effective barrier height. By subtracting the barrier lowering due to the image force $[q(qE/4\pi\kappa\varepsilon_o)^{1/2}/kT]$ one obtains the true barrier. The barrier heights obtained by these two methods should agree if Schottky emission predominates.

If Poole-Frenkel emission dominates, the current characteristics are insensitive to changes in polarity and the type of metal used

as electrodes. The intercept $(V = 0)$ on the ln I vs $V^{1/2}$ curve is a measure of σ_0 which is a function of the trap density. The barrier height of the traps results from the ln I vs. $1/T$ variation. These quantities determine the principal electrical characteristics in such a case.

If tunneling predominates, the current variation with voltage and temperature yields information about the effective mass of the electron in the insulator conduction band as well as barrier heights. The slope of the ln I vs $1/E$ plots for forward and reverse bias gives the barrier at each interface.

CHAPTER III

Conduction Properties of Silicon Nitride

The following experiments established the current mechanisms
present in silicon nitride and to some extent the range of variation
of the I-V characteristics.

A) Current-Voltage Characteristics:

Figure 33 shows the typical behavior of the current with bias.
The data follow a straight line for several decades of ln I plotted
against $V^{1/2}$, the so-called Schottky plot. From eq. 8, the straight
line behavior is characteristic of Schottky emission; however, at the
fields present a straight line also results for a plot of the logarithim
of conductivity against $V^{1/2}$ because the exponent dominates the expres-
sion in the equations for Schottky and Poole-Frenkel emission.

$$J = J_o \exp[b_1 V^{1/2}] \qquad\qquad (45)$$

$$J = AV \exp[b_2 V^{1/2}] \qquad\qquad (46)$$

Using different metals as the electrodes in MIM devices sep-
arates Schottky emission from Poole-Frenkel emission. If Schottky emis-
sion dominates, a difference of only 0.06 eV in the barrier heights at
the two metal-insulator interfaces results in a decade of current dif-
ference at equal and opposite fields. Figures 35 and 36 show the results
for Al-N-Mo and InGa-N-Mo devices. Devices with gold and silicon elec-
trodes yield similar results. The following table gives the work functions
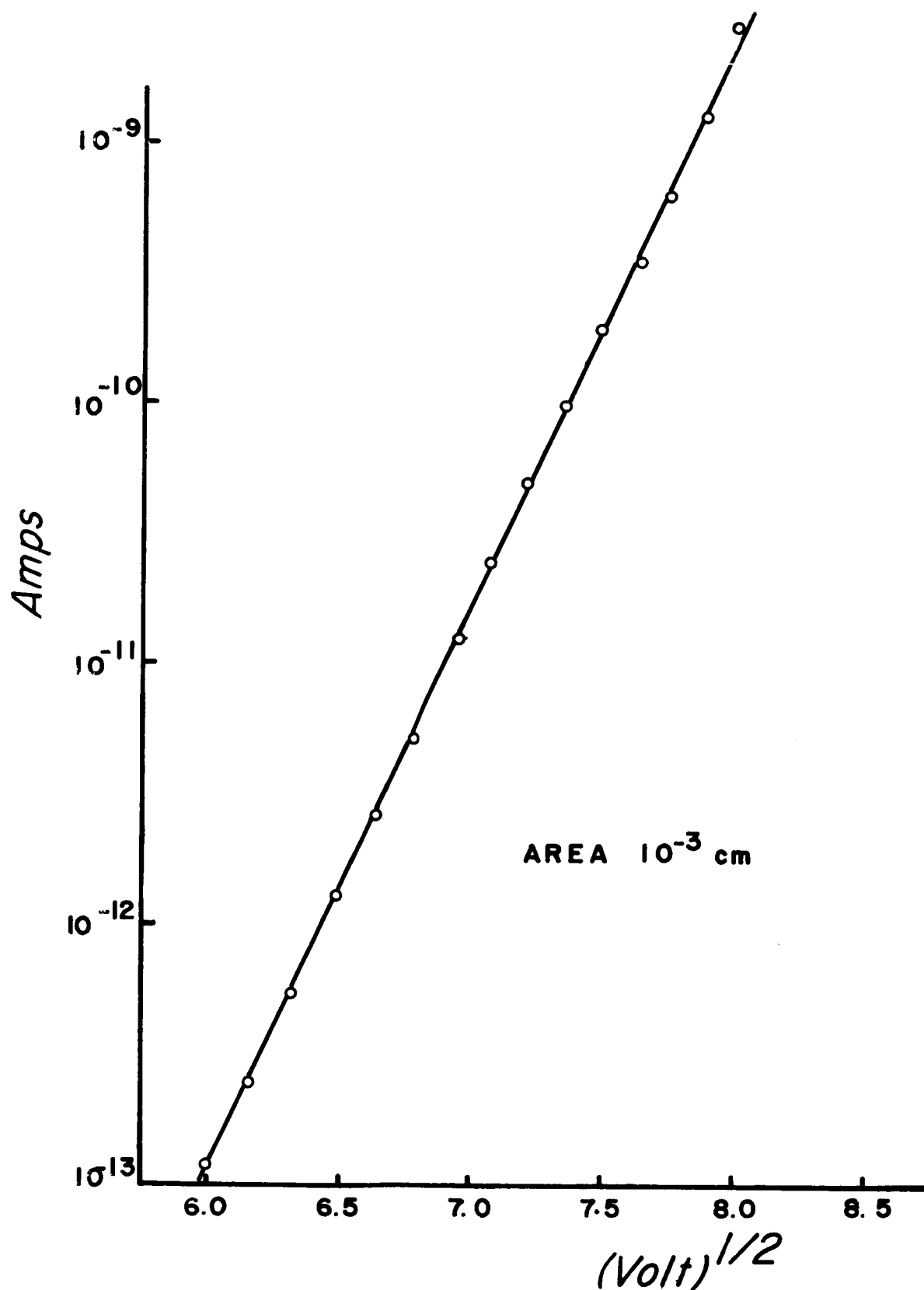
Fig. 33 Ln I vs. $V^{1/2}$ for Metal-Silicon Nitride-Metal Device
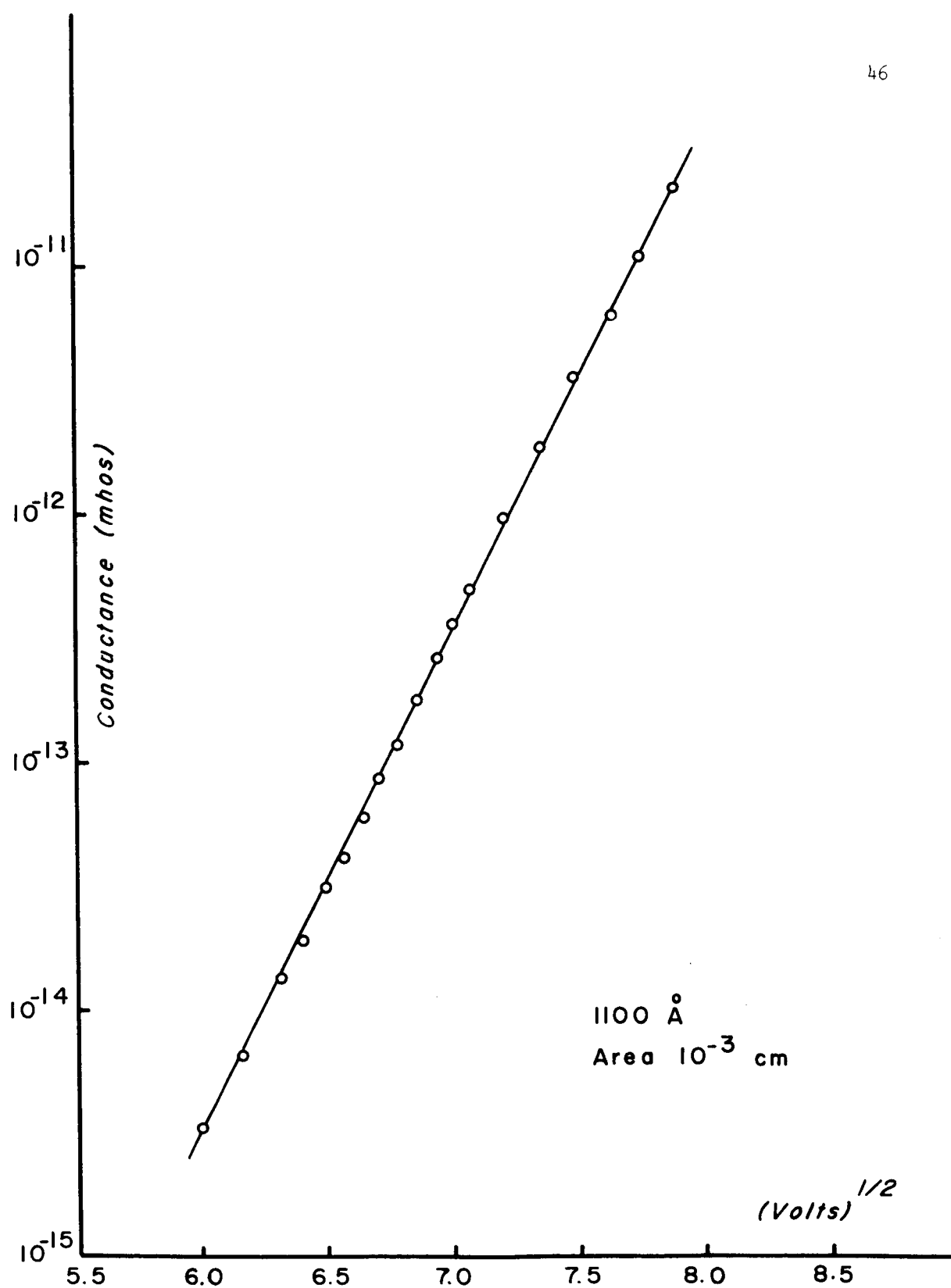
Fig. 34   Conductivity vs. $V^{1/2}$ for the Metal-Silicon Nitride-Metal Device of fig. 33
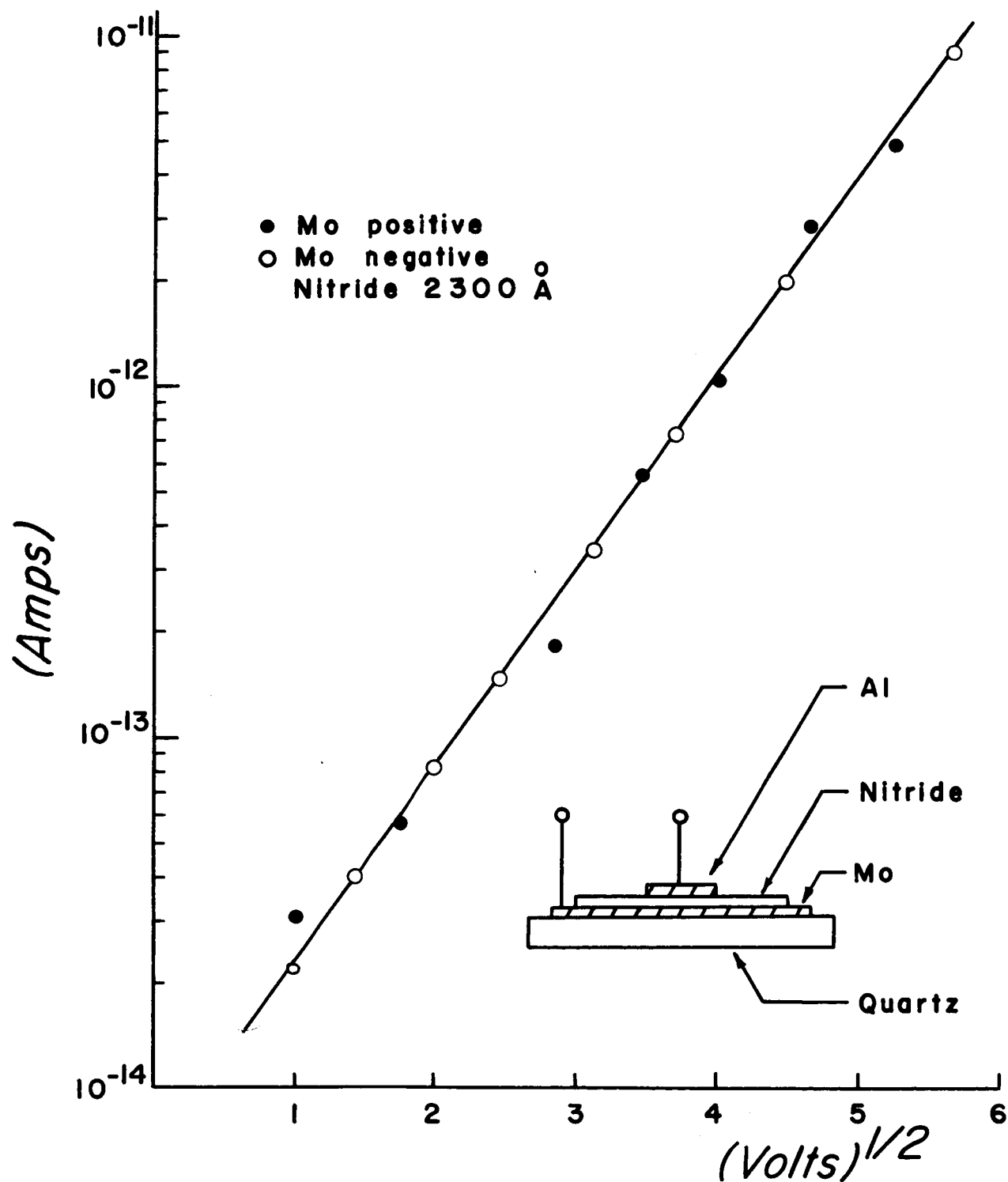
Fig. 35   Current Characteristics of Al-Nitride-Mo Device
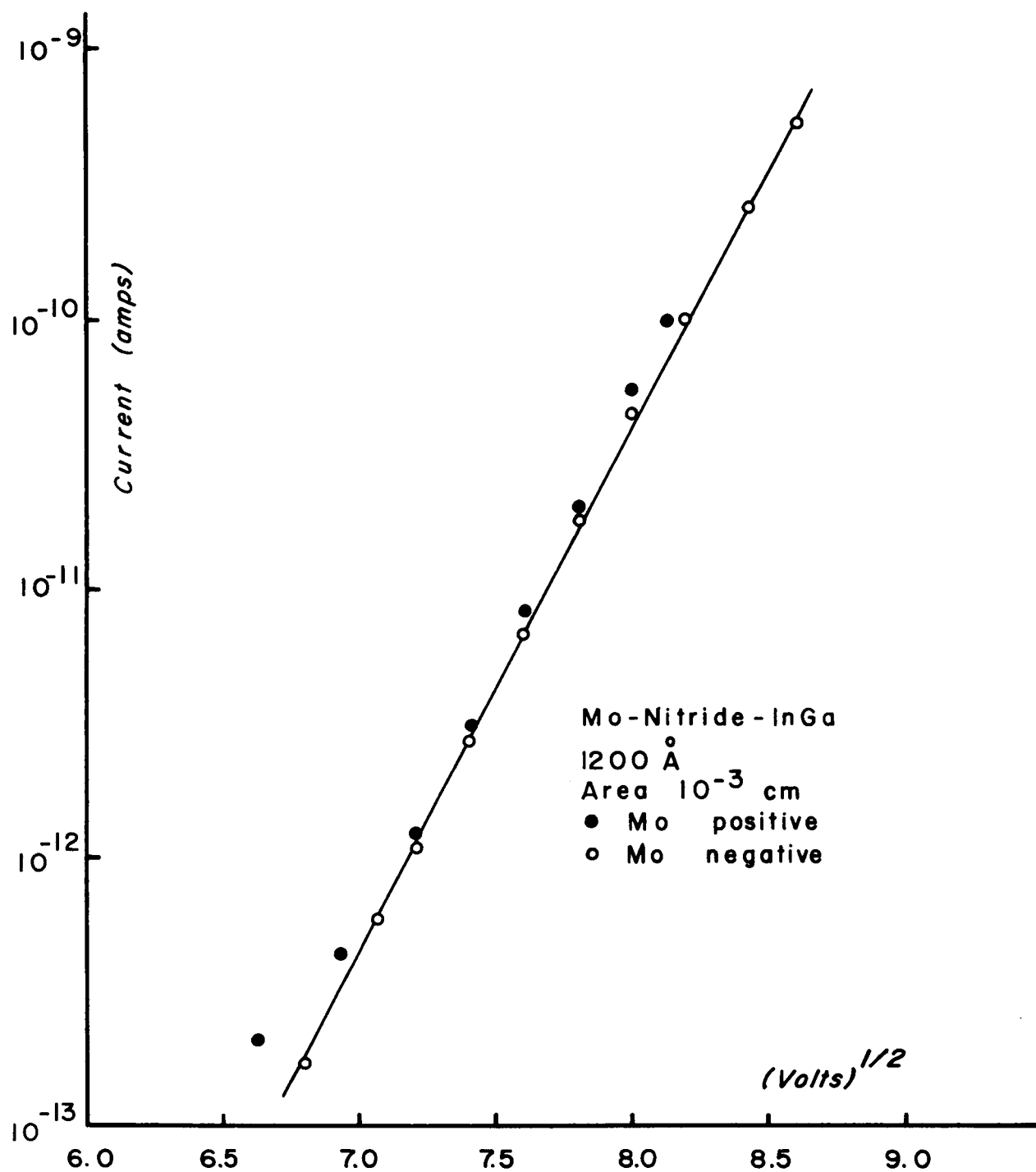
Fig. 36 Current Characteristics of Mo-Nitride-InGa Device

for the metals used.

TABLE I

Work Functions of Metal Contacts

	thermionic work function	photoelectric work function
Mo	4.20 eV	4.34 eV
Al	-------	4.08 eV
In	-------	6.8 (amorphous)
Ga	4.12 eV	-------
Au	4.25 eV	4.82 eV

The fact that the conductivity varies as $\exp(bV^{1/2})$ and that the electrodes have no effect on the current is good evidence that the dominant mechanism is bulk controlled thermal emission.

B) Current Variation With Temperature:

The fact that the current varies as $\exp(bV^{1/2})$ is, however, not conclusive evidence that thermal emission is the mechanism present. O'Dwyer[64] finds that, due to a large space-charge effect, the current varies as $\exp(\text{constant } V^{1/2})$ quite accurately over several decades of current when the mechanism is Fowler-Nordheim tunneling from the metal electrode. Geppart[46] also finds that the presence of space charge affects the I-V characteristics considerably. Hartman[49] et.al. believe that the model of O'Dwyer applies to conduction through SiO. Identification of the current as thermal emission, therefore requires both bias and temperature behavior. Thermal emission models predict an exponential dependence on temperature while Stratton's model predicts a T^2 dependence for tunneling as in eq. 47.

$$J_{(T)} = J(o) + AT^2 \qquad (47)$$

Field   8.7 X 10^{-5} V/cm
2300 Å
Activation Energy   0.67 eV
Barrier 1.0 eV
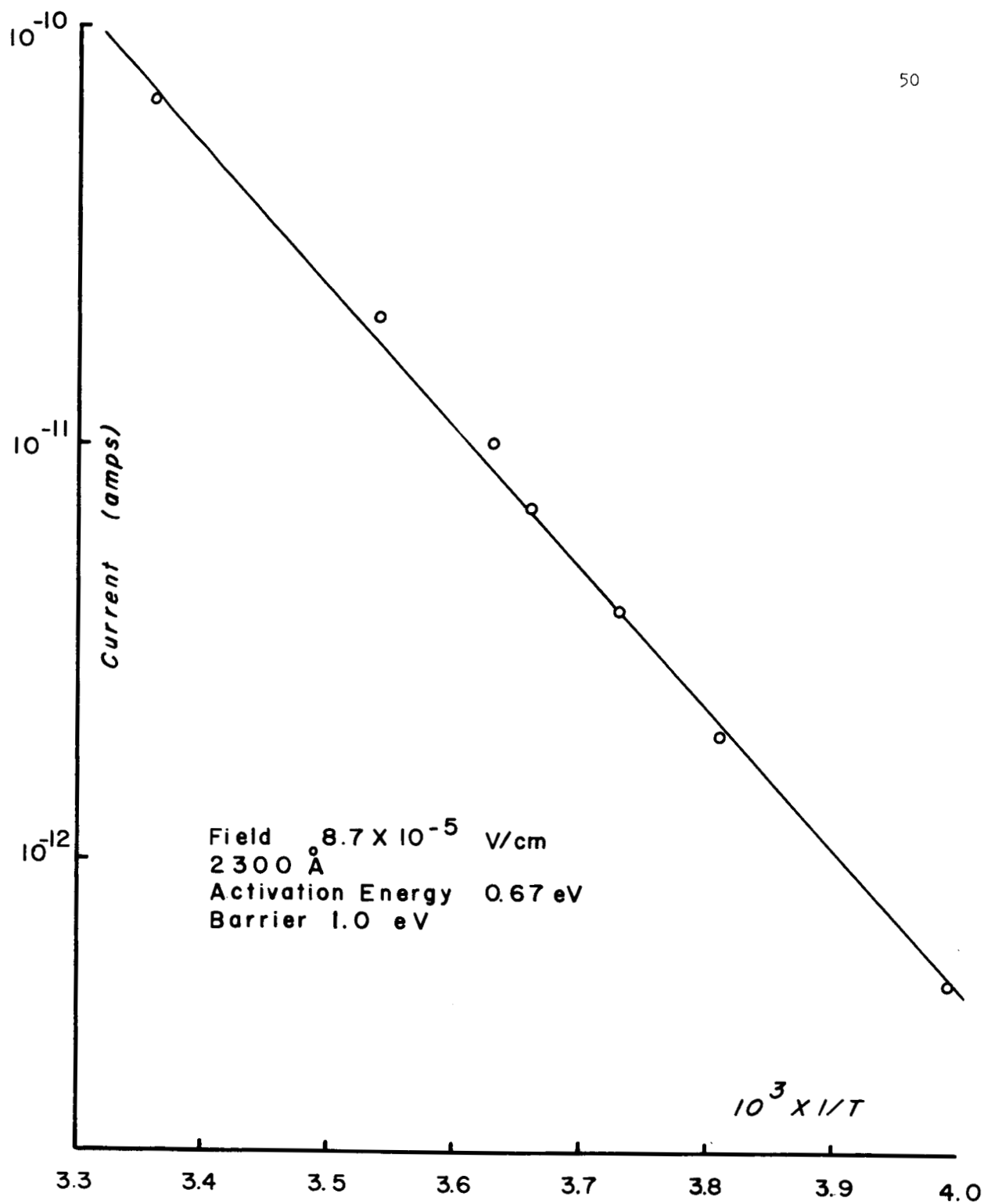
Fig. 37 Current Variation with Temperature for Device of fig. 35
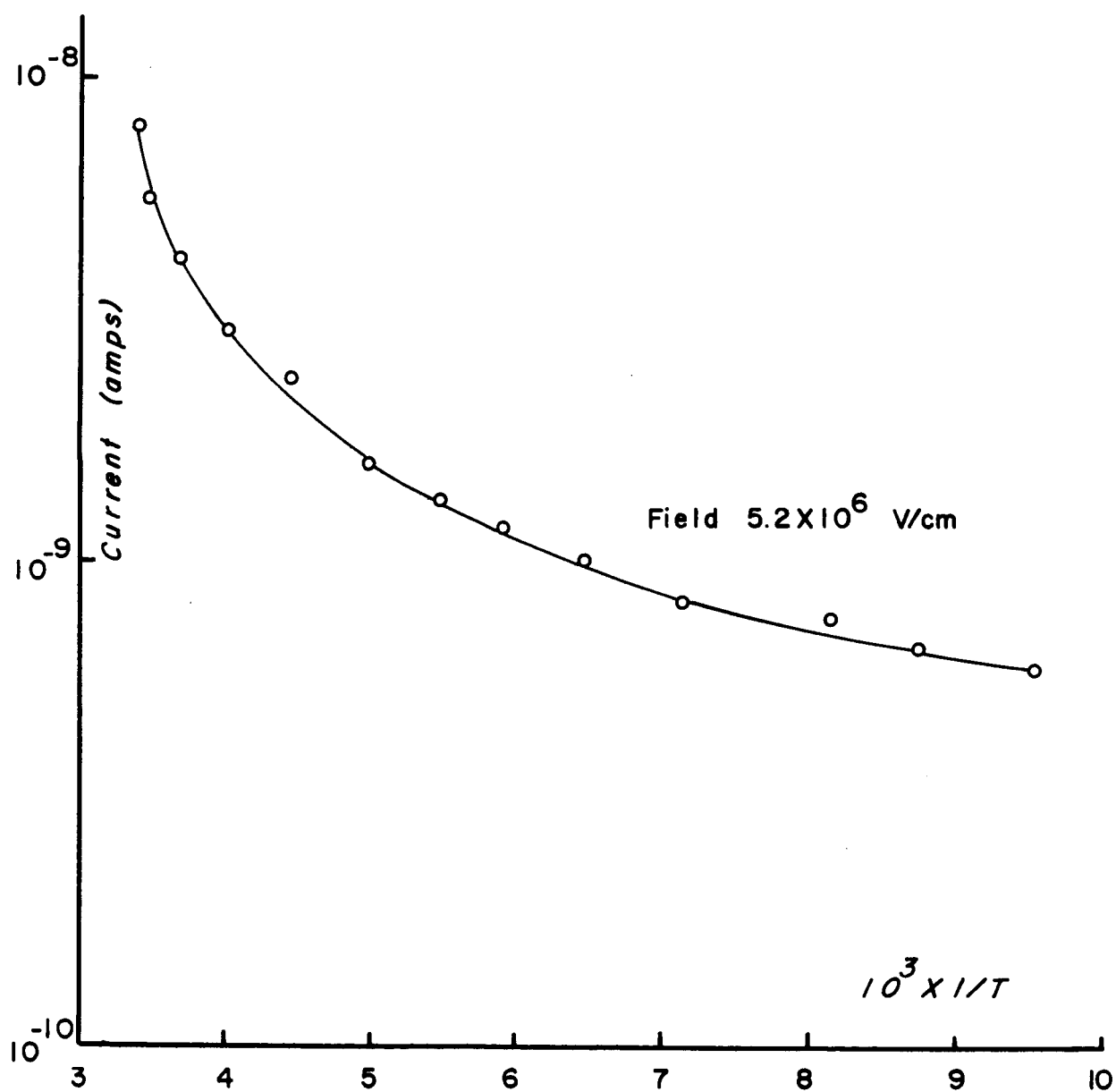
Fig. 38   Current Variation with Temperature for High Resistivity
          Device
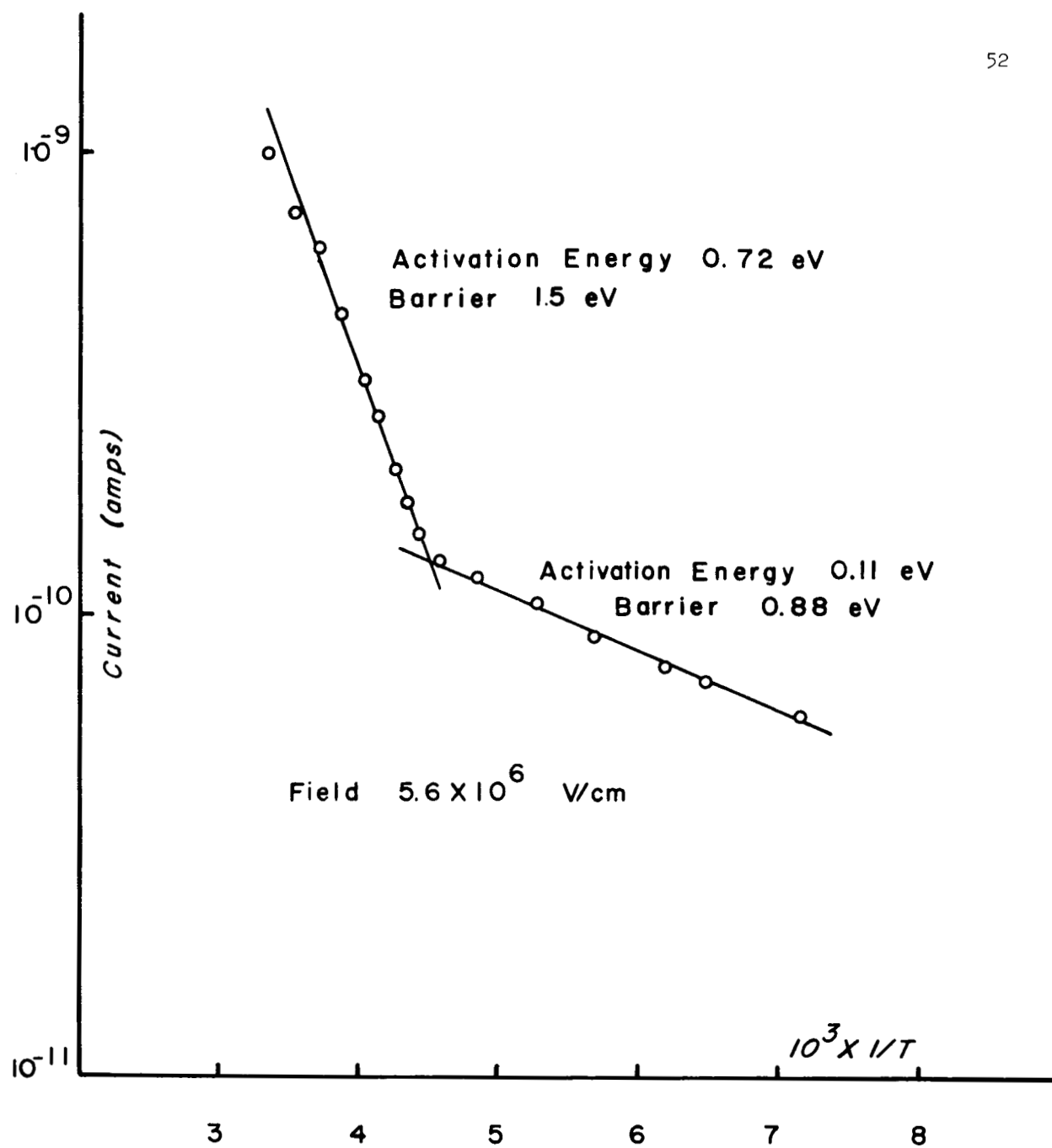
Fig. 39 Current Variation with Temperature for High Resistivity
Device Showing Two Activation Energies

The T^2 dependence of tunneling has been verified by Hartman and Chivian[48],

Wilmsen[79], Fitzgibbons[42] and Meyerhofer and Ochs[63].

Figure 37 shows the current variation with temperature for

the sample of fig. 35. For this sample the current varies as exp (constant/T)

as expected for thermal emission. This device exhibited relatively low

resistivity which is an indication of a low barrier height. The field

in the insulator was 0.87×10^6 V/cm during the temperature test. Other

devices require fields as high as $2 - 6 \times 10^6$ V/cm for currents of similar

magnitude. Figure 38 gives typical temperature characteristics for these

high resistivity devices. While the current deviates from a straight

line, it still depends strongly on temperature. The curve of fig. 38

separates into parts, as in fig. 40,
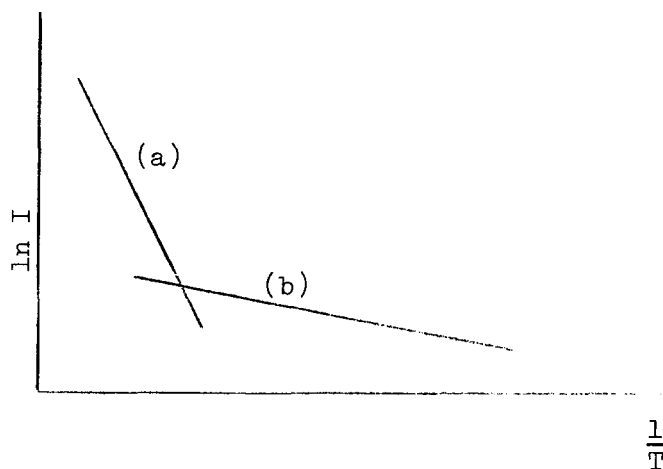
Fig. 40 Separation of current vs. 1/T curve into two parts.

which indicates two different barriers present in the nitride film.

At high temperatures the injection is from the barrier corresponding to

(a) and at low temperatures the injection is over the barrier correspon-

ding to part (b) of the curve. Figure 39 shows the current vs 1/T vari-

ation for a device in which the break is very sharp. With this curve

it is possible to obtain accurate activation energies due to the well

defined break. The slope of the steep portion of the curve of fig. 38

asymptotically approach the slopes of this figure.

From fig. 39, the total current consists of

$$J_T = J_1 + J_2 \tag{48}$$

where

$$J_1 = A_1 e^{-\varepsilon_1/kT} \tag{49}$$

$$J_2 = A_2 e^{-\varepsilon_2/kT} \tag{50}$$

and ε_1 and ε_2 are the activation energies of the two slopes. At
$10^3/T \simeq 4.52$ ($T \simeq 222^\circ$K) J_1 is equal to J_2.

$$J_1 = J_2 \tag{51}$$

$$A_1 e^{-\varepsilon_1/kT} = A_2 e^{-\varepsilon_2/kT}. \tag{52}$$

The constants A_1 and A_2 are functions of the trap densities and the ratio
A_1/A_2 gives an indication of the relative densities of the trap sites.

$$\frac{A_1}{A_2} = \frac{e^{-\varepsilon_2/kT}}{e^{-\varepsilon_2/kT}} \tag{53}$$

Substituting in $\varepsilon_1 = 0.72$ and $\varepsilon_2 = 0.11$ as determined from
the slopes of fig. 39 and T = 222°K results in a ratio

$$\frac{A_1}{A_2} \simeq 5 \times 10^{13} \tag{54}$$

Assuming that J_1 is Poole-Frenkel emission the following
expression holds

$$J = \sigma_0 E \exp[-q\phi/\alpha kT] \exp[(q/kT)(qE/\alpha\pi\kappa\varepsilon_0)^{1/2}] \tag{55}$$

where $\alpha = 1$ as determined by the slope of the Schottky plot.
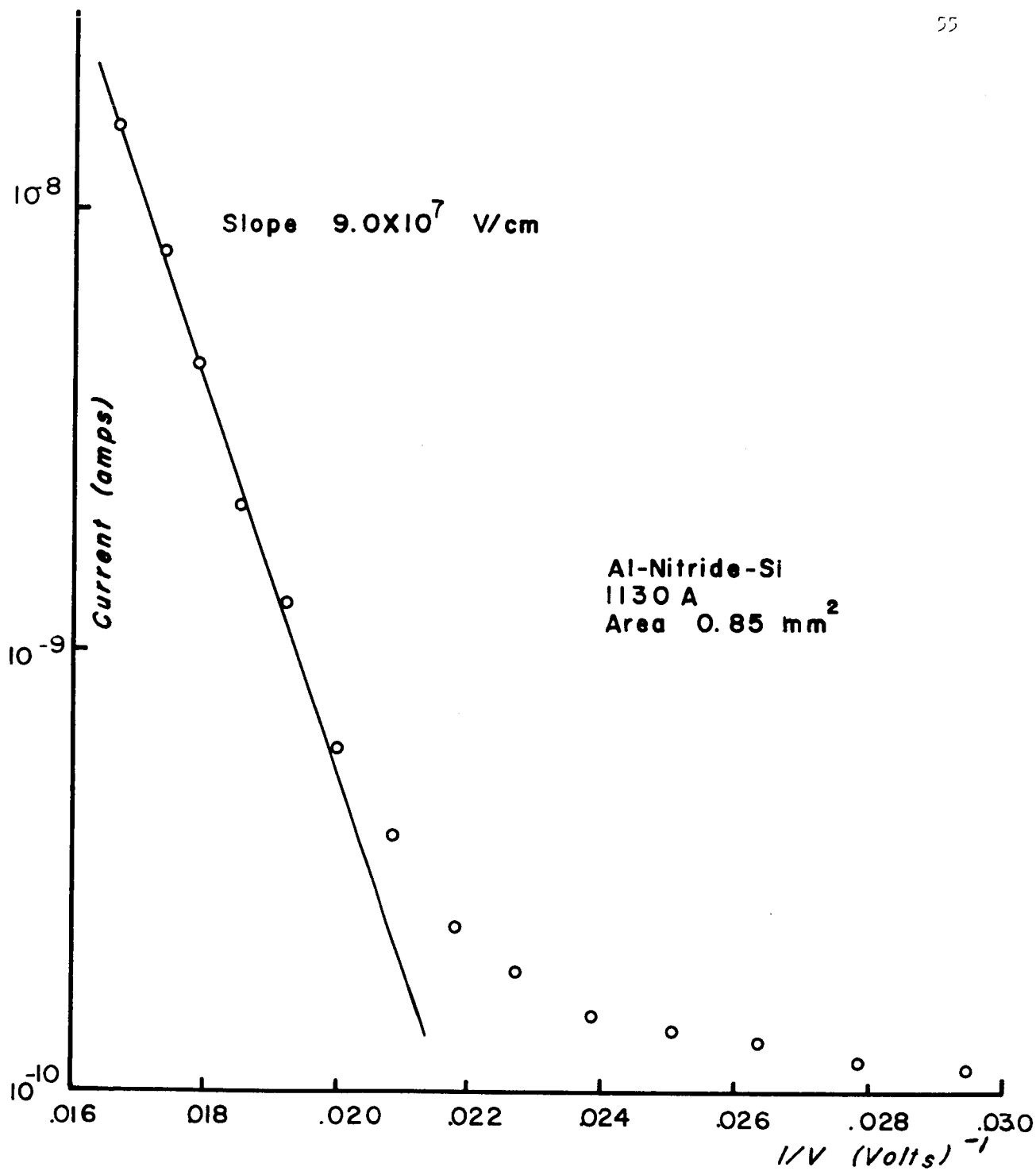
Fig. 41   Fowler-Nordheim Plot of High Resistivity Device Showing
Tunneling at High Fields

Equating eq. 49 and 55 gives

$$\sigma_O \exp[-q\phi/kT]\exp[(q/kT)(qE/\pi\kappa\varepsilon_O)^{1/2}] = A_1 e^{-\varepsilon_1/kT} \qquad (56)$$

or

$$\sigma_O = A_1 = ne\mu , \qquad (57)$$

when μ is mobility,

    n the carrier concentration in the conduction band.

For the case of $\alpha = 1$ and only one donor trap level and one acceptor trap[31] level

$$n = \frac{N_c(N_D - N_A)}{2N_A} \exp [-\varepsilon_1/kT] , \qquad (58)$$

where N_D is the concentration of donor traps

    N_A is the concentration of acceptor traps

    N_c is the effective density of states in the conduction band

$$= (\frac{2\pi mkT}{h^2})^{3/2} .$$

At $T = 222^\circ K$, $J_1 = 0.65 \times 10^{-8}$ amps/cm^2 at a field of 5.6×10^6 v/cm.

$$\sigma = \frac{J_1}{E} = A_1 e^{-\varepsilon_1/kT} = ne\mu e^{-\varepsilon_1/kT} . \qquad (59)$$

Substituting in these values gives

$$ne\mu = 23.2 \ (\Omega - cm)^{-1}. \qquad (60)$$

At $T = 222^\circ K$ and assuming m is the rest mass of an electron

$$N_c \simeq 8.3 \times 10^{18} \ cm^{-3} , \qquad (61)$$

which gives the product

$$(\frac{N_D - N_A}{N_A})\mu = 70 . \qquad (62)$$

For the eq.58 to apply

$$0 < \frac{N_D - N_A}{N_A} > 2 \tag{63}$$

which implies

$$\mu \geq 35 \text{ cm/sec/volt/cm.} \tag{64}$$

Sze[77] observes similar behavior in films of silicon nitride deposited from the $SiCl_4$-NH_3 reaction. He proposes that the current consists of 3 components.

$$J_1 + J_2 + J_3 \tag{65}$$

where $J_1 \propto E \exp[-q(\phi_1-(qE/\pi\kappa\epsilon_o)^{1/2})/kT]$ (66)

$$J_2 \propto E^2 \exp(-E_2/E) \tag{67}$$

$$J_3 \propto E \exp(-q\phi_3/kT) \tag{68}$$

J_1 is the component from Poole-Frenkel emission, J_2 is the component due to field emission from traps and J_3 is a component which results from carriers thermally hopping from one localized site to another.

Sze's current vs. 1/T curves show three parts as shown below.
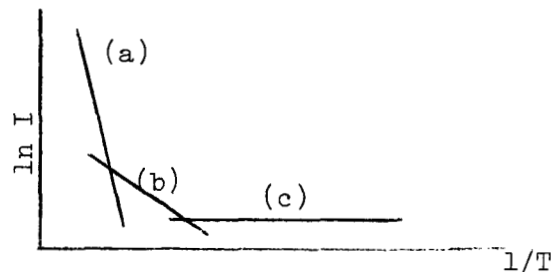
Fig. 42 Current vs. 1/T variation for silicon nitride deposited from the $SiCl_4$-NH_3 reaction (from Sze).

He concludes that part (c) arises from the field ionization of the traps. These specimens show no flat portion corresponding to (c); however, the magnitude of this portion depends strongly on the field at which the temperature data is taken. Perhaps a low bias field precluded observing the tunneling component. Figure 41 indicates tunneling in the films, however. At very high fields ($> 8 \times 10^6$ V/cm) the current follows the characteristic equation for field ionization.

Sze finds that the barrier height from part (a) is 1.3 ± 0.2 eV and that the activation energy from part (b) is typically 0.10 eV. The values from fig. 39 are 1.5 eV and 0.11 eV. These results show good correlation between the films deposited from $SiCl_4$ and those deposited from SiH_4.

C) Current Variation with Thickness

Figure 46 and 47 give the I-V characteristics for a series of devices ranging from less than 80 Å to 1600 Å. The curve for the 1100 Å film marked A is from a device with a quartz substrate. All other curves are from films on silicon substrates. This illustrates the reproducibility of the current characteristics from device to device and the fact that the electrodes and substrates have little effect on the current. Electrode materials for this family of curves include Al, Au, Si, InGa, and Mo.

For the very thin films, the substrate evidently affects the current characteristics. Several attempts to produce metal-nitride-metal device with a thickness less than 100 Å using nickel strips as the base electrode resulted in devices with essentially ohmic current characteristics. The resistivity of the devices ranged from $10^8 - 10^{10}$ ohm-cm with steady and definite capacitance readings corresponding to
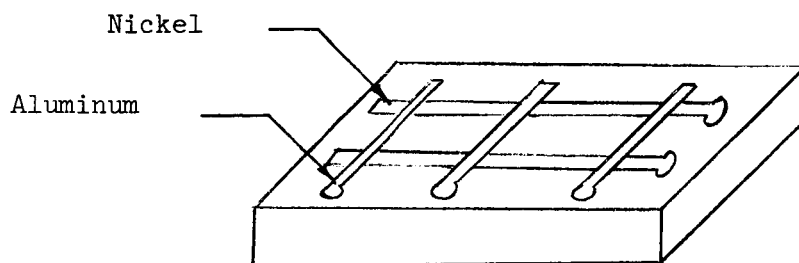
Fig. 43 Configuration used to study films < 150 $\overset{o}{A}$

thicknesses from 49 $\overset{o}{A}$ to 115 $\overset{o}{A}$. Figure 48 gives the I-V characteristic

of one of the Ni-nitride-Al devices. Note that at the high bias, just

before breakdown the current becomes non-ohmic. With silicon substrates

the devices exhibited similar characteristics as with thicker films as

shown in fig. 46. The temperature variation for device (b) is very sim-

ilar to the device of fig. 38. The difference thickness makes in cur-

rent characteristics arises either   from the substrate or from the nickel

electrode. Figure 44 shows a microphotograph of one of the Ni-nitride-

Al devices. Note that near the edge of the metal strip the film is cracked,

due to the mismatch in thermal coefficient of expansion. Such cracks

do not appear for thicker films on molybdenum as shown by fig. 46.

The ohmic characteristics probably arise from the cracking. The crack-

ing indicates that the films differ from those on silicon substrates

and prevents direct comparison.

These experiments indicate that the nitride forms uniform,

pinhole free films less than 100 $\overset{o}{A}$ thick. The consecutive construction

of these devices with no failures indicates the uniformity of the films

at these thicknesses. The area of the top electrode was about 2.0 mm^2.

Base Electrode (Ni)

Top
Electrode
(Al)
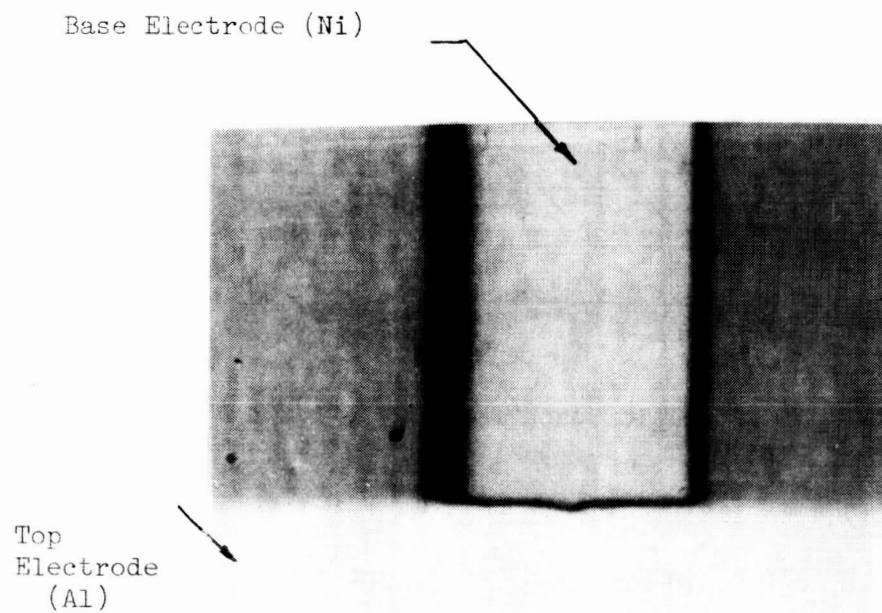
Fig. 44   Al-Nitride-Ni Device showing Cracking at Edges of
Nickel (x50 magnification)

Cracking
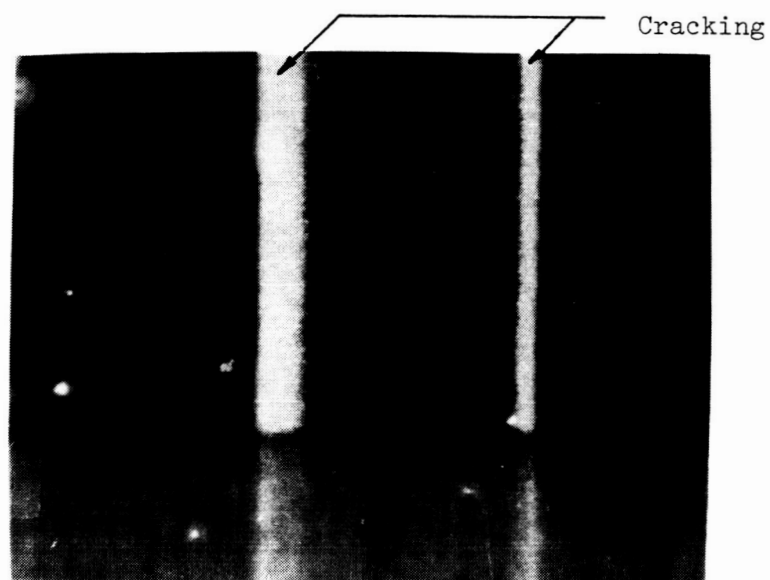
Fig. 45   Al-Nitride-Ni Device with Oblique Lighting
(same device as fig. 44)

At these thicknesses, the surface condition of the substrate is of ex-
treme importance. We find that if no surface irregularities appear
under a x15 microscope, the devices exhibit "good" electrical properties.
To our knowledge, this is the first successful attempt to grow silicon
nitride films less than 100 $\overset{o}{A}$ thick. The results have significance in
immediate device applications.

Figure 50 presents the voltage required to produce 10^{-9} amperes
through the films of fig. 46 and other devices. According to Mead[62]
the linearity of such a plot indicates that the observed currents are
not space-charge-limited due to traps[27]. The space-charge limited cur-
rent for a quasi-continuum of trapping states between the Fermi level
and the conduction band follows the equation

$$I = N_c e\mu(\frac{K\ 10^{-12}}{4\pi e\kappa T_c A})^{T_c/T} L^{-(2T_c/T+1)} V^{(T_c/T+1)} \tag{69}$$

where L is the film thickness

V is the applied voltage

which is non-linear in terms of the film thickness. Lanyon[56] observes
this electrode behavior in vitreous selenuim. Further, any model in
which the electrodes cause the rate limiting elements in the transport
process predicts a deviation from linearity due to low mobility. Mead
concludes that the linearity of such a plot implies that the bulk of
the material limits the current and not the potential barriers at the
electrodes. This interpretation agrees with the model of chapter 2
for the case of the rectifying contact. Figure 50 shows considerable
scatter in the data but none which relates to the metal or the substrate.
No deviation from linearity appears. The scatter rather indicates the
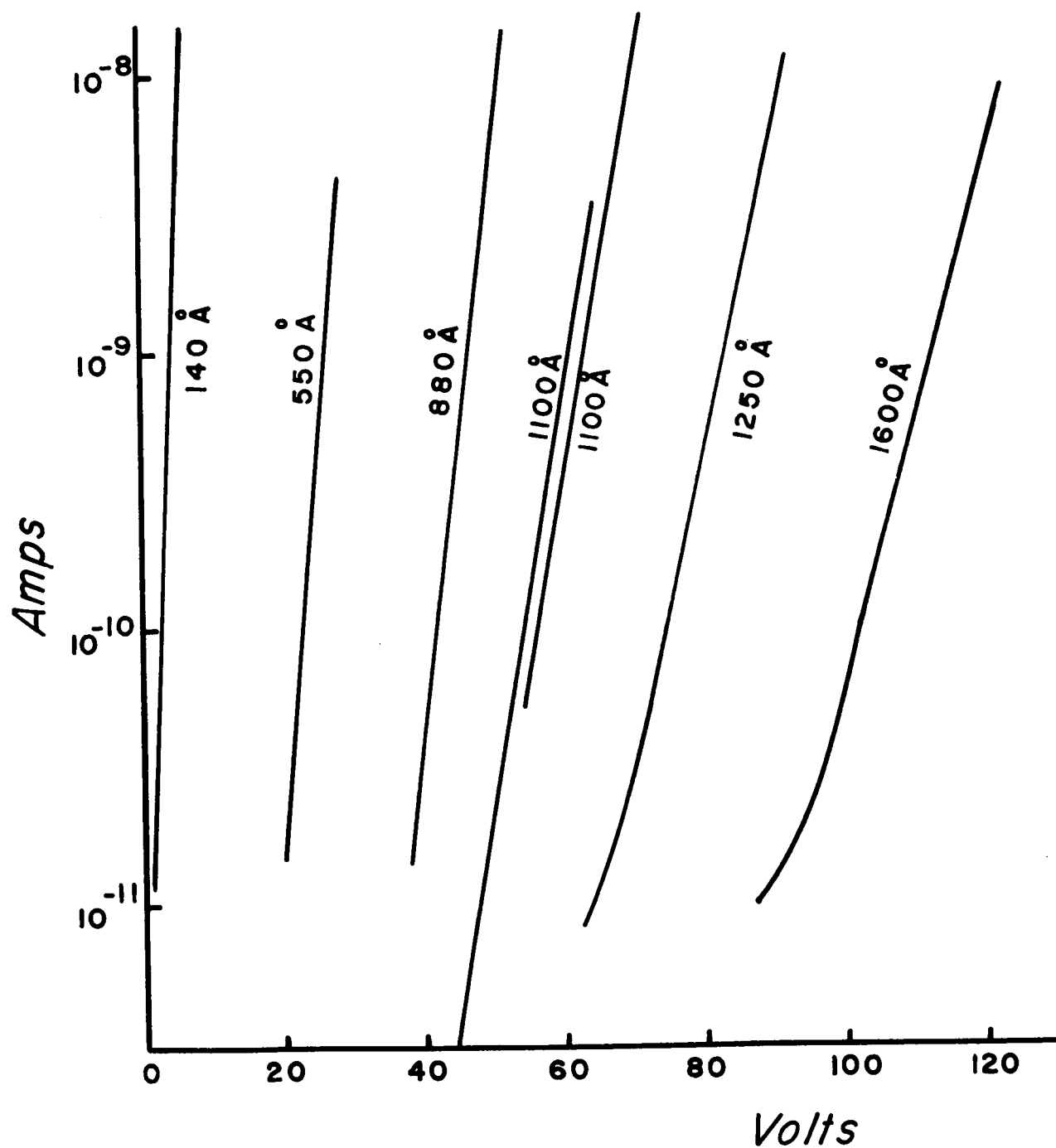
Fig. 46 Current Variation vs. Thickness: 1600 Å – 140 Å
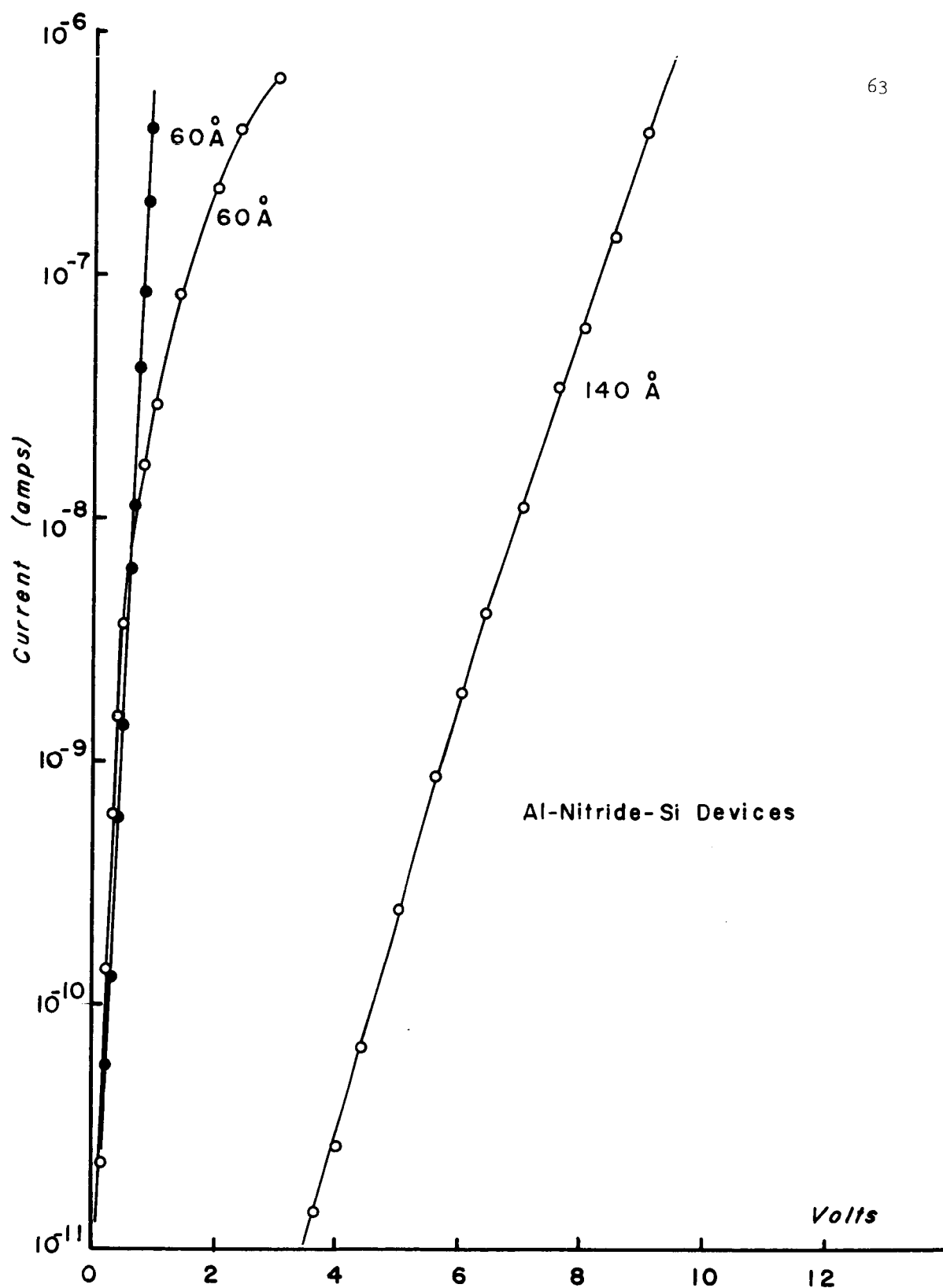
Fig. 47   Current Variation vs. Thickness: 140 Å – 60 Å
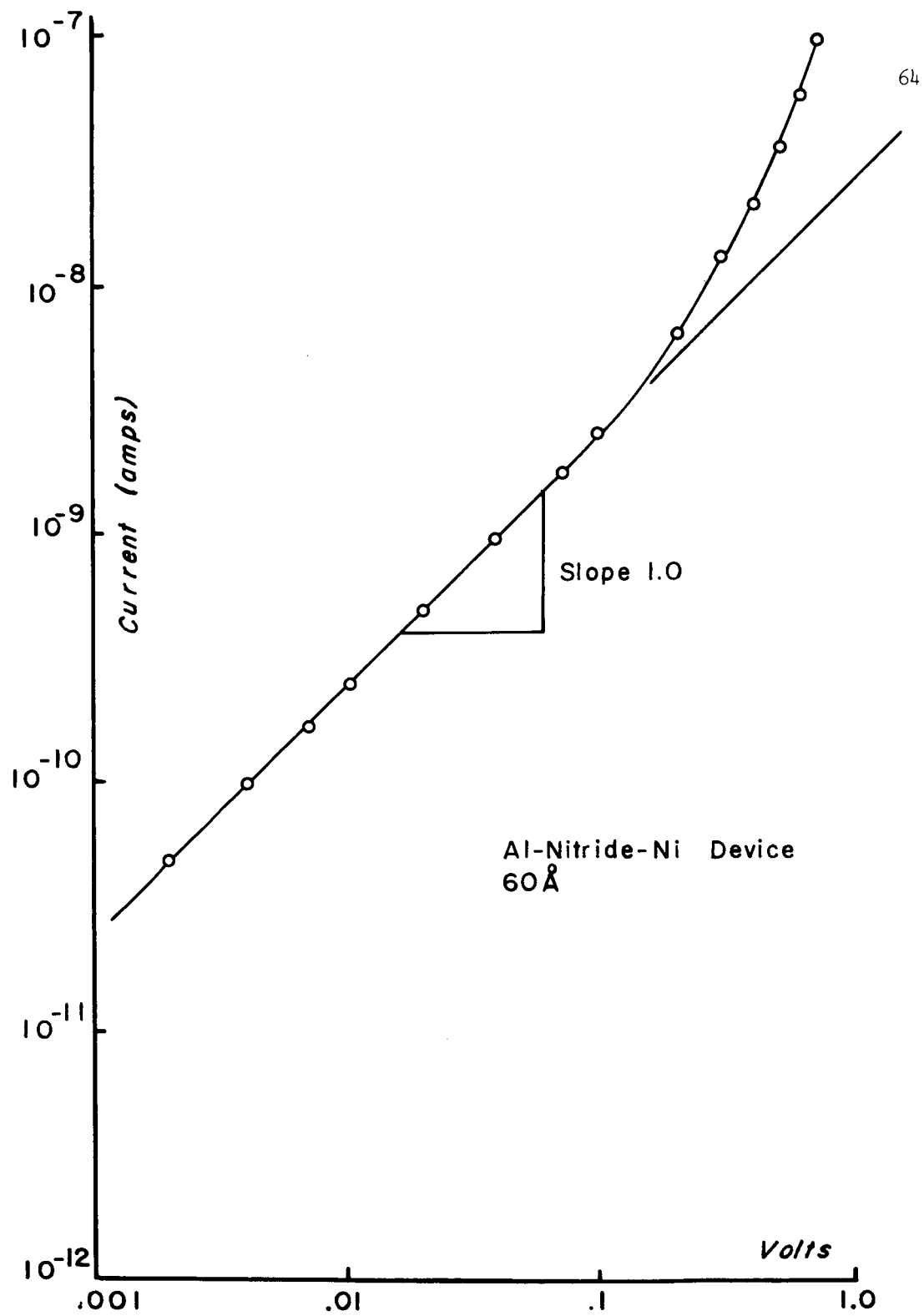
Fig. 48 I-V Characteristics for Al-Nitride-Ni Device with 60 Å
Film Showing Ohmic Behavior
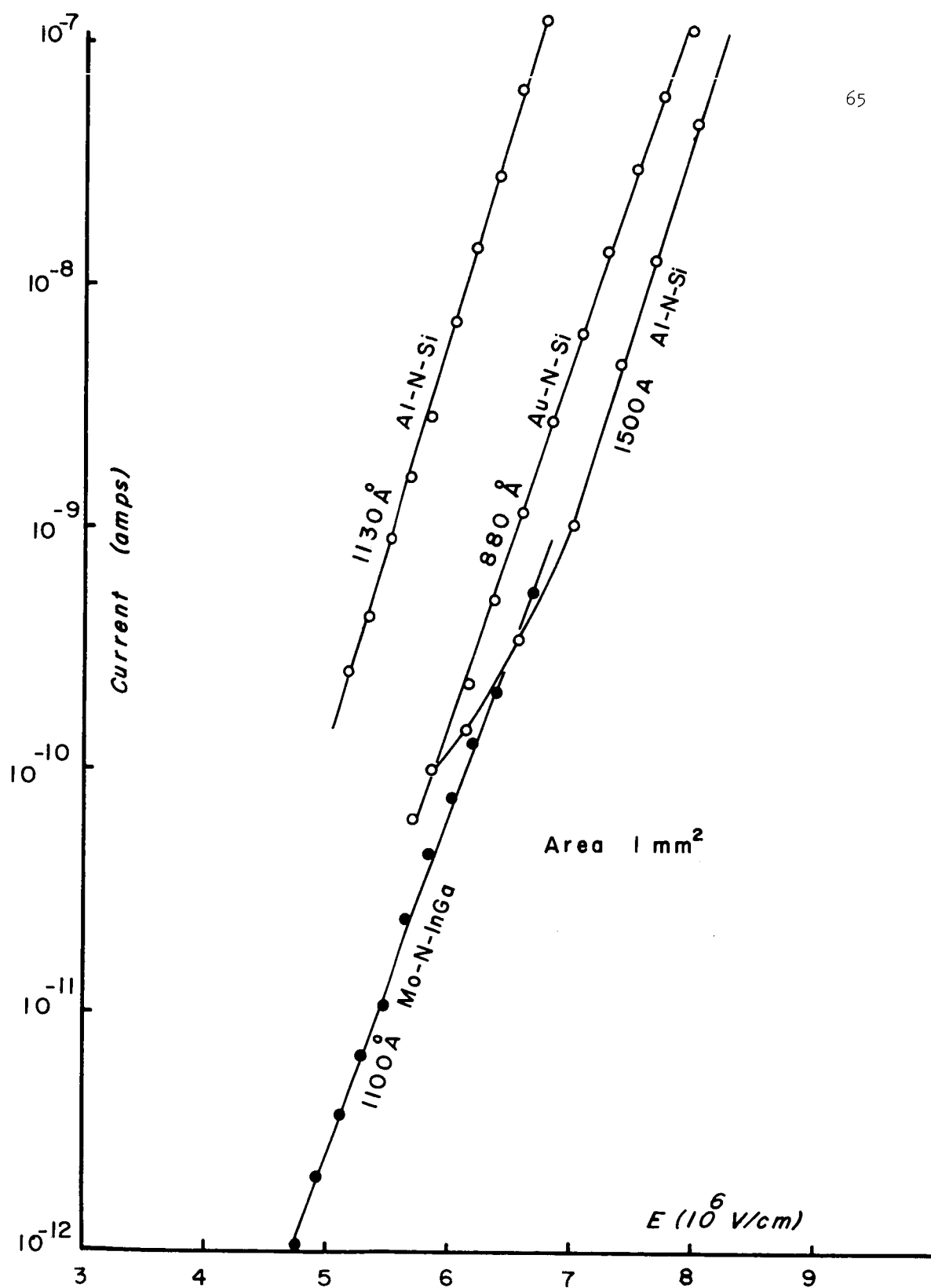
Fig. 49 Ln I Vs. $E^{1/2}$ for Devices with Various Metal Electrodes and Film Thickness
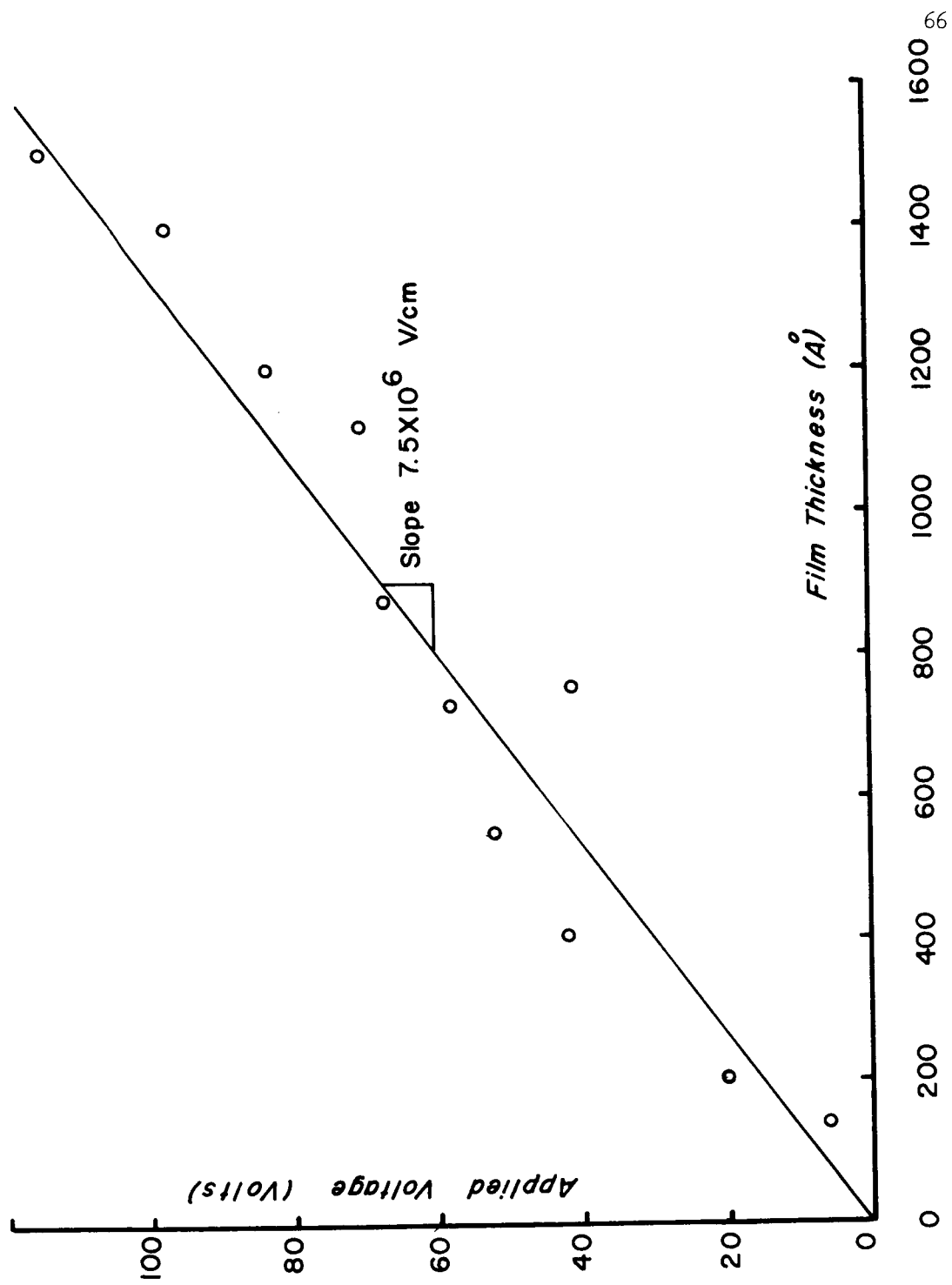
Fig. 50 Voltage Required to Produce 10^{-7} amps/cm^2 for Films of 140-1600 Å
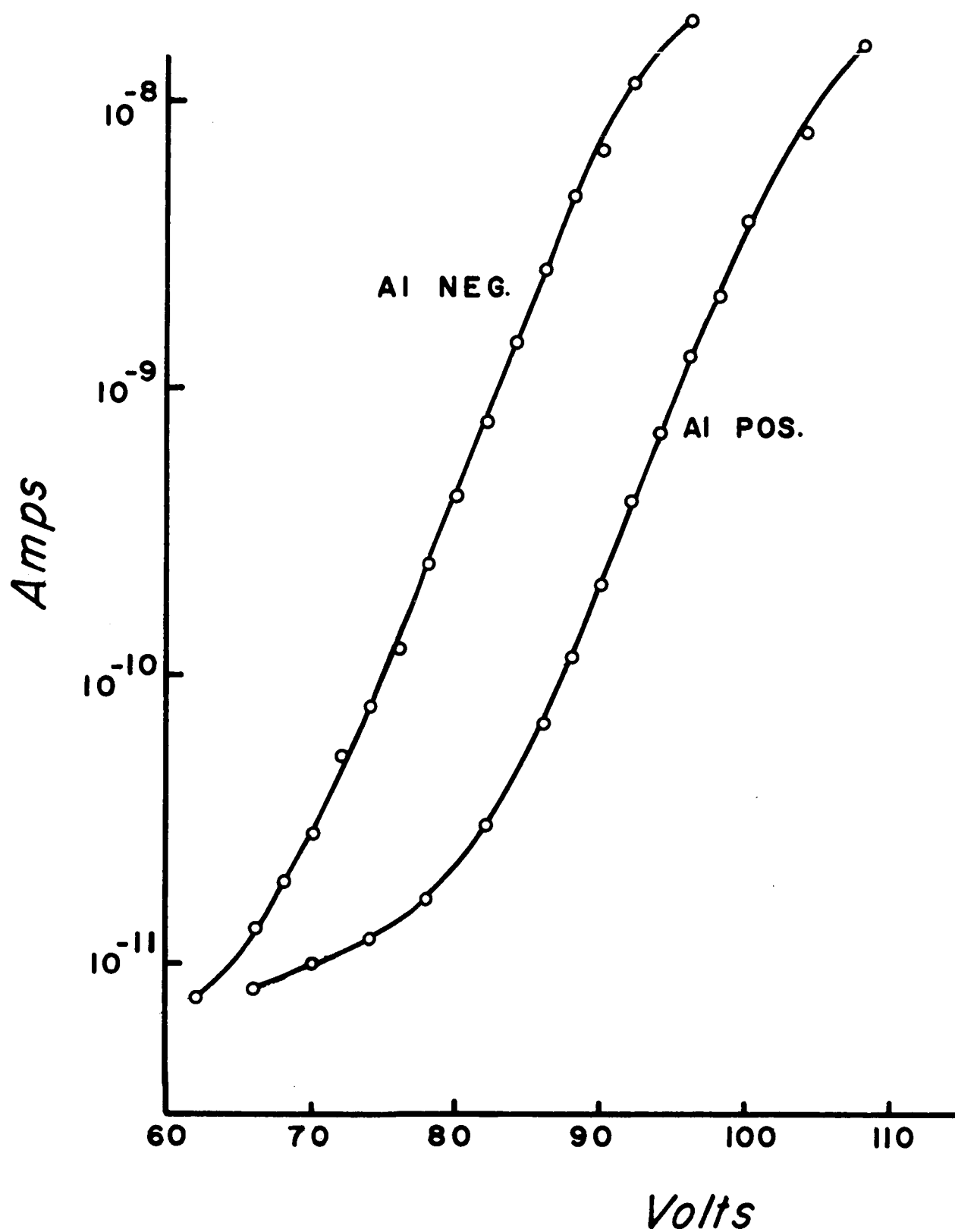
Fig. 51   I-V Characteristics of Al-Nitride-Si Device Showing
Field Penetration into Silicon (p-type Si)

variation in resistivity of the different devices, which in turn depends on the trap densities.

Figure 49 presents curves of ln I vs. $E^{1/2}$ for films of various thicknesses and again indicates that the field controls the current, independent of thickness and interface barrier height.

The only indication of the electrodes in any of the devices is of the form of fig. 51 for an Al-N-Si device. The Si is 0.1 ohm-cm, p-type. The symmetry of the curves and the polarity suggest that polarity dependence is due to a penetration of the field into the bulk of the semiconductor rather than variations in the barrier heights.

D) Slope of Schottky Plots Vs. Thickness:

From the Poole-Frenkel model the slopes of the conductivity vs. $V^{1/2}$ plots are

$$\frac{q}{2kT} \left(q/\pi\kappa\varepsilon_o d \right)^{1/2} < m < q/kT \left(q/\pi\kappa\varepsilon_o d \right)^{1/2} \tag{70}$$

Frenkel[45] points out that the correct value of κ is the electronic component of the dielectric constant (square of the index of refraction = 4) because the field collects the electron before it polarizes the ions. This is subject to experimental test because d and κ are quantities which can be measured independently.

Figure 52 is a plot of the slopes of the various devices versus their thickness. The solid lines represent the limiting values for Poole-Frenkel emission. The lower line also corresponds to the slope expected for Schottky emission. Any points lying on or between the two lines are consistent with the model. The points fall into two general groups, one group which fits the lower value of slope and one

the upper value. The devices in each group also compare in other ways. The devices which show the low values of slope also show low resistivities, while the devices with higher slopes show very large resistivities. The high resistivity devices exhibit tunneling characteristics at the largest fields. A component of current due to tunneling evidently causes the slopes to lie above the line. Hu[52] and Sze[77] observe slopes which lie between the two solid lines.

The fact that the slopes of the log of conductivity vs. $V^{1/2}$ curves agree with the measured dielectric constant is very important. O'Dwyer[64] finds that a large space charge effect can cause the current to be a straight line on a Schottky plot over several decades even when the current injection is by tunneling from the metal into the conduction band of the insulator. However, if the plots of ln I vs. $V^{1/2}$ that O'Dwyer obtains are assumed to be Schottky emission and the dielectric constant calculated from the slopes, one obtains a value approximately an order of magnitude greater than the actual value.

In general the devices which exhibit the higher resistivities and higher slopes are more stable and reach their equilibrium values quicker than do the lower resistivity devices. The readings on all devices are unsteady below currents of 5×10^{-11} amperes and become steady as the current increases. Sze observes an ohmic component at these low currents which he attributes to thermal hopping of carriers between localized levels. Although our readings are unstable in this region, we observe no ohmic component. The time required to reach equilibrium at the low currents is quite long (1-10 min.) similar to effects reported in SiO.

The currents below 10^{-11} amperes are stable and reproducible,
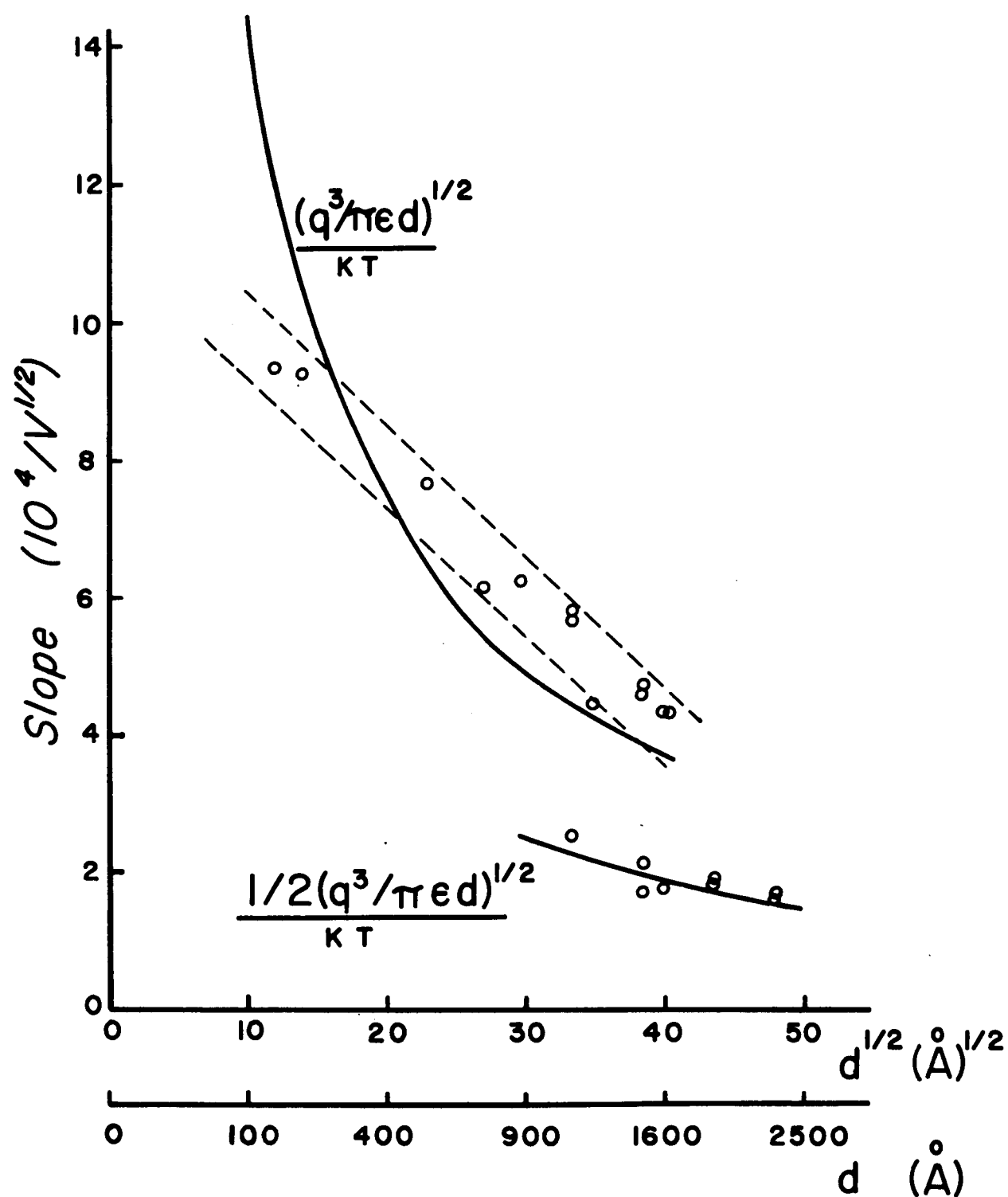
Fig. 52   Variation of the Slopes of the Schottky Plots vs.
Thickness
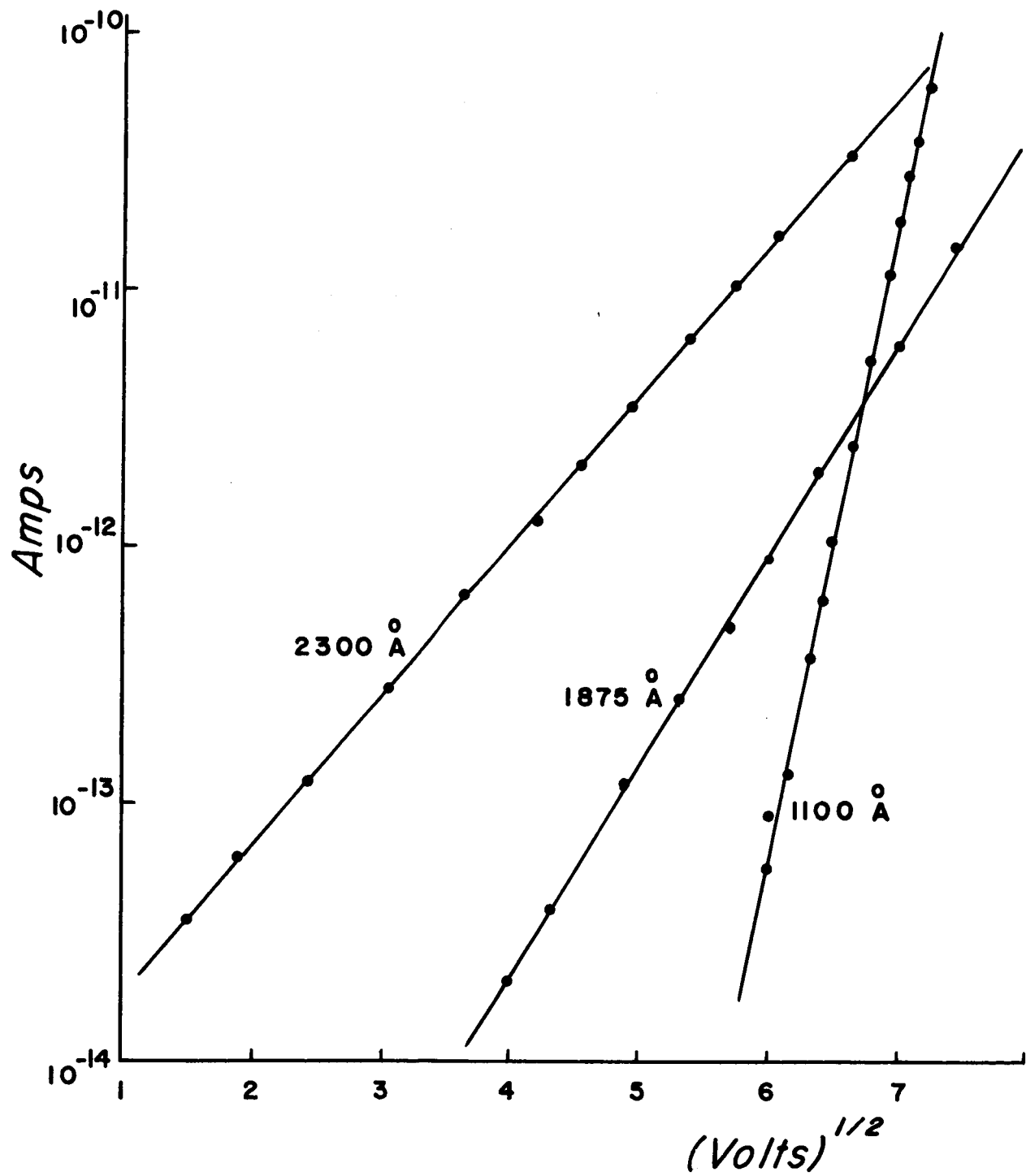
Fig. 53 Variation of Current Behavior in Different Devices

and they reach their equilibrium value quickly. These characteristics
lead to the conclusion that two mechanisms occur in these devices.
The mechanism at the lower fields might be thermal hopping; however,
the instability of the results, the hysteresis effects involved, and the
rather limited range in which this occurs prevent a definite conclusion.
Note that these effects do not occur on all devices (see fig. 52).

E) Further Evidence for Bulk Limited Mechanism:

The differential capacitance vs. bias technique used exten-
sively to study the interface states in Metal-Insulator-Semiconductor
structures sweeps the Fermi level through the forbidden band by bend-
ing the bands at the interface as shown in fig. 54. For simplicity, the
bending of the bands in the insulator is usually neglected; however,
bending occurs just as in the semiconductor. To investigate the pos-
sibility that the barriers at the interfaces are somehow identical for
all the electrodes used, thus masking the dominance of electrode emis-
sion, the capacitance vs. voltage characteristics were measured along
with the I-V characteristics. A relation between the voltages at which
the Fermi level sweeps through the forbidden band and the voltages which
produce currents in the insulator might indicate electrode participa-
tion in current injection.

Figures 55 and 56 give the results of this test. No correla-
tion exists between the sweeping of the Fermi level through the forbid-
den band and the current injection in the device. The current injection
occurs just before breakdown while the voltage required to sweep the
Fermi level through the band gap depends on the surface states present
and is very sensitive to surface preparation and cleaning. This evi-
dence further indicates that the current injection is from the bulk
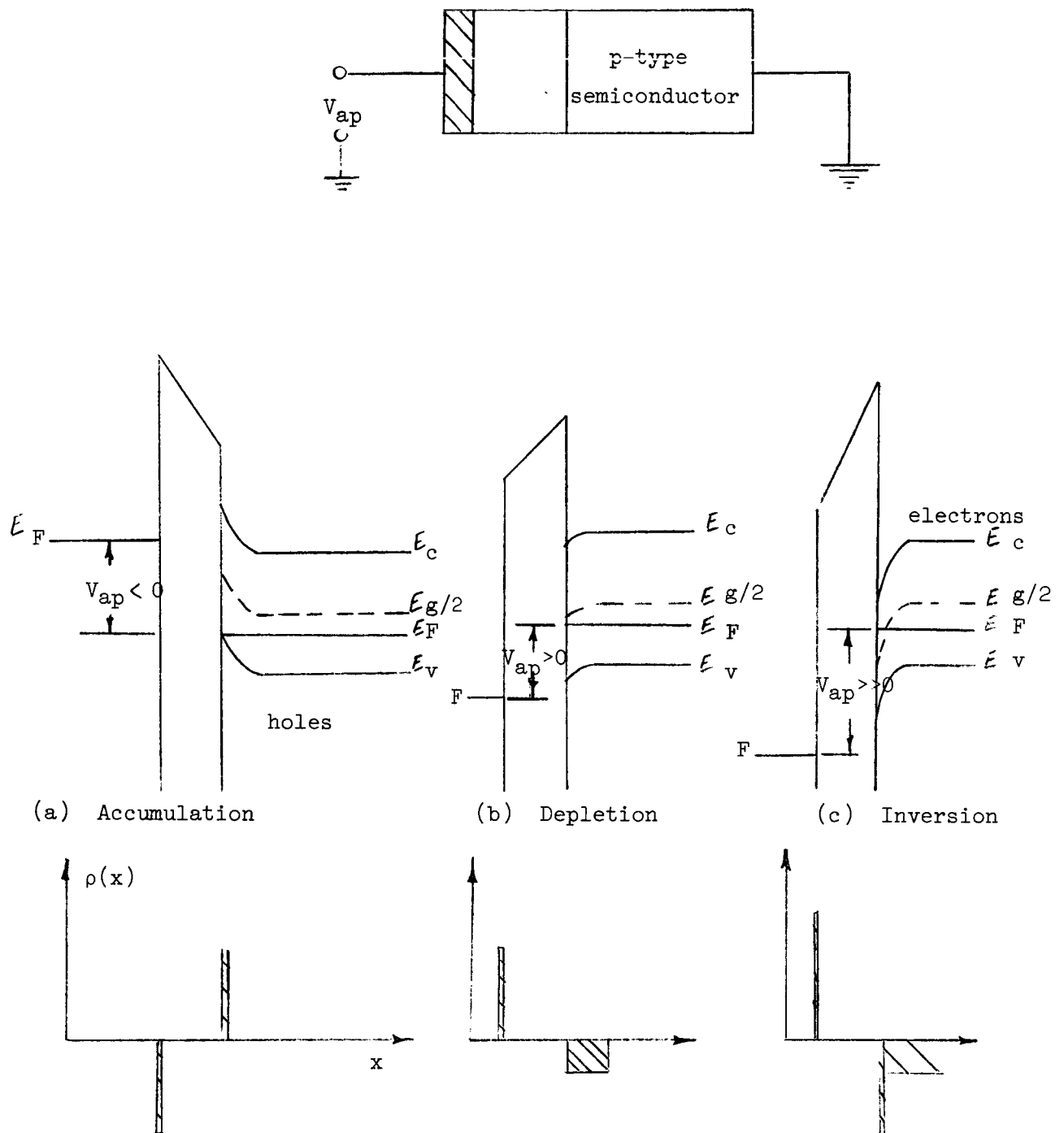
Fig. 54   Energy Bands and Charge Distribution in an MIS Structure
Under Various Bias Conditions in the Absence of Surface
States and Work Function Difference.
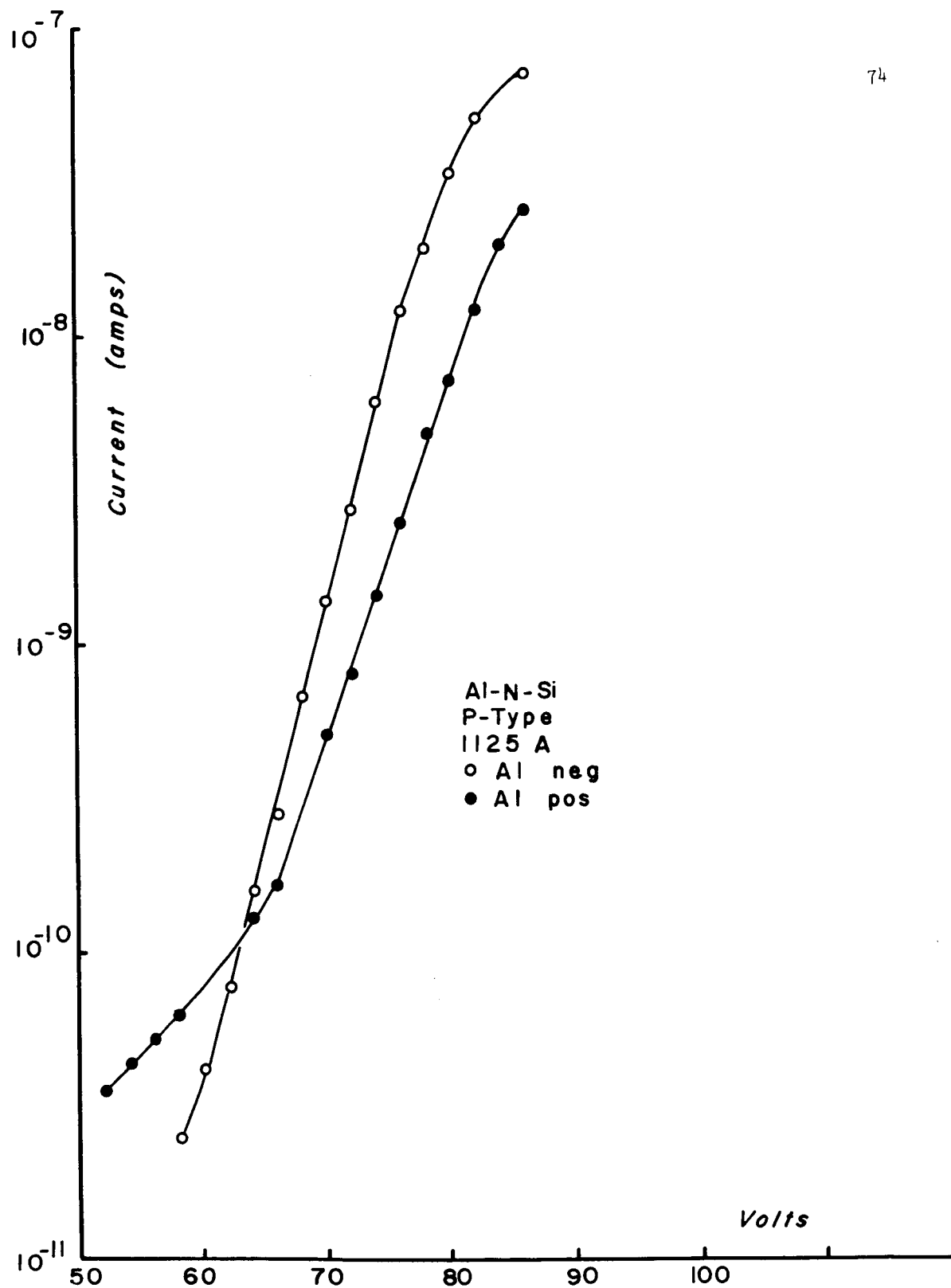
Fig. 55   Current Characteristics for Al-Nitride-Si Device
          (p-type Si, 1125 Å film)
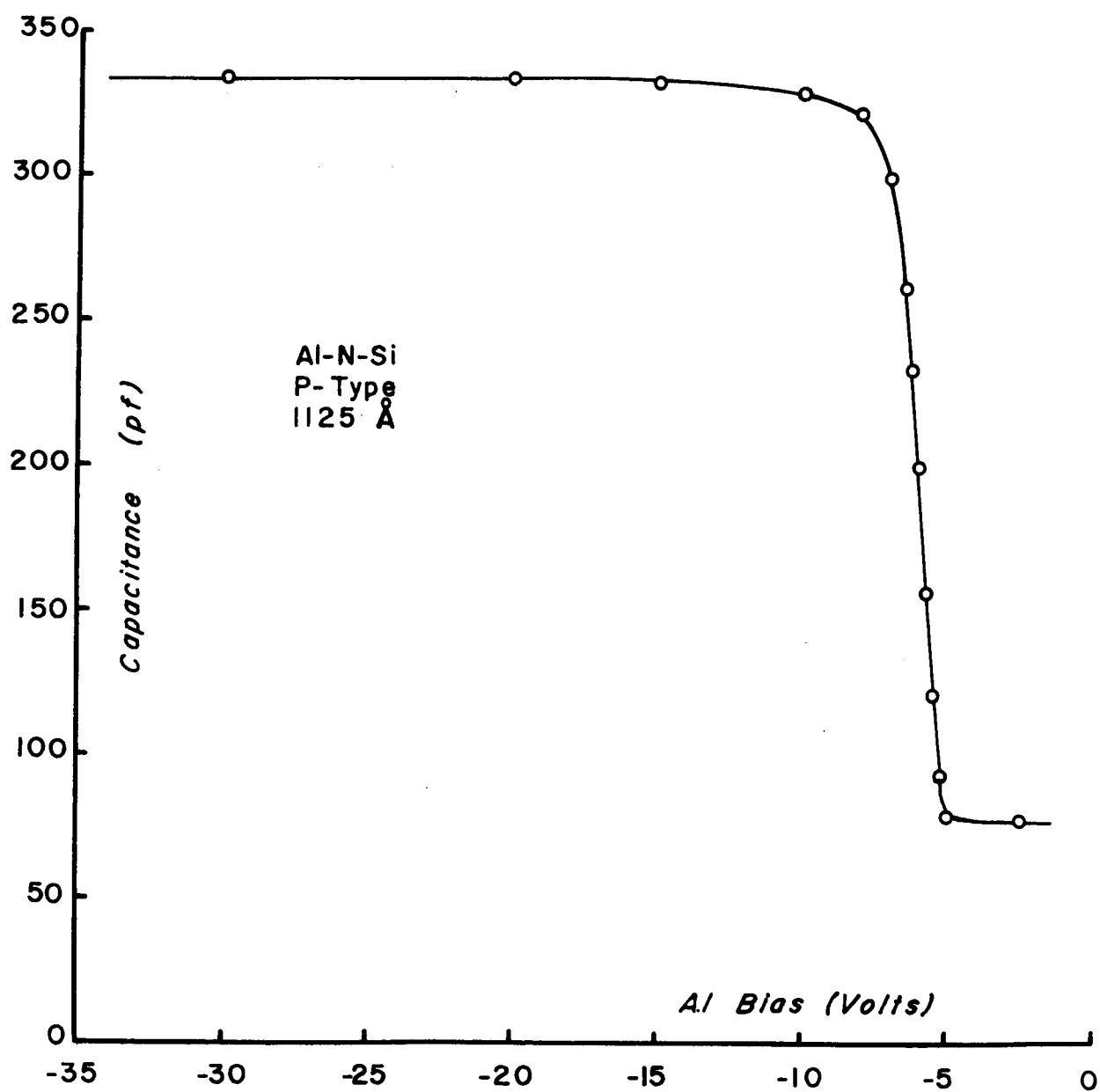
Fig. 56 Capacitance vs. Voltage Characteristics for the
Device of fig. 55

rather than the electrodes.

F) Comparison with Other Workers:

The only information in print on the electrical properties of silicon nitride films is by Hu[51,52] et.al. They report that the current mechanism is Poole-Frenkel emission. The slope of the Schottky plot corresponds to a relative dielectric constant of 7.6 compared to the optical dielectric constant of 4.0. The corresponding trap level was 1.0 ± 0.05 eV from the temperature dependence. The resistivity was 10^{15} ohm-cm at a field of 10^6 v/cm. The films were deposited by RF reactive sputtering.

In an article soon to be published, Sze[77] measures the current voltage characteristics of $Au-Si_3N_4-Mo$ and $Au-Si_3N_4-Si$ structures with film thicknesses ranging from 300 $\overset{o}{A}$ to 3000 $\overset{o}{A}$. His films were deposited by the reaction of $SiCl_4$ with NH_3. He finds that at a given temperature and electric field, the current transport depends very little on the substrate material, the film thickness, or the polarity of the electrodes. He proposes that the current is bulk controlled and is the sum of three contributions. At high fields and high temperatures the current is dominated by the Poole-Frenkel mechanism with a barrier height of 1.3 ± 0.2 eV. The slopes of the Schottky plots give a value of 5.5 for the dynamic dielectric constant. At high fields and low temperatures the dominant mechanism is field ionization of trapped electrons into the conduction band of the dielectric. At low fields and moderate temperatures, the dominant mechanism is thermal hopping of excited electrons between isolated states yielding an ohmic contact and a thermal activation energy of $\simeq$ o.1 eV.

Sze finds that at low temperatures the maximum dielectric

strength approaches 10^7 V/cm and at high temperature where Poole-Frenkel emission dominates the current conduction, the maximum strength decreases as $(\phi_1 - CT)^2$ where ϕ_1 is the barrier height of the traps and C is a function of the thermal conductivity of the films.

Brown[82] reported similar characteristics on films deposited by the SiH_4-NH_3 reaction.

These results resemble those of the above workers in that we find the dominant mechanisms are bulk limited. In particular our results compare with those of Sze in that we observe both the Poole-Frenkel thermal emission and the Fowler-Nordheim field emission. The resistivity of Sze's structures are somewhat lower than the structures in which we observe tunneling. This results in the slope of our Schottky plots being somewhat higher due to a larger contribution from tunneling. These data differ from Sze's in failing to show an ohmic characteristic at the lowest currents. The behavior of the current in this region is unsteady and subject to considerable hysteresis. The mechanism may indeed be thermal hopping, but our devices show ln I as linear with $V^{1/2}$ for as much as four decades. These devices show two different mechanisms act over this region similar to the effects observed by Hartman[49] et.al. on SiO.

G) Band Model for Silicon Nitride:

Based on these results, two groups of behavior exist for silicon nitride. One behavior is characterized by very high resistivities, steeper slopes of the Schottky plots, and larger activation energies. The other group exhibits lower resistivities, lower activation energies, and lower slopes on the Schottky plots. The lower resistivity behavior seems to be more prevalent on thicker devices and

on quartz substrates. These devices also show transient effects and long time constants. The slope of the Schottky plots are very near those expected for Schottky emission from the electrode. The slopes of the high resistivity devices lie near those expected for Poole-Frenkel emission with no compensation. Based on these considerations, the following model appears to apply for silicon nitride.

The current is composed of 3 components.

$$J_T = J_1 + J_2 + J_3 \tag{71}$$

$$J_1 = Ae^{-q\phi_1/kT}e^{-q(qE/4\pi\kappa\varepsilon_o)^{1/2}/kT} \tag{72}$$

$$J_2 = \sigma_o Ee^{-q\phi_2/kT}e^{-q(qE/\pi\kappa\varepsilon_o)^{1/2}/kT} \tag{73}$$

$$J_3 = BE^2 e^{-b/E} \tag{74}$$

J_1 is a thermal emission component where the emission occurs from small islands of silicon within the silicon nitride. These islands of silicon are the result of non-stoichometric conditions in the film.

J_2 is the Poole-Frenkel component of thermal emission. It is a basic property of the nitride material.

J_3 is the field emission component of current. It dominates the behavior at very high fields ($> 7 \times 10^6$ V/cm). The field emission is from the same sites as the Poole-Frenkel emission.

From these conclusions we can draw a band picture for silicon nitride. At approximately 1.5 electron volts below the conduction band

there is a trap level corresponding to the intrinsic properties of

$$E_c$$

0.85 - 1.05 eV

1.5 eV

$$E_v$$
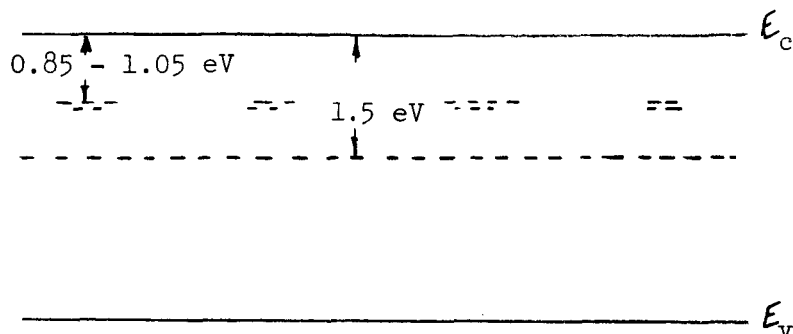
Fig. 57   Band Picture for Silicon Nitride

the silicon nitride. At a level varying from 0.85 to 1.05 eV in the

devices tested a series of trap levels arise from small islands of

silicon embedded in the silicon nitride. The density of these traps

depends on the composition of the reaction gases and probably on the

temperature during the film deposition. If the density of these traps

is small, their presence does not affect the I-V characteristics. They

dominate the current characteristics if their density is large due to

the smaller barrier than that of the intrinsic silicon nitride.

Johansen[53] has proposed this model of internal Schottky emis-

sion to explain the observed current characteristics of SiO_x. A struc-

tural model of SiO, proposed by Brady[88] and supported by x-ray diffrac-

tion experiments, assumes that silicon monoxide is a stoichiometric

mixture of SiO_2 and Si. Johansen proposes that SiO_x is a non-stochio-

metric mixture of the same two components. Similarly, these films

of silicon nitride behave like mixtures of Si_3N_4 and Si. Si_3N_4 is the

formula of bulk silicon nitride and is a crystalline structure.

H) Intrinsic Conductivity:

From chapter two, the expression for Poole-Frenkel emission is

$$\sigma = \sigma_0 e^{q(qE/\pi\kappa\epsilon_0)^{1/2}/kT} \qquad (75)$$

where

$$\sigma_0 = A_1 e^{-q\phi/kT} \qquad (76)$$

depends on the amount of compensation of donor traps with acceptor traps. For the devices with very high resistivities, from fig. 50 the field necessary to produce a current density of 10^{-7} amps/cm^2 is 7.5×10^6 V/cm. Substituting this value in the Poole-Frenkel equation above gives the zero field conductivity

$$\sigma_{E = 0} = \sigma_0 \qquad (77)$$

as

$$\sigma_0 = 6.7 \times 10^{-32} \ (\Omega-cm)^{-1} \qquad (78)$$

the constant A_1

$$A_1 \simeq 10^{-10} \ (\Omega-cm)^{-1} \qquad (79)$$

I) Intrinsic Carrier Concentration:

The carrier concentration, n, relates to conductivity by

$$\sigma = nq\mu = A_1 \qquad (80)$$

where q is the charge on the carrier

μ is the carrier mobility.

From Mott and Gurney, the mobility of a free electron or hole in insulators lies between 1 and 100 cm /sec / per volt/cm. The carrier concentration at room temperature and zero bias is then

$$6.25 \times 10^{+6} < n < 6.25 < 10^{+8} \ cm^{-3} \qquad (81)$$

J) Effective Mass:

Assuming that the field ionization occurs from the same sites as the Poole-Frenkel Emission permits calculation of an approximate value of the effective mass in the conduction band. Chynoweth[36] gives the current expression for tunneling from impurity levels in the forbidden region to the conduction band as

$$J = C_1 E^2 \exp[-\frac{4}{3\hbar q}\sqrt{2m^*}\frac{\psi_T^{3/2}}{E}]\qquad(82)$$

where C_1 is a constant

The slope of Fowler-Nordheim plots (ln J vs. 1/E) are then a measure of the barrier height and effective mass. Substituting values in eq. 82 gives

$$1.25 \times 10^{10} (\frac{m^*}{m_o})^{1/2}\ \text{V/m}\qquad(83)$$

for the slopes of these plots, where we have used

$$\psi_T = q\phi_T\qquad(84)$$

where ϕ_T is 1.5 volts.

The slope of fig. 41 is 9×10^9 V/m giving a relative mass of the carrier in the conduction band of

$$\frac{m^*}{m_o} \simeq 0.40.\qquad(85)$$

Other devices give values ranging from 0.29 to 0.80 but 0.40 is typical.

K) Generation Statistics:

Thorough characterization requires determining the approximate densities of traps necessary to support the steady state Poole-Frenkel current. The exact problem is too complicated for simple analysis; however, an approximate solution appears from the assumptions that (1) one carrier type dominates, and (2) the generation and recombination can be described by an effective density of traps ϕ volts below the conduction band. The second assumption is plausible if we imagine a large density of traps throughout the entire forbidden band in which case traps above the Fermi level a few kT are essentially empty and traps below the Fermi level a few kT have little chance of emission because of the greater barrier height. Emission is then essentially from traps at the Fermi level. This is the same problem of generation-recombination through a single level acceptor (or donor) trap which permits a similar analysis. The barrier height in this case is the energy difference between the Fermi level and the bottom of the conduction band, however the insulator contains a large density of traps at some position in the forbidden band other than at the Fermi level, the barrier height cannot be identified as the position of the Fermi level but is the energy difference between the trap level and the bottom of the conduction band.

The average time required for thermal emission from a trap ϕ volts below the conduction band[23] is

$$\tau = \frac{1}{v_t \sigma_n n} \quad \text{seconds} \tag{86}$$

where v_t is the effective velocity of the electron in the conduction

band

σ_n is the capture cross section of the trap

n is the density of carriers in the conduction band which would

be obtained if the Fermi level were at the trap level.

The correct carrier density is

$$n = N_c e^{-q\phi_{eff}/kT} \qquad (87)$$

where

$$N_c = 2(\frac{2\pi m^* kT}{h^2})^{3/2} \qquad (88)$$

is the effective density of states in the conduction band.

The Poole-Frenkel equation gives the effective barrier height

$$\phi_{eff} = \phi - (\frac{qE}{\pi\kappa\varepsilon_o})^{1/2} \qquad (89)$$

Typical values of the parameters might be

$$v_t = 10^7 \text{ cm/sec.} \qquad (90)$$
$$10^{-22} < \sigma < 10^{-17} \text{ cm}^2 \qquad (91)$$

$$n = 10^{12} \ (\phi_{eff} \simeq 0.5v) \qquad (92)$$

resulting in a mean time for emission of

$$10^{-2} < t < 10^3 \qquad (93)$$

Measured current densities of 10^{-9} amps/cm^2 are obtained for the barrier height used in the above calculation which corresponds to a carrier density of

$$0.625 \times 10^{10}v \simeq 10^8 \text{ cm}^{-3} \qquad (94)$$

which implies a trap density of

$$10^{16} < N_T < 10^{21} \quad cm^{-3}. \tag{95}$$

These seem like reasonable quantities in view of the disordered nature of the material.

CHAPTER IV

Experimental Technique and Technology

Since Sterling and Swann[74], silicon nitride has been formed

by both RF sputtering and chemical vapor deposition. The RF sputter-

ing involves bombarding a cathode of bulk silicon nitride with ions in

a reduced pressure. The advantages of this method include the fact

that the substrate temperature can be low compared to the substrate

temperature involved in the chemical vapor deposition technique. This

allows the films to be deposited on substrates which would melt at the

temperatures required for chemical vapor deposition (e.g. Al). Another

advantage of the low substrate temperature is that the difference in

coefficient of expansion is less important because the expansion is

much less than for chemical vapor deposition. The major disadvantage

of the RF sputtering technique is that the concentration of the two

constitutents cannot be varied with ease and the stoichiometry of the

films is less controllable. The concentration by vapor plating can

be somewhat controlled by conducting the reaction in an atmosphere with

a partial pressure of nitrogen and varying the pressure of the nitrogen.

A) Chemical Vapor Deposition:

Chemical vapor deposition produced the films of this work.

This process involves thermal decomposition of suitable gases into their

elemental components of silicon and nitrogen. The components then

react to form a more stable compound than the original. Suitable gases

are SiH_4 and $SiCl_4$ for silicon and NH_3 for the nitrogen. Silane (SiH_4) decomposes readily at temperatures above $600^{\circ}C$ while the silicon tetrachloride ($SiCl_4$) requires temperatures of $1000^{\circ}C$ or better. The lower temperatures are desirable in work involving semiconductor devices because the higher temperatures affect the pn junction location and doping in the semiconductor substrates. The disadvantage of silane is that it explodes spontaneously with air and requires care to insure that the flow system contains no leaks. The reactions occur according to the equations

$$SiH_4 + NH_3 + energy \rightarrow Si_3N_4 + H_2 \qquad (96)$$

$$SiCl_4 + NH_3 + energy \rightarrow Si_3N_4 + H_2 + Cl_2 \qquad (97)$$

The stoichiometry of the films varies with the mixture of the gases.

This work utilized the silane-ammonia reaction with hydrogen as a carrier. This process has the advantage that most silane which decomposes before reaching the substrate recombines with the hydrogen thus limiting the reaction to the immediate vicinity of the heated substrate.

B) Deposition System:

Wherever possible, the materials used in the deposition system are quartz, stainless steel, and teflon*. These materials minimize contamination to the system and help obtain reproducible results. Tubing and valves are stainless steel, the mixing chamber and reaction chamber are quartz, fittings, for glass to metal seals, are teflon.

---

* Trademark, E.I. Dupont, Co.
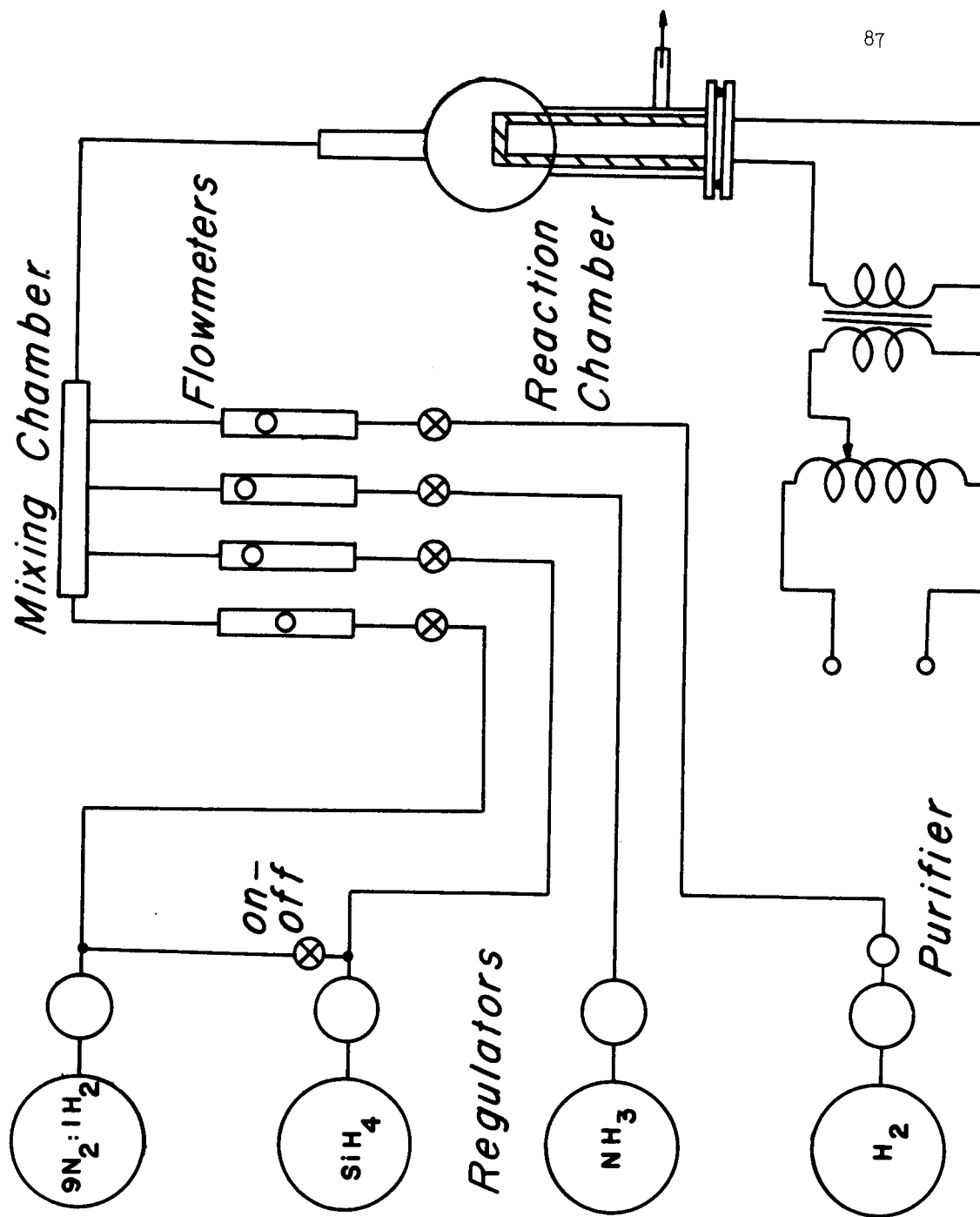
Fig. 58 System for Vapor Deposition of Silicon Nitride

Figure 58 shows a diagram of the system, which resembles systems used
for semiconductor epitaxy. The nitrogen and hydrogen gases are of
commercial quality. The hydrogen flows through two deoxo purifiers
which remove traces of oxygen. Mixing the hydrogen and nitrogen in
a ratio of 9 parts nitrogen to 1 part hydrogen produces the forming
gas which flushes the system. The Matheson Company supplies the silane
and ammonia. The silane is semiconductor grade with a maximum boron
content of 1 part per billion with a resistivity of 50 ohm-cm p-type
after deposition as silicon. The ammonia is 99.99% pure.

From the cylinders, the gases flow to their respective regu-
lators. The pressure used in all work is 10 psi. Flushing the silane
line immediately after the regulator reduces the danger of explosion.
From the regulators the gases flow to a series of metering valves which
regulate the flow during the film deposition. Whitey micrometer con-
trol valves, series #22, control the small flowrates of ammonia and
silane. Next the gases pass through their respective flow meters and
into the mixing chamber at almost atmospheric pressure and room tem-
perature. From the mixing chamber the gases flow into the reaction
chamber where a heated graphite substrate holder decomposes the silane.
The reaction and film deposition occur at the heated portions of the
chamber. After the reaction, burning and venting via a hood insure
safety.

A chromel-alumel thermocouple, as indicated in fig. 59,
determines the temperature of the substrate during deposition. The
thermocouple touching the substrate spoils a small area of the film.
The small areas used for devices avoid the affected area.

Figure 59 shows details of the vertical flow reaction chamber.

Thermocouple

Teflon Fitting

Substrate

Graphite

Stainless Steel

Kovar Metal

To Burn off
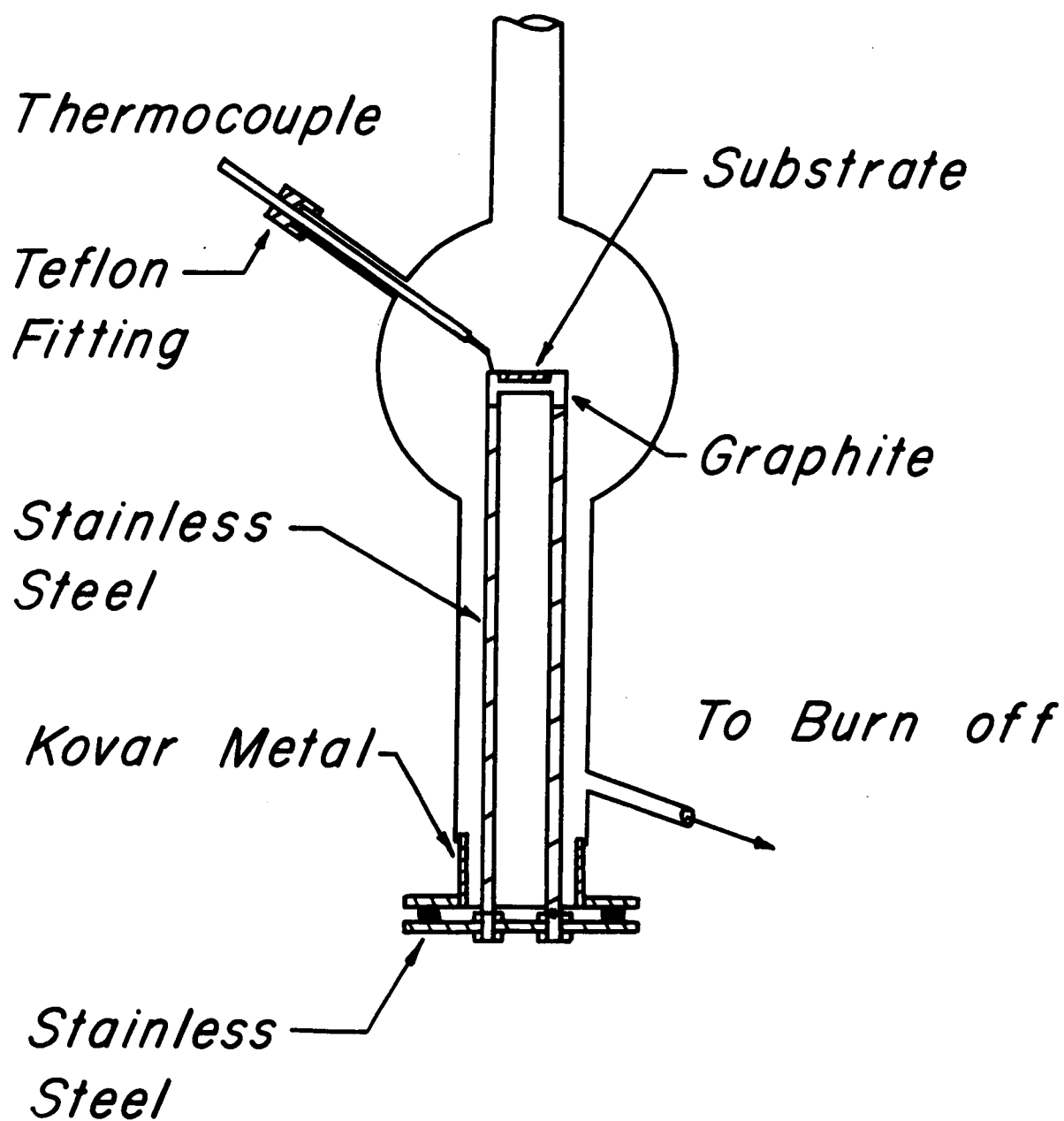
Stainless Steel

Fig. 59 Reaction Chamber

The major problem encountered with the reaction chamber is getting the electrodes through the chamber wall. A glass-to-metal seal using Kovar metal heliarced to a stainless steel flange solves the problem. A neoprene O-ring arrangement allows the removal of the substrate holder and electrodes from the reaction chamber for cleaning and for positioning of substrates.

Ac current heats the graphite holder which tends to vaporize when heated and requires coating. A coat of silicon nitride works well to prevent vaporization. Stainless steel electrodes conduct the current in the reaction chamber. A teflon bushing arrangement (see fig. 59) brings the electrodes through the chamber wall. The power supply to the substrate consists of a 0-220 volt (0-10 amp) variable transformer to control the power input and a 100:1 current transformer to provide current gain for the low resistance circuit. Normal high temperature operation uses 6 volts input to produce 70 amps in the heating element.

C) Film Deposition:

The film deposition follows a symmetrical cycle. First, system flushing with forming gas removes oxygen and other gases which form stable compounds with the reactant gases. After flushing, hydrogen purges the system, providing an atmosphere for the reaction, and acting as a carrier for the silane and ammonia. Power to the substrate heater during the H_2 purge heats the substrate to the desired temperature and allows equilibrium before introduction of the reactant gases. During the substrate heating, the color of the burn off flame changes from a light blue to a bright yellow. This probably indicates trapped gases and organic materials escaping from the substrate and heated

portions of the chamber. The return to a light blue flame indicates that the system has cleansed itself and signals establishment of conditions for introducing the silane and ammonia.

Introducing the ammonia and silane in predetermined quantities and ratios starts the reaction and film deposition, which continues to the desired thickness. Observing the color of the interference fringes gives the film thickness during deposition. The reactant gases are now shut off but the hydrogen remains. Keeping the substrate at the deposition temperatures for two or three minutes insures reaction stoppage before cooling begins. This pause also provides a short anneal period for the film.

After the anneal period, the power to the substrate heater is reduced in steps of 1/3 over a period of from 10-15 minutes. The substrate drops to a temperature below 100°C before final flushing begins. Table II shows a typical film deposition cycle with approximate times and flow rates for the various portions of the cycle.

TABLE II

Flow Rates and Times for Deposition

System Flush	3 - 5 min	10,000 cm^3/min
H_2 Purge and Substrate Heating	7 -12 min	2,000 cm^3/min
Film Deposition	7 -20 min	2,200 cm^3/min
H_2 Purge and Cool Down	15-20 min	2,000 cm^3/min
System Flush	3 - 5 min	10,000 cm^3/min

D) Deposition Behavior Characteristics:

The thickness of the deposited film increases linearly with time as shown in fig. 60. Assuming a constant index of refraction and observing the color of the interference fringes give the thickness. This method is basically inaccurate but taking numerous points elimi- nates random error and allows determination of the deposition rate. The deposition rate is constant since the film is deposited from a chemical reaction and not diffusion limited in the solid, as is the case of thermally grown oxides. No observable differences occur in the deposition of the film on substrates of nickel, molybdenum, molydenum coated quartz, platinum coated quartz, and silicon.

Figure 61 gives the growth rate as a function of silane to ammonia ratio. The slopes of curves give data points similar to fig. 60 which exhibits two distinct regions of the curve. Bean[1] et.al. observes a similar behavior for films deposited from the $SiH_4-NH_3-H_2$ reaction. They correlate the break to a change in the stoichiometry of the film. The break in the curve of fig. 61 occurs at a ratio of ammonia to silane of 7:1 compared to a ratio of 5:1 observed by Bean. Silicon-rich films result at lower concentrations. The fact that the index of refraction increases from the value of 2.0 for silicon nitride to a value approaching the bulk value of silicon (4.02) supports this deduction.

The change in stoichiometry also affects the electrical properties[10]. All work reported here uses ammonia to silane rations greater than 7:1 to insure stoichiometry; however, it would be interest- ing to observe the current variation with silane and ammonia concentrations.
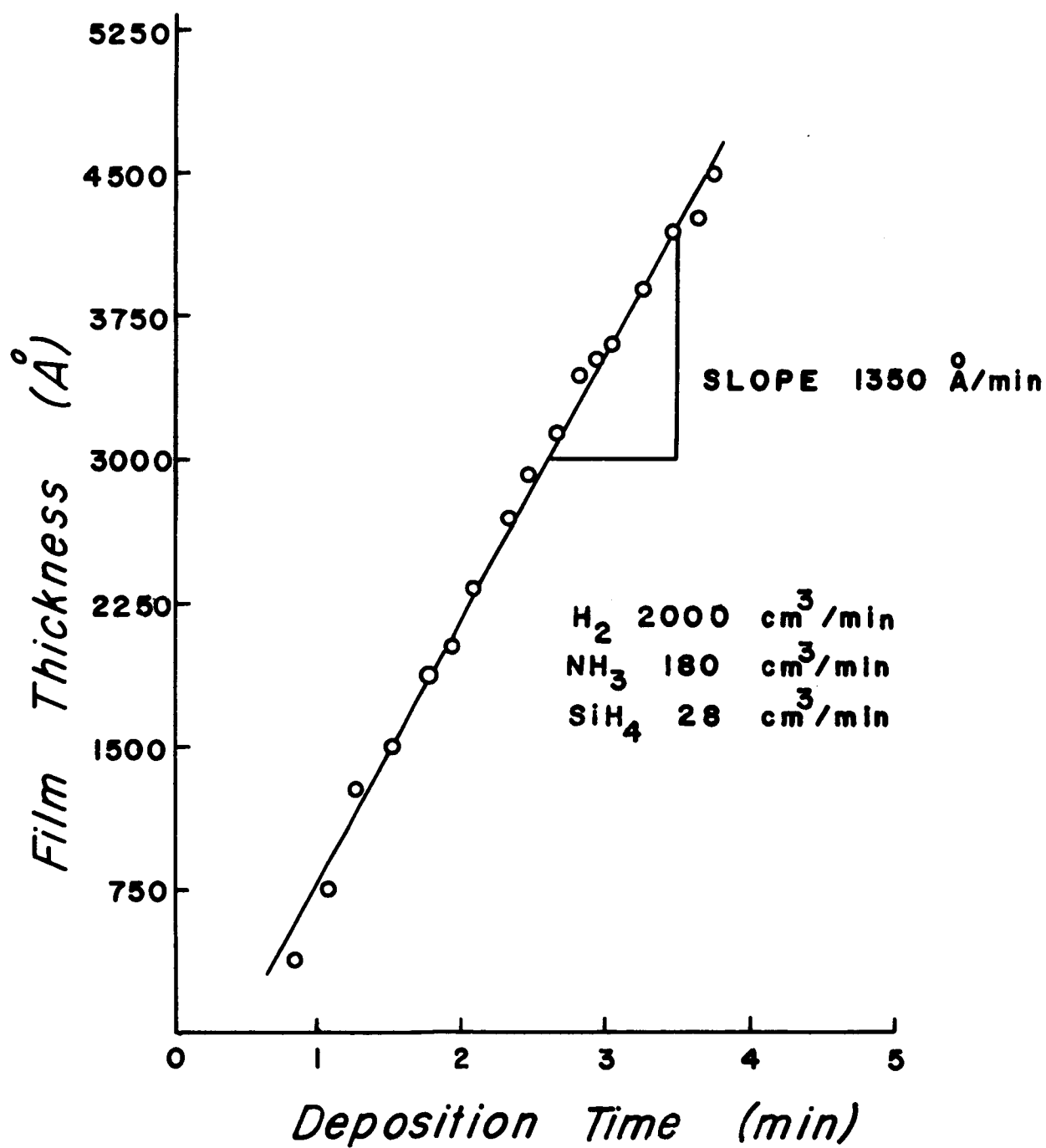
Fig. 60 Film Thickness vs. Deposition Time
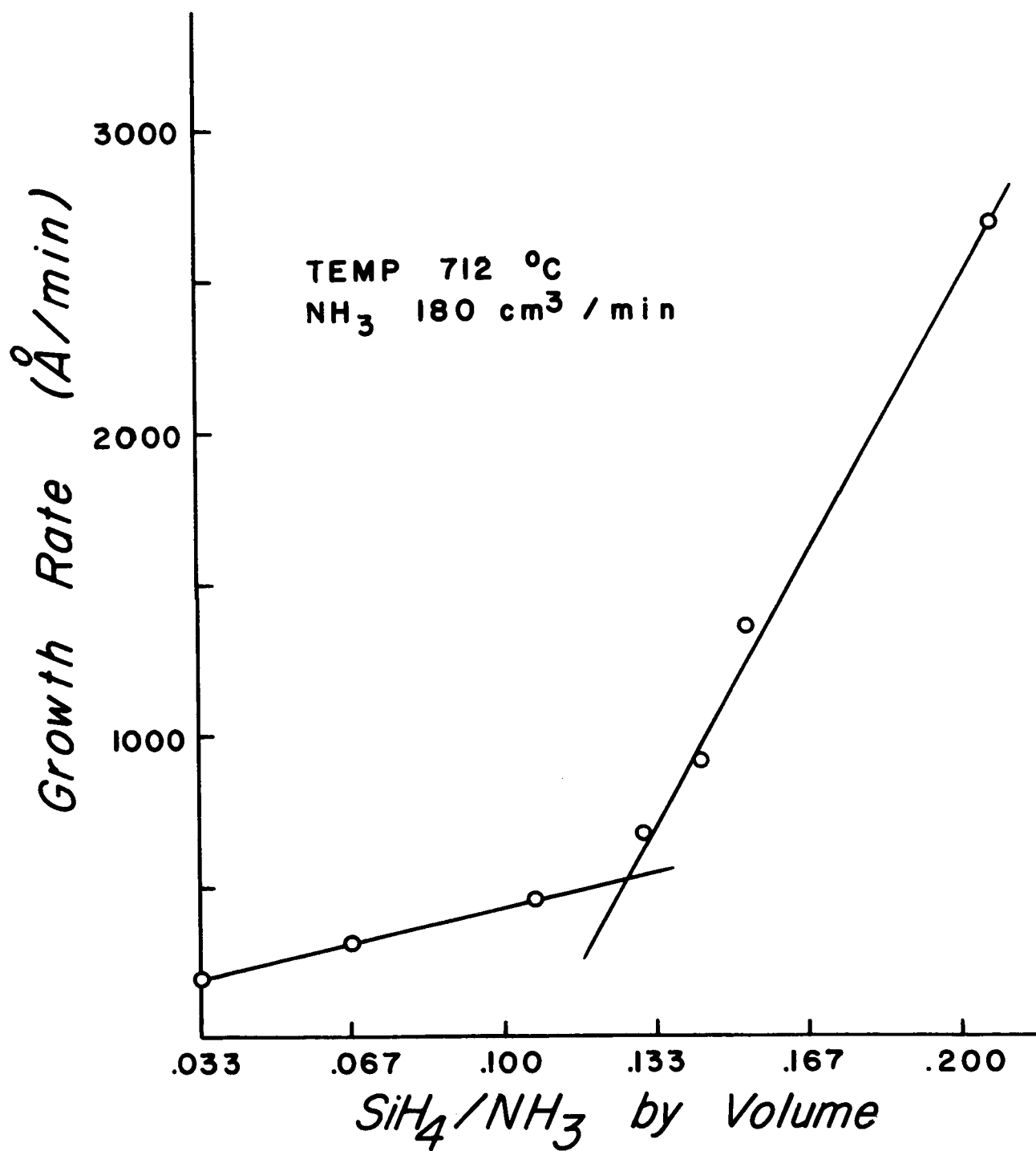
Fig. 61   Growth Rate as a Function of Silane to Ammonia Ratio

E) Substrates:

Substrates used for film deposition include molybdenum, nickel, and platinum films on quartz plates and metallurgically polished nickel and molybdenum wafers, and polished silicon wafers. The quartz plates are 1" x 1" x 1/16" in size. A Varian Associates e-gun evaporates the molybdenum at a pressure of less than 10^{-9} torr in a chemically pumped system. Using an apparatus described by Christian[81], twelve plates are coated in a single pump down and stored in dry air until used.

To reduce aglomeration of the metal at the high deposition temperatures, the substrates must be clean and free of organic films. A mixture of potassium dichromate and sulfuric acid works to remove the organics. The cleaned quartz plates sustain a film of water with no beading.

Nickel and platinum evaporate from a tungsten filament at a pressure of 10^{-5} torr in a diffusion pumped system. Wire, tightly wound onto the filament, serves for the evaporation material. Several attempts to use gold as the base metal on the quartz failed due to aglomeration of the gold at the temperatures involved in the deposition cycle. In general, thin metal films tend to aglomerate at temperatures considerably below their melting temperatures, and metals with melting points in the range of 1200°C or above are best.

Sawing slices of molybdenum and nickel 0.050" thick from a rod of the material, encasing the slice in resin, and polishing with standard metallurgical techniques prepare wafers of these materials. The final polish is with 0.5μ alumina. A mirror finish results on the metals; however, scratches are usually present and the surface is of poorer quality than surfaces of polished silicon. The silicon wafers

are mechanically polished and chemically etched to a mirror finish leaving no scratches visible to the naked eye.

Ultrasonic agitation and vapor degreasing cleans the metal wafers and metal-coated quartz plates. A short etch in hydrofluoric acid removes oxides from the silicon. A further cleaning occurs in the deposition chamber as described in the section on film deposition.

The various substrates differ widely in their thermal coefficient of expansion, e.g.

Silicon	4.2×10^{-6}	per $^{\circ}$C
Molybdenum	4.9×10^{-6}	"
Nickel	10.12×10^{-6}	"
Quartz	0.256×10^{-6}	"

Substrates of molybdenum, silicon, and quartz are satisfactory, and the nitride films appear the same under a x30 microscope for these materials. However, the nickel-nitride mismatch causes the nitride films to crack when the substrate is cooled after film deposition. This cracking is not always immediate. Some films retain their uniform appearance up to 3 or 4 hours after deposition. Bean[1] et.al., by observing the bowing of thin silicon wafers, conclude that the coefficient of expansion of the nitride films exceeds that of the silicon but reasonably close to it. According to Perri and Riseman[83], "mismatches of a factor of 2 can be tolerated if the glass film is thin, about 1.5 microns or less, and the glass is in tension. Greater mismatches can be tolerated if the glass coefficient is lower than the silicon placing the glass in compression."

Failure of the molybdenum to adhere to the quartz plates sometimes causes buckling during periods of high temperature for film deposition.
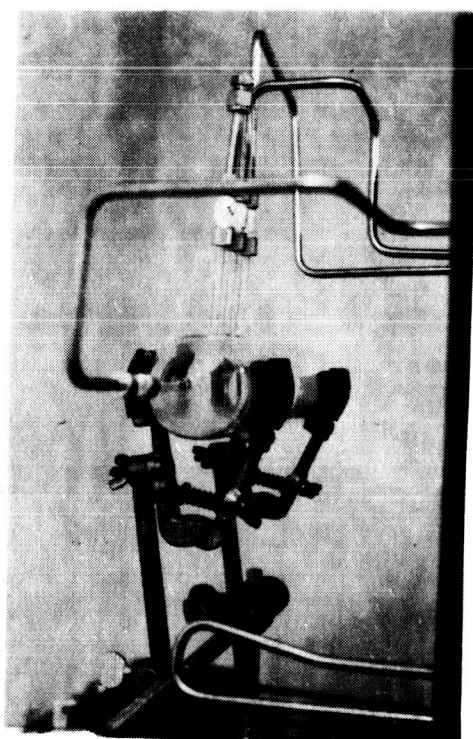
Fig. 62   Mixing Chamber for the Deposition Gases
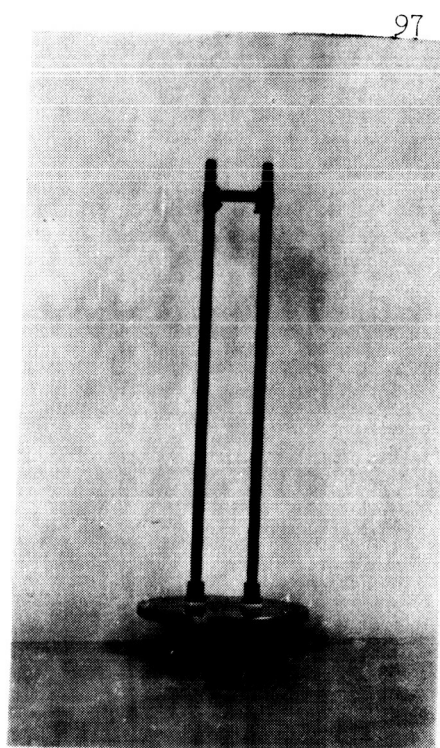
Fig. 63   Substrate Holder with Base Plate to Deposition Chamber
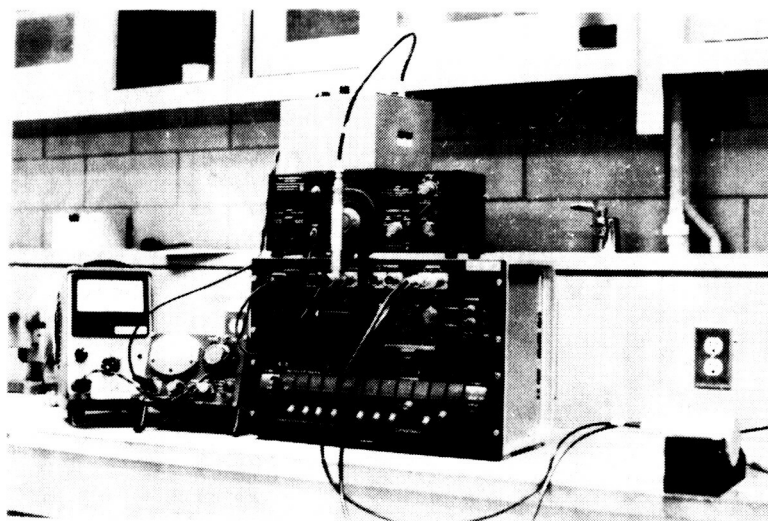
Fig. 64   Capacitance Measurement Arrangement
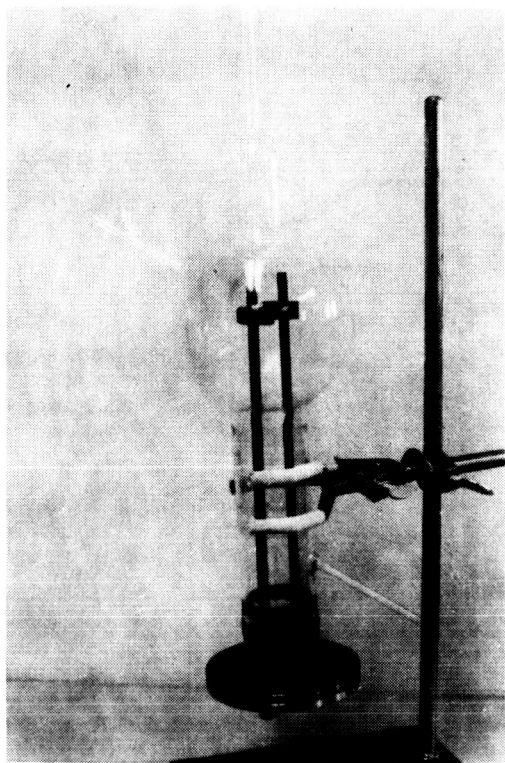
Fig. 65   Reaction Chamber
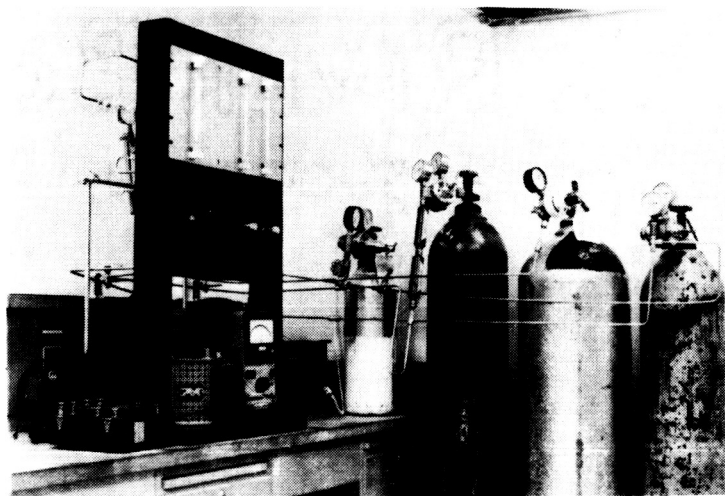
Fig. 66   Gas Flow Apparatus

F) Film Appearance and Structure:

The deposited films appear smooth with no apparent structure under optical microscopes with up to x1000 magnification. Cracks sometimes appear in films with very high growth rates. X-ray diffraction measurements made on the metal and nitride films exhibit no diffraction lines. To check the possibility that the films were too thin for the x-ray diffractometer, measurements were made on a film of aglomerated molybdenum. The aglomerated molybdenum exhibited the characteristic lines and indicated that the films were indeed thick enough for the diffractometer. This also indicates that the smooth films of molybdenum are amorphous. The thicknesses used in the x-ray experiments were approximately 1 micron.

G) Thickness Measurements:

The difficulty of etching the nitride eliminated multiple beam interferometry for thickness measurements. Instead the method of ellipsometry which is non-destructive and capable of extremely high accuracy was used. This involved becoming acquainted with the techniques of ellipsometry, calibrating the Gaertner ellipsometer, and modifing a computer program by McCrackin[84] to run on the Control Data 6020 computer at The University of Texas. The computer program gives tables of readings for the ellipsometer in terms of assumed thickness and index of refraction of the film. Plotting the readings as families of curves with index of refraction and thickness as parameters allows quick conversion of ellipsometer readings to film parameters.

The metal-coated substrates give readings reproducible to ±0.2 degree on the ellipsometer scales. However, due to thickness variations of the nitride films on a substrate, only ±2.0 degrees reproducibility

resulted for the films. This corresponds roughly to $\pm$ 50 $\overset{\circ}{A}$ in thickness. Better accuracy resulted from the ellipsometer for polymer films under 100 $\overset{\circ}{A}$. The thickness measurements from the ellipsometer and from capacitance measurements agreed within $\pm$ 10 $\overset{\circ}{A}$ for the polymer.

The ellipsometer requires a knowledge of the substrate material. Since several different substrates were used in the study of the nitride and accuracies of only $\pm$ 50 $\overset{\circ}{A}$ obtained from the ellipsometer, most thickness measurements were made by observing the color of the interference fringe and comparing the color with a standard by means of a color vs. thickness chart.

Comparing the color of the interference fringes to a color chart gives thicknesses within $\pm$ 100 $\overset{\circ}{A}$. This accuracy is adequate on the thicker films however the error is considerable on films below 1000 $\overset{\circ}{A}$. For the thinner films, the capacitance measurement gives the thickness in terms of the parallel plate capacitor formula. The dielectric constant is discussed elsewhere.

H) Electrical Measurements:

Evaporation of the metal for the base electrode followed by deposition of the nitride film and then evaporation of the top electrode through metal masks constructs the MIM devices. This procedure results in a device with the geometry given in fig. 67. The area of the top electrode varies from 0.3 to 2.0 cm^2 depending on the mask used. Scratching through the nitride film provides a method of making contact to the base electrode.

An indium-gallium paste smeared onto the scratched area assures the pressure contact by wetting both surfaces. Observing the short circuit resistance to record such contact assures the ohmic

nature of the contacts. Attaching a small ball on the In-Ga paste to the contact wire and carefully lowering onto the top electrode completes the connections to the device. Figure 68 shows this arrangement schematically.

Metal

Nitride
Metal
Quartz
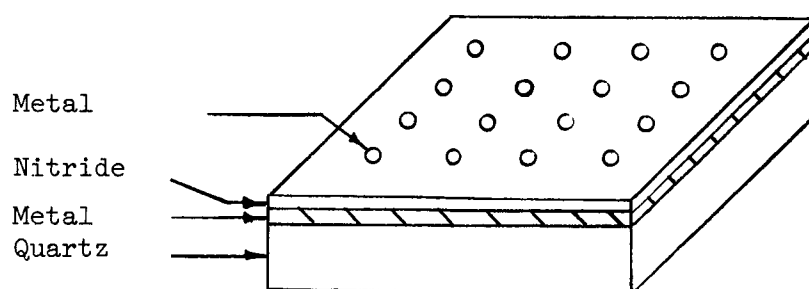
Fig. 67   Geometry of MIM Devices

Nitride
Base Electrode
Quartz

In-Ga Paste
Top Electrode
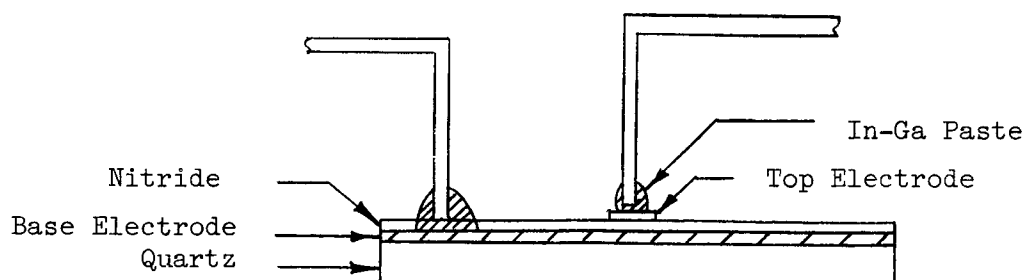
Fig. 68   Method of Making Contacts to the MIM Devices

A special sample holder, shown in figures 70 and 71, that
completely encloses the devices insures that changes in the surrounding
electromagnetic field do not disturb the readings. The adjustable
pressure contacts can be placed on any spot on the sample. Figure 69
is a schematic of the electrical circuit used to take the readings.
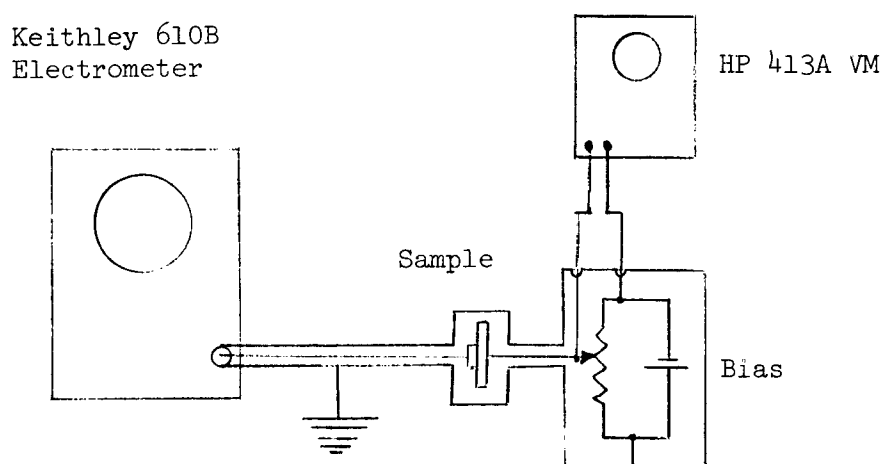
Fig. 69 Electrical Measurement Circuit

A Keithley 610 B electrometer or Hewlett-Packard 425 A
micromicro - ammeter measures the current, and a Hewlett-Packard 413A
dc voltmeter measures the voltage.

Several methods of taking the readings give the same results.
The quickest way to take the readings is to apply the maximum voltage
to be used in the test, (field of 8-9 x 10^6 V/cm), allow the reading
to stabilize, and then remove the bias and take the data point by point.
When the bias is first applied, the current decreases slowly until an
equilibrium value is reached. This usually requires 3-5 minutes.
After stabilization the readings can proceed from the lowest value
readable on the current meter. The bias is then re-increased and the
data points obtained. The current settles to its equilibrium value in
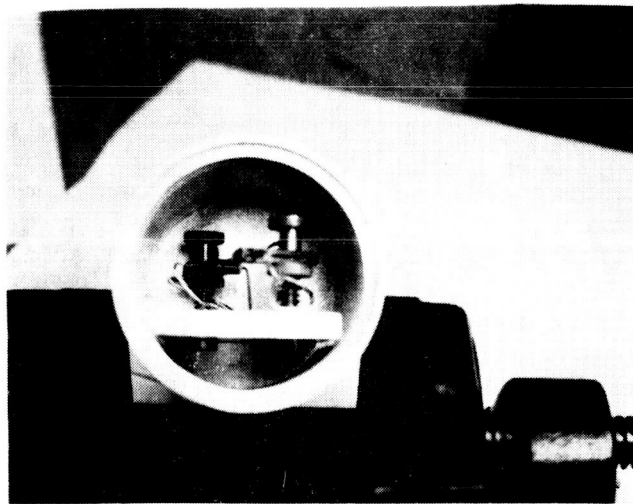
Fig. 70 Sample Holder Inside Metal Cover with Backplate Removed
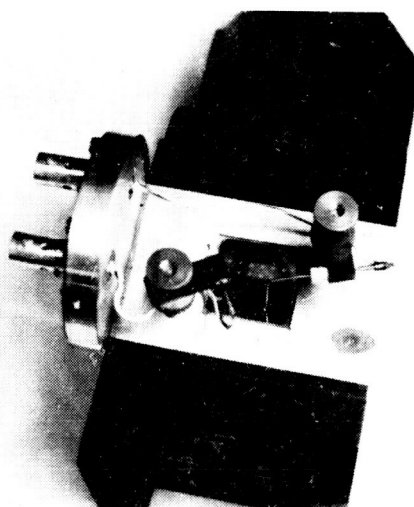
Fig. 71 Sample Test Jig Showing Sample in Place

a few seconds. For readings taken at the first bias application, a considerably longer time is required at each data point before stabilization.

At current readings below 10^{-11} amperes, the considerable fluctuations in the current observed become stable as the bias is increased. Readings below 10^{-11} amperes exhibit considerable hysteresis and are difficult to reproduce; however, readings above this value are immediately reproducible within the accuracy of the bias setting. The lower readings seem to be particularly affected when the polarity is reversed.

I) Dielectric Constant:

The parallel plate capacitance formula expresses the relative dielectric constant in a manner which is convenient for experimental use. This formula is

$$C = \kappa \varepsilon_0 A/d$$

where κ is the relative dielectric constant

      ε_0 is the permittivity of free space

      C   is the capacitance

      d   is the thickness of the films.

Measuring the dimensions of the top electrode using a microscope with a calibrated eyepiece determines the area. A General Radio 1620A capacitance bridge, capable of six figure accuracy from 20 Hz to 100,000 Hz, measures the capacitance and dissipation factor of the device. The index of refraction of silicon nitride films is 2.0 with the composition used in this study[1,2]. Using this value for the index of refraction, the color of the interference fringes gives the thickness of the film to an accuracy of approximately $\pm$ 100 Å. A series of capacitance readings, with thicknesses ranging from 500 Å to 1500 Å, averages out the

error from the approximate thickness determination. Plotting $C/\varepsilon_0 A$ versus

$1/d$ yields a straight line whose slope is the relative dielectric constant.

Figure 72 is the result of such measurements. The slope or relative

dielectric constant is 5.5. One other point is known on the curve,

namely $C/\varepsilon_0 A = 0$ and $1/d = 0$. This point is relevant because the best

fit of the data is a straight line with a slope of 6.2; however, this

line does not go through the origin. The value of 5.5 is somewhat low

for the dielectric constant of silicon nitride. A value of 6.2 seems

to be the most common; however, variations from 5.4 to 9.2 occur. The

dielectric constant is a function of the relative amount of silicon

present in the film. With extremely silicon-rich films the value ap-

proaches that of pure silicon (11.8). The films used in this study are

low in silicon content which probably explains the low value of the

dielectric constant; however, another possibility is that a significant

amount of oxygen impurity is present which tends to lower the dielec-

tric constant to the value of silicon dioxide (4.8).

J) Capacitance Measurements:

At zero bias, the metal-nitride-metal capacitors are stable to

as much as five significant figures at frequencies from 100 to 100,000 Hz.

With an applied field of approximately 2×10^6 V/cm across the device

the balance drops to four significant figures. One some devices, we

observe a very low capacitance reading compared to the value expected

for the thickness of the film as a result of the indium - gallium paste

not wetting the top electrode metal. Reproducible capacitance readings

result only when the indium-gallium paste wets the metal contact.

On the metal-nitride-semiconductor capacitors there was some

frequency dependence at zero bias. Since the semiconductors were p-type
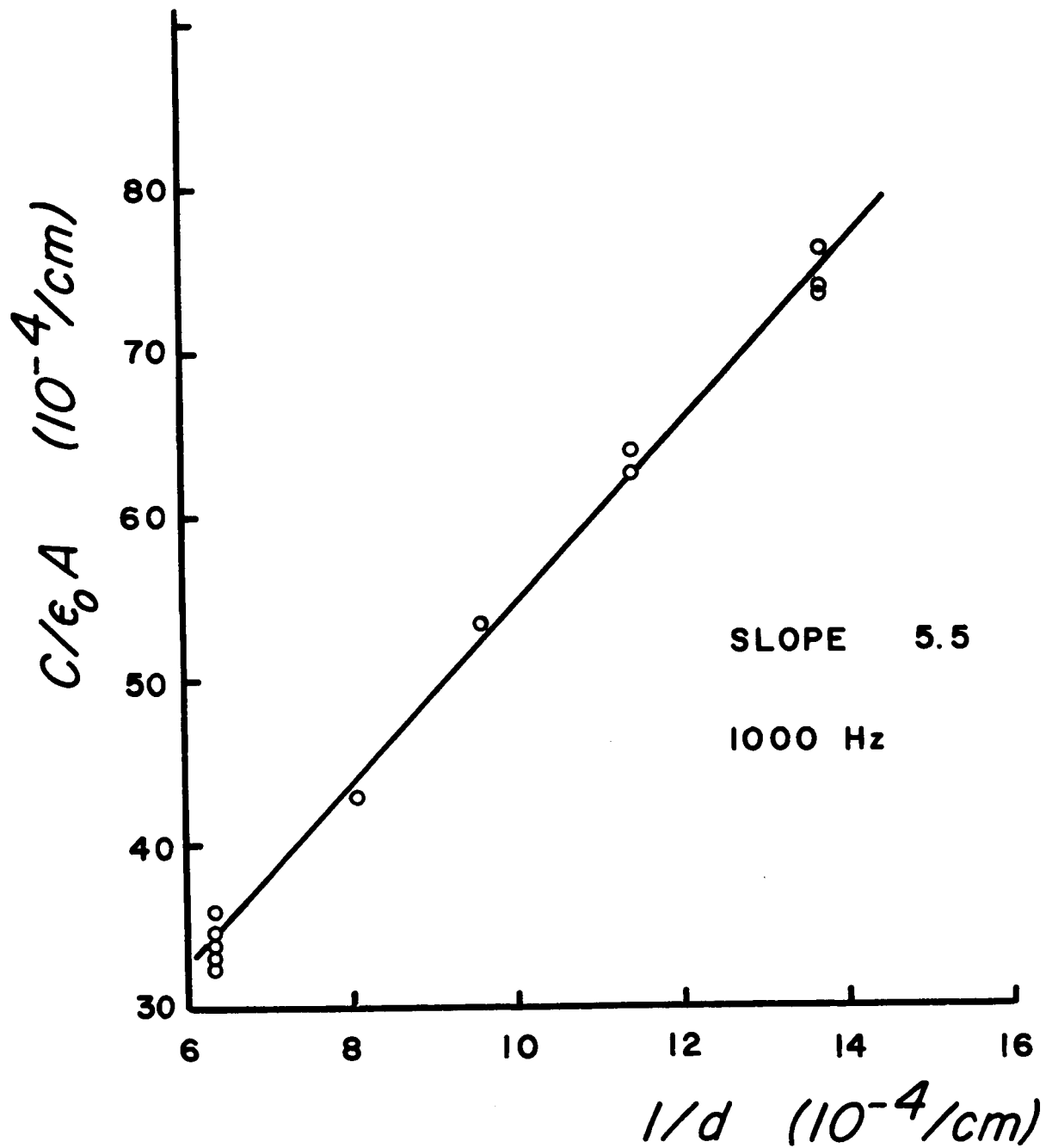
Fig. 72 Capacitance vs. Reciprocal Film Thickness

and there is no frequency dependence in the MIM devices, we concluded
that the surface of the semiconductor was inverted and that the obser-
ved frequency dependence was due to the response of the surface states.

CHAPTER V

Results, Conclusions and Suggestions for Future Work

Results of this work include the design and construction of a system for the deposition of silicon nitride from the reaction of silane and ammonia and obtaining properties of the nitride films such as growth rate, appearance, structure, dielectric constant, and current behavior. The experiments indicate the potential range of the nitride properties and the versatility of chemical vapor deposition for forming films. A review of the transport mechanisms of thin film insulators shows clearly how to analyze the I-V data in light of present theories and knowledge.

The breakdown strength of the films is approximately 1×10^7 V/cm. which is better than thermally grown silicon dioxide by approximately a factor of two. The nitride films are uniform and pinhole free in regard to their electrical characteristics down to 50 $\overset{o}{A}$ which suggests the use of silicon nitride in thin film tunneling devices. Indeed the nitride seems well suited for several devices and adapts easily to manufacturing processes in use.

At high fields, but before breakdown, a measurable current flows in the nitride. A study of the behavior of this current as a function of field, temperature, contacts, thickness, and substrates leads to the following conclusions: (1) For fields up to 8×10^6 V/cm the current varies as exp $(cV^{1/2})$. In general two different behaviors

appear: a) a steady, reproducible current with no hysteresis effects usually dominates at current densities above 10^{-9} amps/cm^2, and b) a current which exhibits slow transient effects and which requires a much wider voltage variation to produce the same current variation. Figures 33 and 35 illustrate the two types of behavior. Figure 53 shows the current variation in different devices. On a few devices a definite change in current behavior appears as the bias increases (note the 1250 Å and 1600 Å curves on fig. 46). Because of the different behavior during the measurements and the large difference in the slopes of the Schottky plots (fig. 52) two different mechanisms seem assured.

(2) Properties of the bulk control the current. No observable differences occur with substrates of quartz or silicon and contacts of molybdenum, aluminum, gold, indium-gallium, or silicon. The outstanding fact here is the lack of control of the electrodes. On devices with film thicknesses of less than 80 Å and 0.1 Ω-cm p-type silicon substrates no differences appear to relate to the difference in barrier heights. At some thickness, theory predicts electrode control due to direct metal-metal tunneling; however, there is a noticeable lack of electrode effect even at these very thin films. It should be noted that our work at these very thin films is qualitative at best and should not be regarded as definitive. We were mainly interested in determining how the nitride behaved at these thicknesses, and variations in the surface roughness probably determines the detailed characteristics. However, we have established that the nitride is continuous below 80 Å and that the current behavior is similar to that seen for thicker films for silicon substrates. For quartz substrates with

nickel strips for base electrodes the current appears ohmic below 200 $\overset{o}{A}$. Several devices on each of five samples exhibited this behavior. The samples were manufactured consecutively with stable capacitive readings which indicated thicknesses ranging from 49 $\overset{o}{A}$ to approximately 140 $\overset{o}{A}$. The resistivity ranged from 10^8 to 10^{10} Ω-cm in these samples. Cracking of the nitride due to the thermal mismatch between the nitride and quartz or between the nitride and nickel probably causes this behavior. A x30 microscope shows this cracking clearly.

(3) Field ionization occurs in the very high resistivity devices at fields above a $7 - 8 \times 10^6$ V/cm. Assuming that the barrier is the same as that for Poole-Frenkel gives a typical value of 0.4 m_o for the electron mass in the conduction band.

(4) The current depends strongly on temperature. The usual variation is 1 to 2 decades between room temperature and liquid nitrogen tem-peratures. On the low resistivity devices the current is clearly exponential over two decades of current; however, on the high resis-tivity devices the current starts out strongly temperature dependent and becomes less so. The ln I vs. 1/T curves separate into two linear parts. Part (a) corresponds to a barrier height of 1.5 eV and part (b) to a barrier height which varies from 0.85 to 1.05 eV on the devices tested. We associate the 1.5 eV barrier with the high resis-tivity devices and the lower barrier with the low resistivity devices.

The investigation uncovered several interesting phenomena not directly related to the major problem but which probably warrant further study.

(1) The nature and cause of the ohmic behavior on the quartz for films below 200 $\overset{o}{A}$ should be examined. The ellipsometer and electron

microscope measure distances comparable to the diameter of atoms and would be helpful in this study.

(2) The current characteristics as a function of deposition temperature and gas composition were not obtained. This type of study would determine over what range the conductivity of the nitride can be varied and perhaps explain the variation in conductivity seen from device to device.

(3) A more complete study of films below 100 $\overset{o}{\text{A}}$ would determine at what thickness tunneling dominates and enable comparison of the nitride properties to those of other dielectrics which have been studied extensively in this range.

(4) A study of the details of the field penetration into the semiconductor in MIS devices should yield information about surface state participation in the conduction mechanisms. Wilmsen[79] observes surface state effects in MIS tunneling devices with polymer film insulators. However, more information about the field penetration, as functions of substrate resistivity, surface state density, film thickness, etc., is needed for a complete understanding of this effect.

(5) On the very thin films the capacitance of the MIM devices is in the 10^{-9} farad range. These are large values compared to values commercially available in microelectronic devices. A study of these capacitors with temperature and frequency would evaluate their practical limits.

(6) Diffusion of substrate ions into the dielectric has been suggested as the source of the surface state charge. Deposition of the nitride on a variety of semiconductor substrates, measuring the short circuit current[86] and C-V characteristics should yield information

on this supposition. The short circuit current determines if diffusion is present and the magnitude of the charge. The C-V curve gives the magnitude of the surface charge. A comparison of these two values on different semiconductors might give new information as to the origin of surface charge. This study would also yield information on ionic diffusion and conduction.

(7) The surface properties probably control the electric characteristics at the very thin films. A study of the surface topology using the ellipsometer and electron microscope would determine if a correlation exists.

Bibliography

SYMPOSIUM ON SILICON NITRIDE--Sponsored by the Electrochemical Society
held in Philadelphia, October 9-14, 1966

1. Kenneth E. Bean, Paul S. Gleim, and W.R. Runyan, "Some Properties of Vapor Deposited Silicon Nitride Films Using the SiH_4-NH_3-H_2 System"

2. T.L. Chu, J.R. Szedon, and C.H. Lee, "Interface Characteristics of Silicon-Silicon Nitride Structures"

3. J.J. Comer and N.C. Tombs, "Structural Properties of the Silicon Nitride System"

4. V.Y. Doo and D.R. Nichols, "Effect of Reactant Composition on Pyrolytic Silicon Nitride Films"

5. M.J. Grieco, F.L. Worthing, and B. Schwartz, "Silicon Nitride Thin Films from $SiCl_4$ and NH_3: Preparation and Properties"

6. S.M. Hu and L.V. Gregor, "Silicon Nitride Films Prepared by Reactive Sputtering"

7. S.M. Hu, "Electronic Conduction in Silicon Nitride and Silicon Dioxide Films"

8. Alan R. Janus and George A. Shirn, "Some Properties of Thin Films of Silicon Nitride Prepared by Sputtering"

9. H. Lawrence and C. Simpson, "Stability Properties of Nitride Film on Silicon"

10. C.H. Lee, T.L. Chu, and G.A. Gruber, "Properties of Silicon Nitride Films"

11. L.A. Murray and J.H. Scott, "Optical Properties and Deposited Silicon Nitride"

12. T.W. O'Keeffe, T.L. Chu, and C.H. Lee "Chemical and Physical Properties of Electron Irradiated Silicon Nitride Layers."

13. Herbert R. Philipp, "Optical Properties of Silicon Nitride"

14. J.H. Scott and J.A. Olmstead, "Low-Temperature Deposition of Si_3N_4"

15. F.A. Sewell, "Capacitance-Voltage Measurements of Metal-Silicon Nitride-Silicon Systems"

16. Alan G. Stanley, "Radiation Effects in Silicon Nitride Insulated Gate Field-Effect Transistors"

17. J.R. Szedon, T.L. Chu, and G.A. Gruber, "Comparison of Electron Irradiation Effects in Metal-Insulator-Silicon Structures Using Nitrides and Oxides"

18. H.A.R. Wegener and N.C. Tombs, "Silicon Nitride Passivated Planar Devices"

BOOKS

19. D. Corson and P. Lorrain, <u>Introduction to Electromagnetic Fields and Waves</u>, W.H. Freeman and Co., San Francisco, 1962.

20. A.J. Dekker, <u>Solid State Physics</u>, Prentice-Hall, Englewood Cliffs, New Jersey, 1957.

21. C. Kittel, <u>Solid State Physics</u>, John Wiley and Sons, Inc. 2nd ed. New York, 1963.

22. A. Many, Y. Goldstein, N. B. Grover, <u>Semiconductor Surfaces</u>, North-Holland Publishing Co. Amsterdam 1965.

23. J.L. Moll, <u>Physics of Semiconductors</u>, McGraw-Hill, New York, 1964.

24. N.F. Mott and D.W. Gurney, <u>Electronic Processes in Ionic Crystals</u>, Dover Publications, 1964

25. N.F. Mott and H. Jones, <u>The Theory of the Properties of Metals and Alloys</u>, Dover Publications, New York 1958

26. R.L. Ramey, <u>Physical Electronics</u>, Wadsworth Pub. Co., Belmont, Calif. 1961

27. A. Rose, <u>Concepts in Photoconductivity and Allied Problems</u>, no. 19 Interscience Tracts on Physics and Astronomy, John Wiley and Sons, Inc., New York, 1963.

28. F. Seitz, <u>The Modern Theory of Solids</u>, McGraw-Hill Book Company, Inc. New York 1940.

29. R.A. Smith, <u>Semiconductors</u>, Cambridge University Press, Cambridge 1964.

30. J.T. Wallmark and H. Johnson, <u>Field-Effect Transistors</u>, Prentice-Hall, Englewood Cliffs, New Jersey, 1966

31. S. Wang, <u>Solid State Electronics</u>, McGraw-Hill, New York, 1966

32. J.M. Ziman, <u>Principles of the Theory of Solids</u>, Cambridge University Press, Cambridge, 1964

JOURNAL ARTICLES

33. H.W. Becke and J.P. White, "Gallium Arsenide FET's Outperform Conventional Silicon MOS Devices," _Electronics_ vol. 40, no. 12, June 12, 1967, pp. 82-90.

34. C.R. Crowell and S.M. Sze, "Current Transport in Metal-Semiconductor Barriers" _Solid-State Electronics_, vol. 9, pp. 1035-1048, Sept. 1966.

35. R.W. Christy, "Electrical Properties of Thin Polymer Films" Part II Thickness 50 - 150 A, _J. Appl. Phys._, vol. 35, no. 7, July 1964, pp. 2179-2184,

36. A.G. Chynoweth, "Internal Field Emission" _Progress in Semiconductors_, John Wiley and Sons, Inc., New York, 1960.

37. V.Y. Doo, "Silicon Nitride, A New Diffusion Mask" _IEEE Trans. Electron Devices_, Vol. ED-13, no. 7, July, 1966, pp. 561-563.

38. P.R. Emtage and W. Tantraporn, "Schottky Emission Through Thin Insulating Films" _Phys. Rev. Lett._, vol. 8, no. 7, April 1, 1962 pp. 267-268.

39. P.R. Emtage, "Enhancement of Metal to Insulator Tunneling by Optical Phonons" _J. Appl. Phys._ vol. 38, no. 4, 15 March 1967, pp. 1820-1825.

40. L. Esaki and P.J. Stiles, "Study of Electronic Band Structure by Tunneling Spectroscopy: Bismuth" _Phys. Rev. Lett._ 14 902, May 1965.

41. L. Esaki and P.J. Stiles, "New Type of Negative Resistance in Barrier Tunneling," _Phys. Rev. Lett._ 16, 1108, June 1966.

42. E.T. Fitzgibbons, _Current Mechanisms in Thin Polymer Films_, Master's Thesis, The University of Texas, Austin, Texas June, 1967.

43. R.H. Fowler and L. Nordheim, "Electron Emission in Intense Electric Fields" _Proc. Roy. Soc._, A119, 173, 1928.

44. R.I. Frank and J.G. Simmons, "Space-Charge Effects on Emission-Limited Current Flow in Insulators" _J. Appl. Phys._, vol. 38, no. 2, Feb. 1967, pp. 832-840.

45. J. Frenkel, "Pre-Breakdown Phenomena in Insulators and Electronic Semiconductors" _Phys. Rev._ vol 54, pp. 647, 1938.

46. D.V. Geppert, "Space-Charge-Limited Tunnel Emission into an Insulating Film" _J. Appl. Phys._, vol. 33, no. 10, Oct. 1962.

47. M. Hacskaylo, "A Relationship Between the Schottky Emission Mechanism and Energy Bands of Thin-Films Metal-Insulator-Metal Configuration" _J. Appl. Phys._ vol. 35, no. 10, Oct. 1964 pp. 2943-2947.

48. Thomas E. Hartman and J.S. Chivian, "Electron Tunneling Through Thin Aluminum Oxide Films" Phys. Rev., vol. 134, no. 4A, 18, May 1964 pp. A1094-A1101.

49. T. Hartman, J.C. Blair, and R. Bauer , "Electrical Conduction Through SiO Films, J. Appl. Physics, vol. 37, no. 6, May 1966, pp. 2469-2474.

50. H. Hirose and Y. Wada, "Dielectric Properties and DC Conductivity of Vacuum-Deposited SiO Films", Jap. J. Appl. Phys., vol. 3, no. 4, April, 1964, pp. 179-190.

51. S.M. Hu, "Properties of Amorphous Silicon Nitride Films", J. Electrochem. Soc., vol. 113, no. 7, July, 1966, pp. 693-698.

52. S.M. Hu, et.al. "Evidence of Hole Injection and Trapping in Silicon Nitride Films Prepared by Reactive Sputtering" Appl. Phys. Lett. vol. 8, no. 3, Feb. 1, 1967, pp. 97-99.

53. I.T. Johansen "Electrical Conductivity in Evaporated Silicon Oxide Films" J. Appl. Phys. vol. 37, no. 2, Feb. 1966, pp. 499-507.

54. N. Klein, "The Maximum Dielectric Strength of Thin Silicon Oxide Films" IEEE Trans. Electron Devices vol. ED-13 no. 12, Feb. 1966.

55. Walter Kohn, "Theory of the Insulating State", Phys. Rev., vol. 133, no. 1A, 6 Jan. 1964, pp. A171-A181.

56. H.P.D. Langon, "Electrical and Optical Properties of Vitreous Selenium, Phys. Rev. vol. 130, no. 1, April 1, 1963, pp. 134-143.

57. T.J. Lewis, "Some Factors Influencing Field Emission and the Fowler-Nordheim Law", Proc. Roy. Soc. 68B, pp. 938-943, 1955.

58. T.J. Lewis, "High Field Electron Emission From Irregular Cathode Surfaces", J. Appl. Phys., Vol. 26, no. 12, Dec. 1955, pp. 1405-1410.

59. T.J. Lewis "Theoretical Interpretation of Field Emission Experiments" Phys. Rev, vol. 101, no. 6, March 15, 1956, pp. 1694-1698.

60. H.T. Mann, "Electrical Properties of Thin Polymer Films, Part I, Thickness 500-2500 Å. J. Appl. Phys., vol. 35, no. 7, July 1964, pp. 2173-2179.

61. C.A. Mead, "Operation of Tunnel-Emission Devices," J. Appl. Phys. vol. 32, no. 1, April 1964, pp. 646-652.

62. C.A. Mead, "Electron Transport Mechanisms in Thin Insulating Films", Phys. Rev. vol, 128, no. 5, Dec. 1, 1962, pp. 2088-2093.

63. D. Meyerhofer and Stefan A. Ochs, "Current Flow in Very Thin Films of Al_2O_3 and BeO", J. Appl. Phys., vol. 34, no. 9, Sept. 1963.

64. J.J. O'Dwyer, "Current-Voltage Characteristics of Dielectric Films"
    J. Appl. Phys. vol. 37, no. 2, Feb. 1966, pp. 599-601.

65. C. Van Opdorp and H.K.J. Kanerva, "Current-Voltage Characteristics
    and Capacitance of Isotype Heterjunctions", Solid State Electronics
    vol. 10, pp. 401-421. Oct. 1967.

66. S.R. Pollack, "Schottky Field Emission Through Insulating Layers"
    J. Appl. Phys., vol. 34, no. 4 (part 1), April 1963, pp. 877-880.

67. S.R. Pollack and C.E. Morris, "Electron Tunneling Through Asymetric
    Films of Thermally Grown Al_2O_3" J. Appl. Phys., vol. 35, no. 5,
    May 1964.

68. A. Rose, "Space-Charged-Limited Currents in Solids", Phys. Rev., vol. 97,
    no. 6, March 15, 1955, pp. 1538-1544.

69. E. Schibli and A.G. Milnes, "Injected Carrier Flow in a Semi-Insu-
    lator containing a Density Gradient of a Deep Impurity", Solid
    State Electronics, vol. 10, pp. 97-107.

70. J.G. Simmons, "Intrinsic Fields in Thin Insulation Films Between
    Dissimiliar Electrodes", Phys. Rev. Lett., vol. 10, no. 1,
    1 Jan. 1963, pp. 10-12.

71. J.G. Simmons, "Generalized Formula for the Electric Tunnel Effect
    Between Similar Electrodes Separated by a Thin Insulating Film",
    J. Appl. Phys., vol. 34, no. 6, June 1963, pp. 1793-1803.

72. J.G. Simmons, "Potential Barriers and Emission-Limited Current Flow
    Between Closely Spaced Parallel Metal Electrodes", J. Appl. Phys.
    vol. 35, no. 8, Aug. 1964, pp. 2472-2481.

73. A.G. Stanley and H.A.R. Wegener, "Effects of Electron Irradiation
    Metal-Nitride-Semiconductor Insulated Gate Field-Effect Transis-
    tors" Proc. IEEE (letters), vol. 54, no. 5, May 1966, pp. 784-785.

74. H.F. Sterling and R.C.G. Swann, "Chemical Vapor Deposition Promoted
    by R.F. Discharge," Solid State Elec., vol. 8, no. 8, 1965,
    pp. 653-655.

75. R. Stratton, "Field Emission From Semiconductors", Proc. Roy. Soc.
    vol. 68B, pp. 746-757, 1955.

76. R. Stratton, "Volt-Current Characteristics for Tunneling Through
    Insulating Films, J. Phys. Chem. Solids, vol. 23, 1963, pp. 1177-1190.

77. S.M. Sze, "Current Transport and Maximum Dielectric Strength of
    Silicon Nitride Films," to be published in the J. App. Phys.

78. N.C. Tombs, H.A.R. Wegener, R. Newman, B.T. Kenney, A.J. Coppola,
    "A New Insulated-Gate Silicon Transistor" Proc. IEEE (letters)
    vol. 54, no. 1, Jan. 1966, pp. 87-88.

79. C.W. Wilmsen, Tunneling Between a Metal and Silicon Separated by a
    Polymer Insulator, Dissertation, University of Texas, 1967.

80. G. Zeidenbergs and R.L. Anderson, "Si-GaP Heterojunctions", Solid-
    State Electronics, vol. 10, pp. 113-123.

81. J.H. Christian, "Ionic Diffusion in the Al-Al$_2$O$_3$-Al Structure"
    Thesis, University of Texas, August 1966.

82. G. Brown, W.C. Robinette, and H. Carlson, "Electrical Characteristics
    of Silicon Nitride Films," A Late Newspaper, presented at the
    Fall meeting of the Electrochemical Society, Philadelphia, Oct.1966.

83. J.A. Perri and J. Riseman, "New Dimensions in IC's Through Films of
    Glass," Electronics, vol. 39, no. 20, Oct. 3, 1966.

84. F.L. McCrackin, E. Passaglia, R.R. Stromberg and H.L. Steinberg,
    "Measurement of the Thickness and Refractive Index of Very Thin
    Films and the Optical Properties of Surfaces by Ellipsometry"
    J. of Research, A. Phys and Chem. vol. 67A, no. 4, July-Aug. 1963,
    pp. 363-377.

85. B.E. Deal, A.S. Grove, and E.H. Snow, "Characteristics of the Sur-
    face State Charge (Q_{ss}) of Thermally Oxidized Silicon," J. Elec-
    trochemical Soc., vol. 114, March, 1967.

86. J.H. Christian and H.L. Taylor "Ionic Diffusion at the Aluminum-
    Aluminum Oxide Interface," J. Appl. Phys. (to be published
    in September 1967).

87. W.H. Hartwig "Metal-Insulator-Semiconductor Tunneling as a Basis
    for Digital Transducer Action," Bull. Am. Phys. Soc., Series II
    vol. 12, no. 5 1967.

88. Brady, J. Phys. Chem. 63, 1119 (1959).

VITA

Jerry R. Yeargan was born in Kirby, Arkansas, January 31, 1940, the son of Edd O. and Tacy P. Yeargan. He finished Kirby High School in 1957 and attended Henderson State Teachers College from September 1957 to June 1959. In September, 1959, he entered The University of Arkansas and completed the degree of Bachelor of Science in Electrical Engineering in the summer of 1961. He worked with the Science Service Division of Texas Instruments Incorporated from July 1961 to September 1963 when he entered graduate school at The University of Arkansas. He entered graduate school at The University of Texas in June 1964 and received the degree of Master of Science in Electrical Engineering from The University of Arkansas in January 1965.

His Research Engineer appointment in the Electronic Materials Research Laboratory at The University of Texas followed his experience as teaching assistant in Electrical Engineering at The University of Arkansas and at The University of Texas.

He is a member of Eta Kappa Nu, Tau Beta Pi, Pi Mu Epsilon, Sigma Xi, the Institute of Electrical and Electronic Engineers, the American Physical Society, and the Electrochemical Society. He married the former Jane Evans of Murfreesboro, Arkansas in August, 1959.

His papers include

"Solid State Electronics," with H.L. Taylor, Texas Engineering and Science Magazine, vol. 2, no. 2, Dec. 1965, pp. 8-12.

"MOS Capacitance-Dissipation Properties," with D.R. Harbison and H.L. Taylor, 1966 SWIEEECO Record.

"Deposition of Silicon Nitride on Metal Coated Substrates, with H.L. Taylor, 1967 SWIEEECO Record.

"I-V Characteristics of Mo-Si$_3$N$_4$-Metal Structures," with H.L. Taylor, J. Electrochemical Soc., vol. 114, no. 3, March, 1967, pp. 58C.

"Silicon Nitride Conduction Mechanisms," Invited paper at NASA seminar on Future Trends in Digital Transducers, NASA, Houston, May, 1967.

Permanent address: % Vance Evans
                       Box KK
                       Murfreesboro, Arkansas

This dissertation was typed by Linda Johnson.